Studies on Synthesis and Properties of Helicenes and Helicene-like Compounds

Keisuke Uematsu

2022

Contents

Abbreviations ……vi

Chapter 1 General Introduction …….1

1.1 Helicenes …….3
1.2 Synthesis of helicenes and helicene-like compounds …….4
1.2.1 Photocyclization …….5
1.2.2 Diels–Alder cycloaddition …….6
1.2.3 Friedel–Frafts reaction …….7
1.2.4 Reaction of biaryl dianions with dielectrophiles …….7
1.2.5 Intramolecular cycloisomerization …….9
1.2.6 Intermolecular cycloisomerization ……..12
1.2.7 Olefin metathesis ……..13
1.2.8 Cross-coupling reaction ……..13
1.3 Properties of helicenes ……..15
1.3.1 Molecular recognition ……..15
1.3.2 Photoluminescence property ……..17
1.3.3 Helicene aggregates and helicene oligomers ……..20
1.4 Summary ……..23
1.5 References ……..26

Chapter 2 Transformation of Thia[7]helicene to Aza[7]helicenes and [7]helicene-like Compounds via Aromatic Metamorphosis ……..29

2.1 Introduction ……..31
2.2 Synthesis ……..36
2.2.1 Synthesis of 3,3'-dibromo-4,4'-biphenanthrene ……..36
2.2.2 Aromatic metamorphosis of thia[7]helicene ……..37
2.2.3 Optical resolution of aza[7]helicenes ……..40

2.3 Photophysical properties ……42
2.3.1 Absorption and fluorescence properties ……42
2.3.2 Chiroptical properties ……44
2.4 Theoretical calculations ……45
2.5 Conclusion ……54
2.6 Experimental section ……55
2.6.1 General ……55
2.6.2 Synthetic procedure ……56
2.6.3 X-ray crystallography ……63
2.6.4 Theoretical calculations ……63
2.7 References ……64

Chapter 3 Synthesis and Properties of Spiro-Double Silole-fused [7]Helicene-like Compound ……67

3.1 Introduction ……69
3.2 Synthesis ……71
3.3 X-ray crystallographic analysis ……72
3.4 Photophysical properties ……76
3.4.1 Absorption and fluorescence properties ……76
3.4.2 Chiroptical properties ……77
3.5 Theoretical calculations ……78
3.6 Conclusion ……84
3.7 Experimental section ……85
3.7.1 General ……85
3.7.2 Synthetic procedure ……85
3.7.3 Theoretical calculations ……86
3.8 References ……87

Chapter 4 Synthesis and Properties of [7]Helicene and [7]Helicene-like Compounds with a Cyclopenta[1,2-*b*:4,3-*b*']dithiophene or Dithieno[2,3-*b*:3',2'-*d*]heterole Skeleton …...89

4.1 Introduction …...91
4.2 Synthesis …...92
4.3 X-ray crystallographic analysis …...95
4.4 Photophysical properties …...99
4.4.1 Absorption and fluorescence properties …...99
4.4.2 Chiroptical properties ….104
4.5 Theoretical calculations ….104
4.6 Conclusion ….111
4.7 Experimental section ….112
4.7.1 General ….112
4.7.2 Synthetic procedure ….113
4.7.3 X-ray Crystallography ….121
4.7.4 Theoretical calculations ….121
4.8 References ….123

Chapter 5 Conclusion and Perspective ….125

List of Publications ….129

Acknowledgements ….131

Abbreviations

Ac	acetyl
APCI	atmospheric pressure chemical ionization
Ar	aryl or aromatic ring
a.u.	arbitrary unit
B3LYP	Becke three-parameter hybrid functional combined with Lee–Yang–Parr correlation functional
br	broad (spectral)
Bu	butyl
calcd	calculated
CD	circular dichroism
CI	configuration interaction
cod	1,5-cyclopentadiene
Cp	cyclopentadienyl
CPL	circularly polarized luminescence
Cy	cyclopentadienyl
d	doublet (spectral)
δ	chemical shift of NMR signal in ppm
dba	dibenzylideneacetone
DFT	density functional theory
DMSO	dimethyl sulfoxide
ε	molar absorption coefficient
ESI	electrospray ionization
Et	ethyl
h	hour
HOMO	highest occupied molecular orbital
HPLC	high-performance liquid chromatography
HRMS	high-resolution mass spectrometry
Hz	hertz
ICT	intramolecular charge transfer
^{i}Pr	isopropyl
IUPAC	International Union of Pure and Applied Chemistry
J	coupling constant
λ	wavelength
LDA	lithium diisopropylamide
LUMO	lowest unoccupied molecular orbital
m	multiplet/multiple resonances (spectral)
M	mol·dm^{-3}
Me	methyl
Mes	2,4,6-trimethylphenyl/mesityl
min	minute
m.p.	melting point
nbd	norbornadiene
Nf	nonafluorobutanesulfonyl
NMR	nuclear magnetic resonance
ORTEP	Oak Ridge thermal ellipsoid plot
Ph	phenyl
Φ_f	quantum yield
PL	photoluminescence
Pr	propyl
q	quartet (spectral)
R_f	relative mobility
s	singlet (spectral)
S	singlet (electronic state)
S_NAr	nucleophilic aromatic substitution
t	triplet (spectral)
^{t}Bu	tertiary butyl
TD	time dependent
Tf	trifluoromethanesulfonyl
THF	tetrahydrofuran
TMEDA	*N*,*N*,*N*′,*N*′-tetramethylethelene-diamine
TOF	time of flight
Ts	*p*-toluenesulfonyl/tosyl
UV-vis	ultraviolet and visible

Chapter 1

General Introduction

1.1. Helicenes

Helicenes are a class of polycyclic aromatic compounds in which benzene and other aromatic rings are *ortho*-fused and angularly arranged to form nonplanar helical structures.[1–4] According to IUPAC nomenclature, the structures with five or more *ortho*-fused aromatic rings are classified as helicenes.[5] Helicenes composed of *n ortho*-fused aromatic rings are called as [*n*]helicenes or (numerical prefix)helicenes. For example, the helicene with six *ortho*-fused benzene rings, phenanthro[3,4-*c*]phenanthrene, is named as [6]helicene or hexahelicene (Figure 1.1). The helicenes can be categorized into two types. One is carbohelicene which contains only carbon atoms in the helical skeleton, and the other is heterohelicene with at least one heteroaromatic ring. When aromatic ring(s) in a helicene skeleton is replaced with non-aromatic ring(s), such as cyclopentadiene, silole, and phosphole, the resulting compound is not a helicene, but called as a helicene-like compound. The defining structural feature of helicenes is helical chirality induced by an intramolecular steric repulsion. In accordance with the helicity rule proposed by Cahn, Ingold, and Prelog in 1966, helicenes with a right-handed helical conformation are described as (*P*)-helicenes (plus), and those with a left-handed ones are described as (*M*)-helicenes (minus).[6]

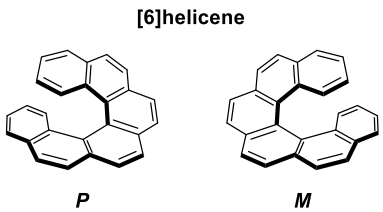

Figure 1.1. The structure of [6]helicene.

Helicenes have been known over one hundred years. For many years from the first synthesis of helicenes, they have been challenging synthetic targets mainly from the view point of their aesthetic and curious structures. More recently, it has been found that their π-extended nonplanar structure and chirality endow them with unique properties, offering applications in a variety of fields such as catalysts, nonlinear optics, and circularly polarized luminescent materials. The chemistry of helicenes has now grown as an important research field, and a wide range of researches are in progress in the world.

1.2. Synthesis of helicenes and helicene-like compounds

The first helicene, 3,4-diazadibenzo[*c*,*g*]phenanthrene, was reported by Meisenheimer and Witte in 1903.[7] Then, [5]helicene, dibenzo[*c*,*g*]phenanthrene, was synthesized in 1918 as the first example of carbohelicenes.[8] In 1955, Newman and coworkers prepared enantiomerically pure [6]helicene for the first time.[9] They synthesized [6]helicene in a racemic form by using Friedel–Crafts acylation, and then separated *P*- and *M*-isomers through charge-transfer complexation with enantiomerically pure 2-(2,4,5,7-tetranitro-9-fluorenylideneaminooxy)propionic acid. After this report, the studies in helicenes have made significant progress. A variety of helicenes have been synthesized until now, particularly in the last few decades, leading to elucidation of structure–property relationship in helicenes. Obviously, the development of synthetic methodologies for helicenes has greatly contributed to significant progress of the chemistry of helicenes. The representative synthetic methodologies are summarized below.

1.2.1. Photocyclization

The photocyclization of stilbene derivatives is a typical method to synthesize helicenes. Irradiation of the stilbene precursors in the presence of iodine as an oxidant operates cyclization and the following dehydrogenation, affording helicene skeletons. For example, [7]helicene was synthesized by photocyclization of 1,2-di(phenanthren-3-yl)ethene (Figure 1.2a).[10] Recently, the synthesis of [16]helicene, the largest carbohelicene ever reported, was achieved by photocyclization (Figure 1.2b).[11] The asymmetric synthesis by photocyclization was achieved by using circularly polarized light.[12] The (*M*)-[6]helicene was selectively synthesized under irradiation with right-handed circularly polarized light. In general, high dilution condition is required to prevent an undesirable intermolecular [2+2] dimerization. Such a requirement would be disadvantageous for a large scale synthesis. Nevertheless, the photocyclization approach has been one of the most common methods because the reaction procedure is very simple and the stilbene precursors can be easily prepared by Wittig reaction and so on.

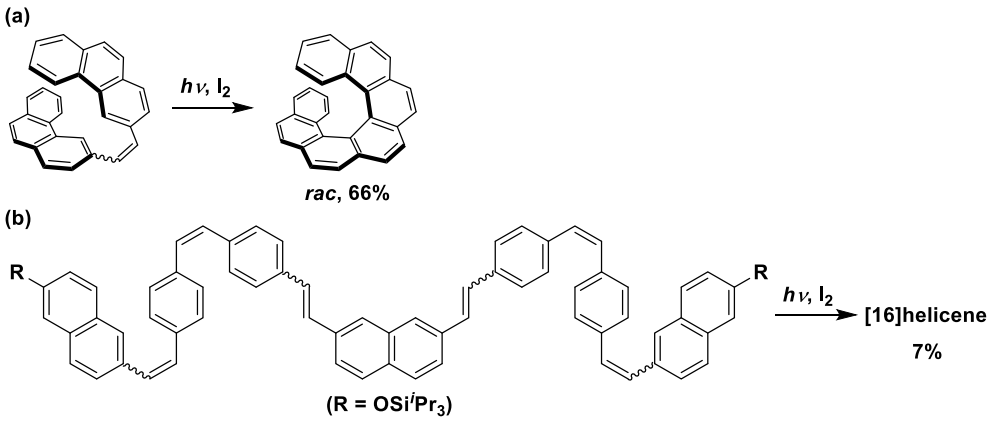

Figure 1.2. Photocyclization of the stilbene precursors.

1.2.2. Diels–Alder cycloaddition

The synthesis of helicenes via the Diels–Alder cycloaddition has also been reported. The Diels–Alder cycloaddition is applicable to dienes and dienophiles with various substituents, therefore useful for the synthesis of multi-substituted helicenes. For example, a series of helicene-like compounds have been prepared by using the reaction of divinylarenes with 1,4-benzoquinone (Figure 1.3a).[13,14] The quinone unit can be reduced to the hydroquinone one to afford fully aromatic helicenes. Asymmetric synthesis has also been achieved by using the benzoquinone with a chiral auxiliary (Figure 1.3b).[15,16] In addition, heterohelicenes can be synthesized by using dibenzoheteroles with vinyl substituents (Figure 1.3c).[17,18] The Diels–Alder cycloaddition is superior in that it can be applied to a large scale synthesis.

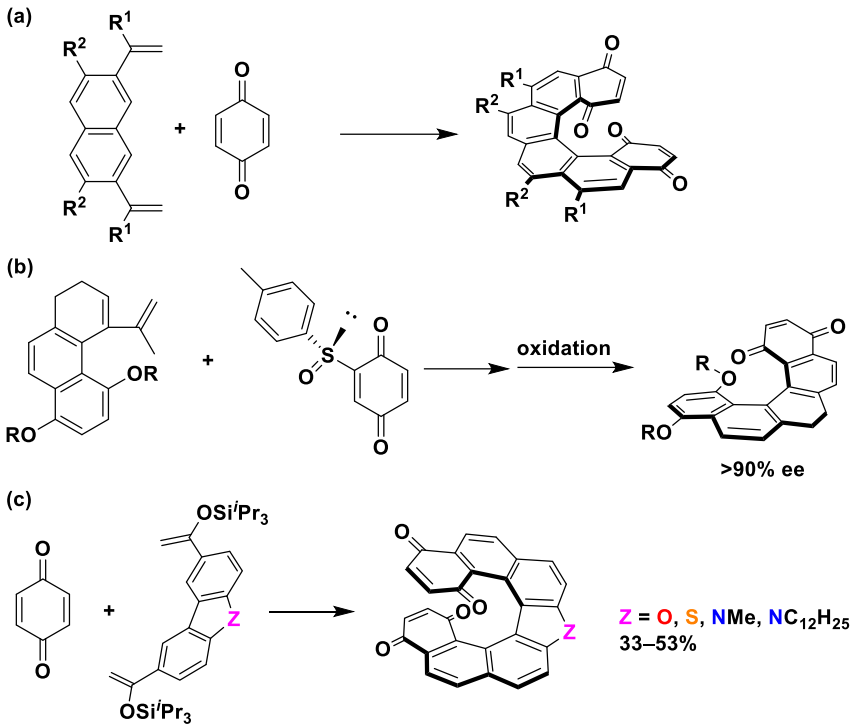

Figure 1.3. Synthesis of helicenes and helicene-like compounds via Diels–Alder cycloaddition.

1.2.3. Friedel–Frafts reaction

Intramolecular Friedel–Crafts-type reaction has also been used for the synthesis of helicenes. Ichikawa and coworkers have reported the synthesis of helicenes from 1,1-difluoro-1-alkenes with two aryl groups (Figure 1.4a).[19,20] The helicene structure is constructed by the domino Friedel–Crafts-type cyclization in the presence of $FSO_3H{\cdot}SbF_5$ and the subsequent dehydrogenation. Gaucher and coworkers have achieved the synthesis of diamino[6]helicenes from dinitrile precursors using the intramolecular Friedel–Crafts-type cyclization (Figure 1.4b).[21]

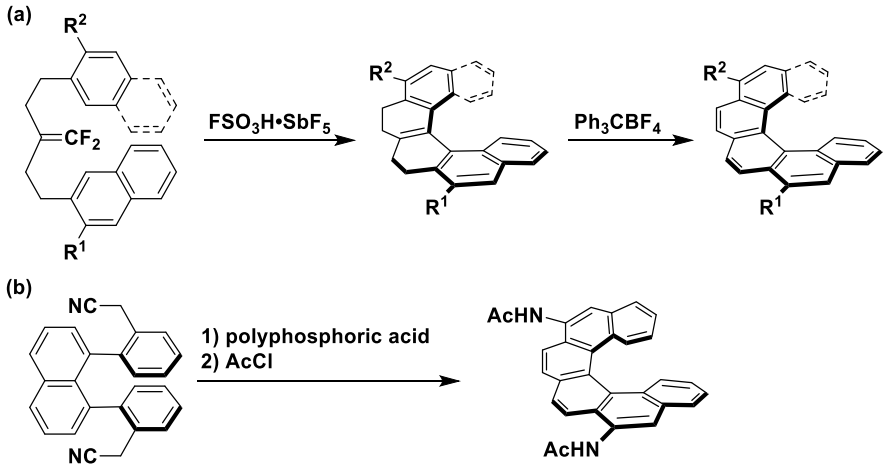

Figure 1.4. Synthesis of helicenes via Friedel–Crafts reaction.

1.2.4. Reaction of biaryl dianions with dielectrophiles

The reaction of biaryl dianions with dielectrophile is a classical and simple method for constructing phenanthrene, fluorene, and dibenzoheterole (borole, silole, phosphole, thiophene, germole, etc.) skeletons and have been applied to helicene synthesis. A

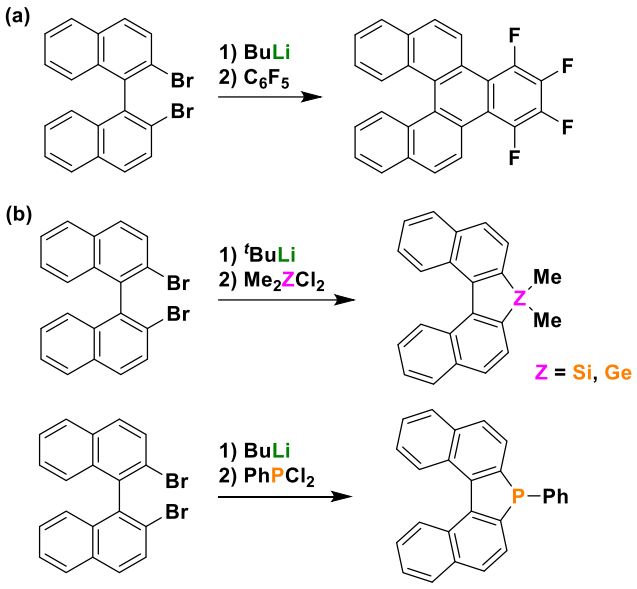

Figure 1.5. Synthesis of [5]helicenes and [5]helicene-like compounds.

variety of [5]helicene and [5]helicene-like compounds can be prepared from 2,2'-dibromo-1,1'-binaphthalene as a common starting material. In 2005, Piers and coworkers reported a facile synthesis of the fluorine-substituted [5]helicene through bromine–lithium exchange and the subsequent reaction with hexafluorobenzene (Figure 1.5a).[22] The trapping with heteroatom-centered dielectrophiles was found to give a series of [5]helicene-like compounds with silole, phosphole, and germole units (Figure 1.5b).[23–25]

Rajca and coworkers prepared thia[7]helicene and bisthia[7]helicene which contains only thiophene rings in the helical skeletons.[26,27] These thiahelicenes were synthesized from the 3,3'-bidithieno[2,3-*b*:3',2'-*d*]thiophene skeleton. It is well known that the 2-position (α-position) of a thiophene ring can easily be deprotonated with a lithium reagent, giving an anionic species. Therefore, the dianion was prepared from the 3,3'-bidithieno[2,3-*b*:3',2'-*d*]thiophene derivative with lithium diisopropylamide (LDA) and

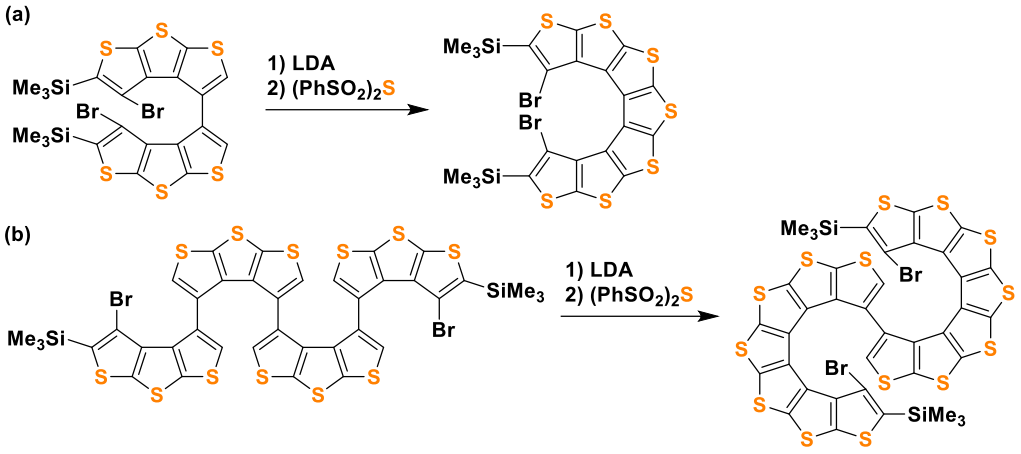

Figure 1.6. Synthesis of thiahelicenes via the reaction of the dianion with the sulfur dielectrophile.

treated with bis(phenylsulfonyl)sulfide to give the thia[7]helicene (Figure 1.6a). The bisthia[7]helicene was also synthesized from quaterdithieno[2,3-*b*:3',2'-*d*]thiophene by the same method (Figure 1.6b).

1.2.5. Intramolecular cycloisomerization

In the last two decades, a variety of transition metal-catalyzed reactions have been applied to helicene synthesis. The typical reaction for synthesizing helicenes and helicene-like compounds is the [2+2+2] cycloisomerization.[28] Easy preparation of substrates, wide substrate scope, and applicability to the asymmetric synthesis make this method useful. The pioneering work was reported by Stará, Starý, and coworkers in 1998. The [7]helicene-like compounds were prepared from the triynes through cobalt-catalyzed [2+2+2] cycloisomerization (Figure 1.7a).[29] Three rings are constructed in one-step. Following this pioneering work, a variety of helicenes and helicene-like compounds have been synthesized by using this methodology. For example,

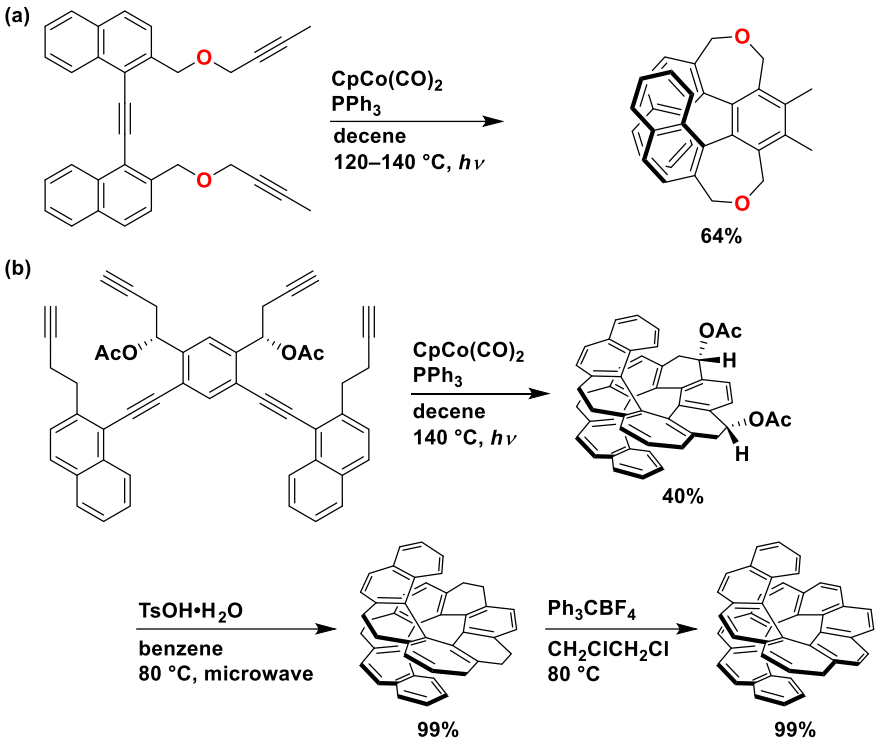

Figure 1.7. Synthesis of helicenes and helicene-like compounds by Co-catalyzed [2+2+2] cycloisomerization of triynes.

[11]helicene was successfully synthesized via double intramolecular [2+2+2] cycloisomerization from the hexayne precursor (Figure 1.7b).[30] In addition to cobalt catalysts, other metal catalysts can be used for this intramolecular cycloisomerization strategy. The synthesis of [7]helicene, which can be prepared by photocyclization (*vide supra*), was achieved by the Ni-catalyzed [2+2+2] cycloisomerization of the diene-triyne compound (Figure 1.8a).[31] Tanaka and coworkers have reported asymmetric synthesis of a variety of helicene-like compounds by applying the [2+2+2] cycloisomerization reaction with chiral rhodium catalysts (Figure 1.8b).[32,33]

In addition to the intramolecular [2+2+2] cycloisomerization of triynes, another type of metal-catalyzed intramolecular cycloisomerization has been applied to helicene

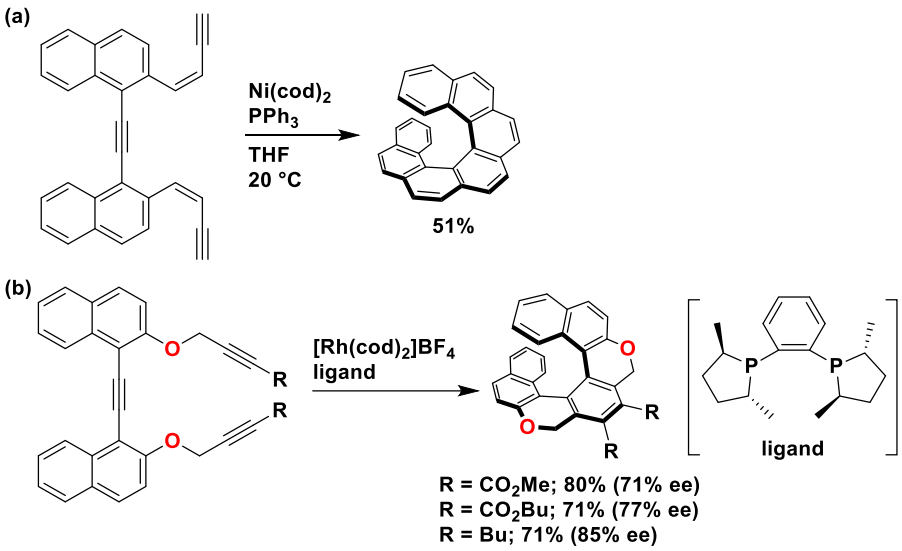

Figure 1.8. Synthesis of helicenes and helicene-like compounds by Ni and Rh-catalyzed [2+2+2] cycloisomerization.

synthesis. In this cycloisomerization, the alkynylated biaryls are converted to the phenanthrene skeleton by virtue of metal catalysts. In 2009, Storch and coworkers reported the synthesis of [6]helicenes by using platinum-catalyzed double cycloisomerization (Figure 1.9a).[34] The silole- and cyclopentadiene-fused [7]helicene-like compounds were also prepared through the double cycloisomerization catalyzed by $PtCl_2$ (Figure 1.9b).[35,36]

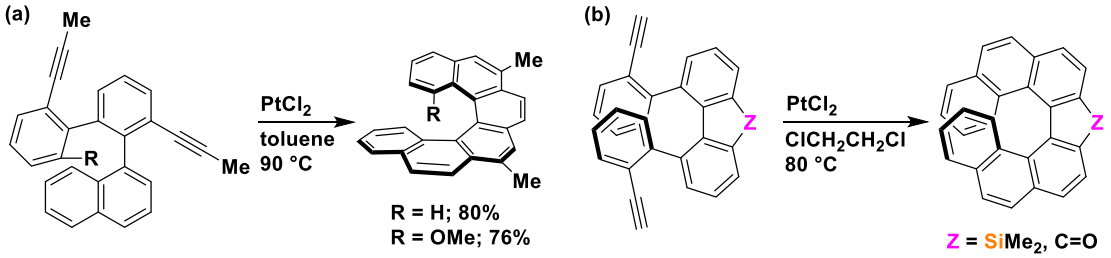

Figure 1.9. Synthesis of helicenes and helicene-like compounds by Pt-catalyzed double cycloisomerization.

1.2.6. Intermolecular cycloisomerization

The intermolecular version of the [2+2+2] cycloisomerization was also used in the construction of helicene skeletons. Tanaka and coworkers have prepared various kinds of helicene-like compounds by metal-catalyzed intermolecular [2+2+2] cycloisomerization. For example, enantio-enriched [9]helicene-like compounds were synthesized by intermolecular double [2+2+2] cycloisomerization with chiral rhodium catalysts (Figure 1.10a).[37] Phosphole-fused [7]helicene-like compounds were also obtained by using the same method (Figure 1.10b).[38]

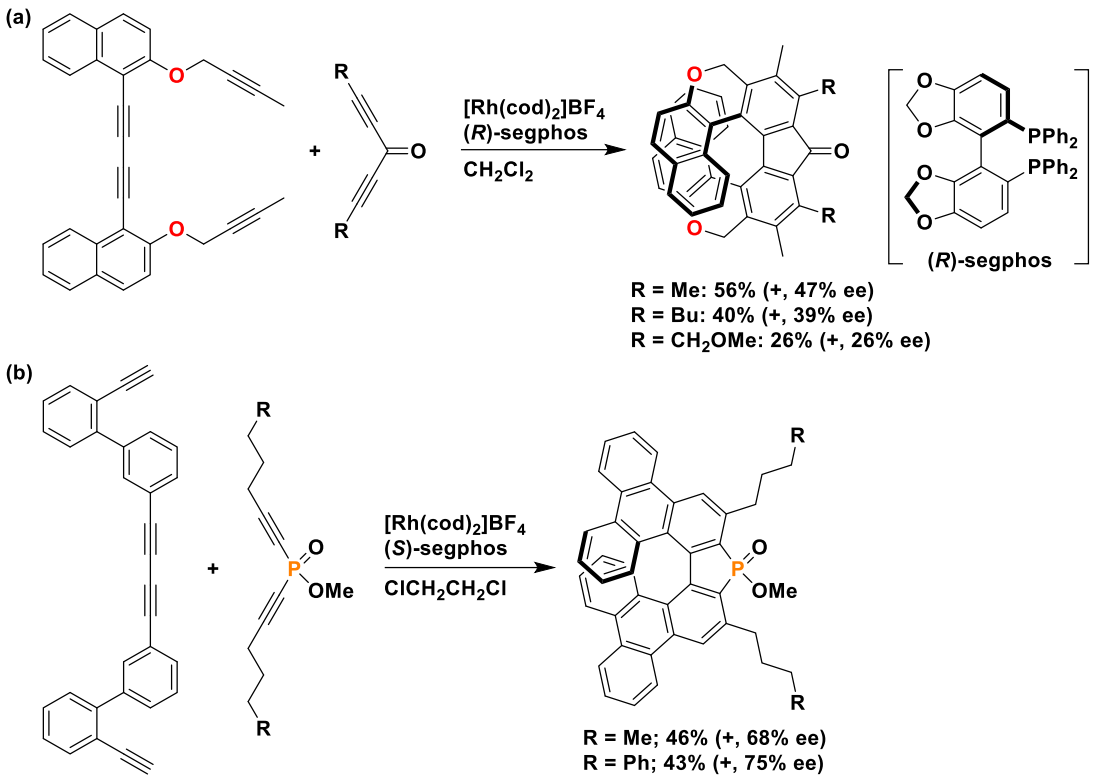

Figure 1.10. Synthesis of helicene-like compounds by Rh-catalyzed double [2+2+2] cycloisomerization

1.2.7. Olefin metathesis

The ring-closing olefin metathesis is often used for the synthesis of cycloalkenes, and the synthesis of helicenes is no exception. Collins and coworkers have successfully synthesized [5]-, [6]-, and [7]helicenes from the corresponding divinylbiaryl precursors with a ruthenium-based second-generation Grubbs catalyst (Figure 1.11a).[39] They have also achieved asymmetric synthesis by this method. Helicenes with high enantiopurity (up to 80% ee) were obtained from racemic starting materials through kinetic resolution (Figure 1.11b).[40]

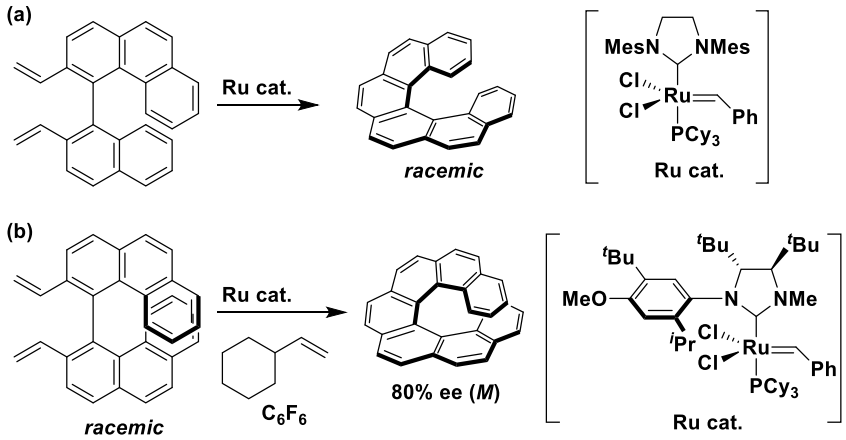

Figure 1.11. Synthesis of helicenes by olefin metathesis.

1.2.8. Cross-coupling reaction

Significant efforts have been devoted into the development of transition metal-catalyzed carbon–heteroatom bond-forming reactions in the last few decades. These reactions have provided facile synthetic routes to polycyclic aromatic compounds. For example, carbazole derivatives can be prepared by the palladium-catalyzed double *N*-

arylation of primary amines with 2,2′-dihalobiphenyls or biphenyl-2,2′-ylene disulfonate, while the related carbon–oxygen bond-forming reaction can give dibenzofurans from 2′-hydroxybiphenyl-2-yl halides or sulfonate.[41,42] In 2005, Nozaki and coworkers applied these strategies to the synthesis of aza- and oxa[7]helicenes.[43] The aza[7]helicene was synthesized by palladium-catalyzed double *N*-arylation of aniline with 4,4′-biphenanthrene-3,3′-diyl disulfonate (Figure 1.12a). The intramolecular *O*-arylation of the corresponding monosulfonate gives the oxa[7]helicene (Figure 1.12b). Both starting compounds for these transformations can be prepared from 4,4′-biphenanthrene-3,3′-diol. Nozaki and coworkers also prepared the phosphole-fused [7]helicene-like compound by applying the palladium-catalyzed carbon–phosphorus bond-forming reaction (Figure 1.12c).[44]

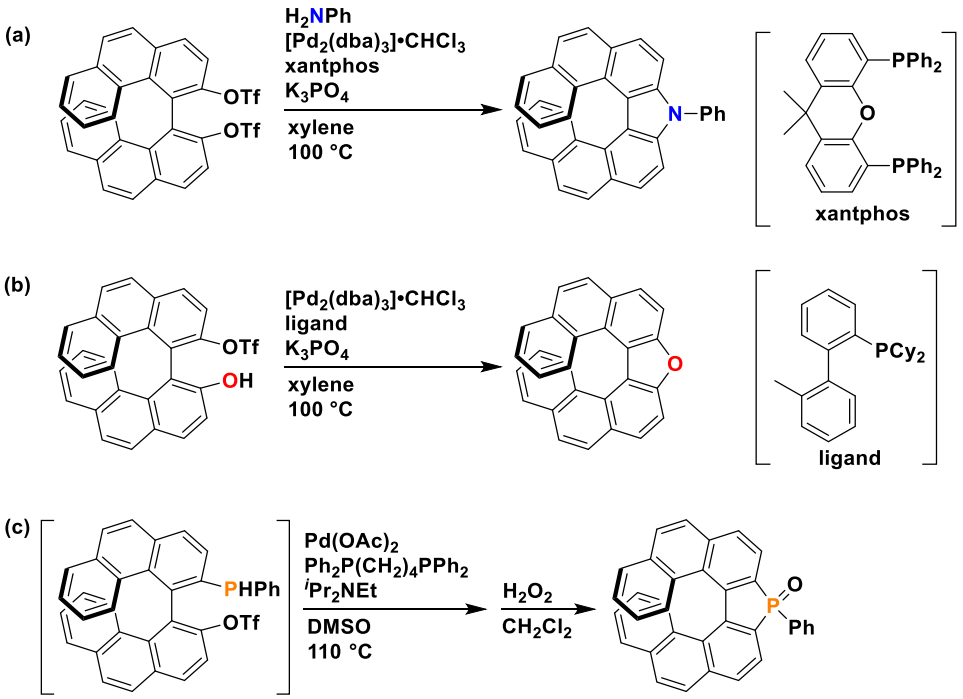

Figure 1.12. Synthesis of helicenes and the helicene-like compound by cross-coupling reaction.

1.3. Properties of helicenes

Significant research efforts have been devoted to helicenes to elucidate their structure–property relationship and found that their π-extended nonplanar structure and chirality endow them with unique properties. Aggregated structures of helicenes have also attracted researchers' attention because some physicochemical properties can be enhanced through aggregation compared to those from a single molecule.

1.3.1. Molecular recognition

There are some reports on the molecular recognition of helicene derivatives. Goddard and coworkers reported the [6]helicene with two diphenylphosphino groups at the terminal benzene rings.[45] This helicene is the first helicene-based diphosphine ligand for metal-catalyzed asymmetric reactions. The rhodium-catalyzed hydrogenation of dimethyl itaconate in the presence of an optically active (−)-helicene diphosphine gave the *S*-isomer with a moderate enantioselectivity (39% ee) (Figure 1.13a). The phosphine ligand containing two twisted benzo[*c*]phenanthrene units were also developed and applied to the same reaction to give a much improved enenatioselectivity (96% ee) (Figure 1.13b).[46] [5]HELOL composed of two [5]helicenols was found to work as a bidentate ligand in the asymmetric catalytic addition of diethylzinc to benzaldehyde (Figure 1.13c).[47] The corresponding enantio-enriched alcohol (81% ee) was obtained in 93% yield.

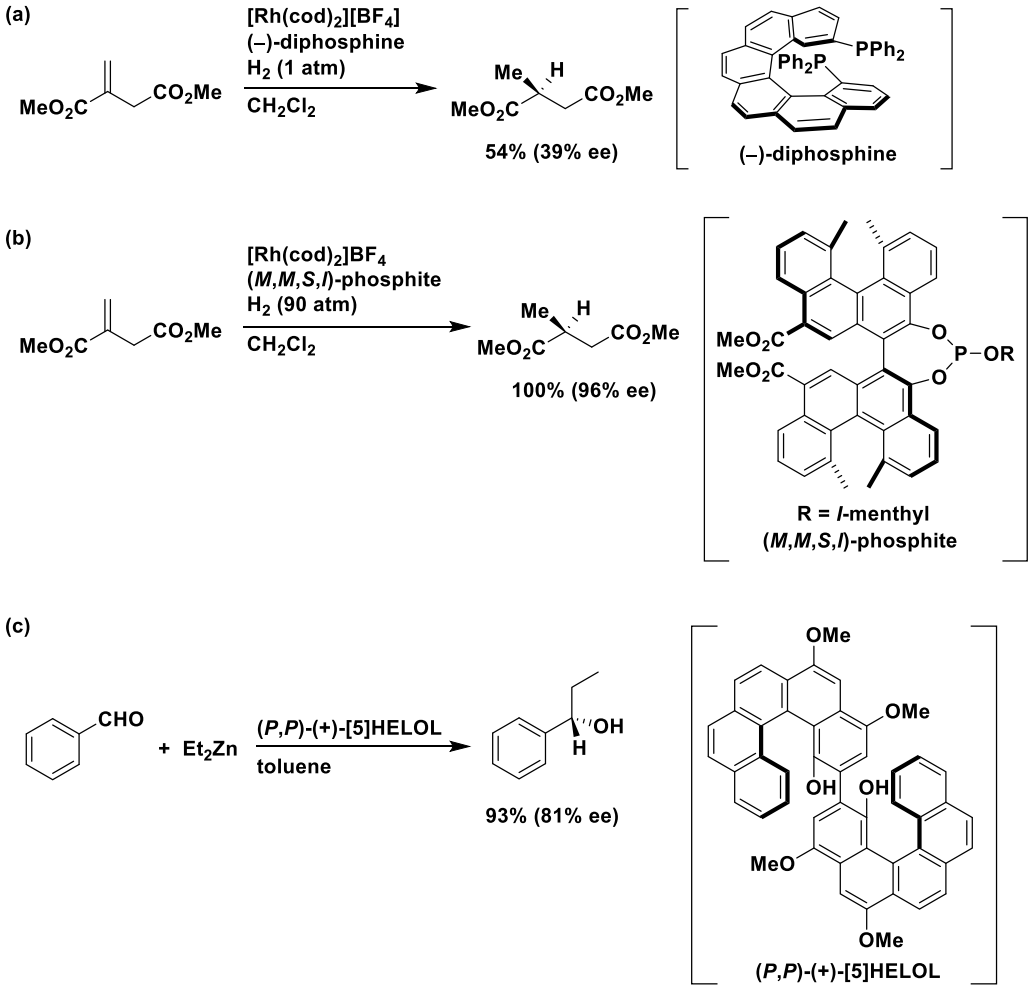

Figure 1.13. Helicene ligands for asymmetric reactions.

Nakazaki and coworkers reported the crown ethers with a helicene moiety.[48,49] When the crown ethers containing the (*M*)-[5]helicene moiety was treated with methyl (±)-phenylyglycinate hydrochloride, it gave the complex with methyl (*S*)-phenylyglycinate more favorably (Figure 1.14). On the other hand, the crown ethers containing the (*M*)-[6]helicene moiety forms the complex with methyl (*R*)-phenylyglycinate more selectively. Therefore, the two crown ethers exhibited the opposite chiral recognition ability although their helicene moieties have the same helicity.

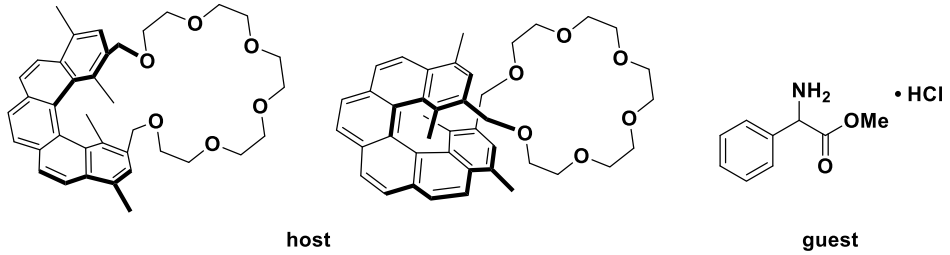

Figure 1.14. Molecular recognition with crown ethers containing a helicene moiety.

The reason for such an opposite chiral recognition ability would be attributed to the difference in helicity of the ether units. According to the CPK molecular models, the (*M*)-[5]helicene moiety induces *P*-helicity in the ether unit, while (*M*)-[6]helicene moiety gives *M*-helicity in the ether unit.

1.3.2. Photoluminescence property

Unsubstituted helicenes with only benzene rings exhibit low fluorescence quantum yield ($\Phi_f \leq 4\%$)[50,51] due to the fast intersystem crossing and a small oscillator strength for the $S_1 \rightarrow S_0$ transition.[52,53] In order to develop helicenes with enhanced fluorescence property, significant research efforts have been devoted until now. One promising approach is introduction of substituents on carbohelicene cores. By introducing electron-withdrawing groups at the 5- and 10-positions and electron-donating groups at the 2- and 13-positions of [5]helicene, the $S_1 \rightarrow S_0$ transition is allowed, and a large Φ_f is achieved (Figure 1.15a).[54] For [7]helicene, the $S_1 \rightarrow S_0$ transition also changes depending on the position of the functional groups (Figure 1.15b).[55] Another promising approach is replacement of at least one benzene ring in carbohalicenes with five-membered ring(s), such as cyclopentadiene and heteroles, giving heterohelicenes and

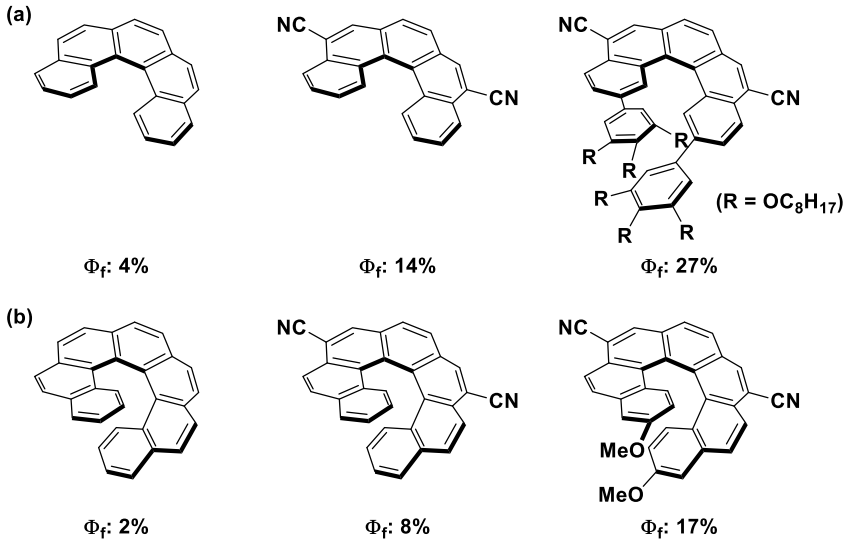

Figure 1.15. Enhanced fluorescence properties by introducing functional groups on carbohelicenes.

helicene-like compounds. Hasobe and coworkers reported the synthesis and properties of the tetrathia[9]helicene and its oxidized derivative with four sulfone groups (Figure 1.16).[56] The tetrathia[9]helicene showed low fluorescence quantum yield (3%), while its sulfone derivative exhibited high fluorescence quantum yield of 27%. This enhancement would be attributed to effective suppression of intersystem crossing pathways. It is well known that the net rate constant of intersystem crossing is generally affected by the energy gap (ΔE_{ST}) between the lowest singlet and triplet excited states. The ΔE_{ST} of the sulfone derivative (1.02 eV) is much larger than that of its parent

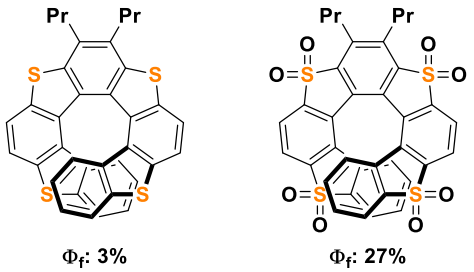

Figure 1.16. Thia[9]helicene and its sulfone derivative.

tetrathia[9]helicene (0.60 eV). This result indicates that the helicene with sulfone unit(s) in their helical skeleton possesses a large ΔE_{ST} and can suppresses the corresponding intersystem crossing pathways, achieving a high fluorescence quantum yield.

The silole-fused [7]helicene-like compound mentioned above (Figure 1.9b) also shows much higher fluorescence quantum yield (23%)[35] than carbo[7]helicene (2%)[50] in solution (Figure 1.17). Moreover, its quantum yield in the solid state (17%) is high among helicenes and helicene-like compounds. Nozaki and coworkers also reported that cyclopentadiene-fused [7]helicene-like compounds exhibits high fluorescence quantum yields (up to 40%).[36] Similarly, the cyclopentadiene-fused [7]helicene-like compounds with triphenylene moieties reported by Tanaka and coworkers shows the same level of fluorescence quantum yield (up to 32%).[38]

These helicene-like compounds exhibit circularly polarized luminescence (CPL). CPL has attracted growing interest because it can be applied to display devices, sensors, data storage, biological probes, and so on.[57,58] Therefore, numerous research efforts have been devoted to the development of circularly polarized luminescent organic materials. The crucial parameter of CPL is the luminescence dissymmetry factor, g_{lum},

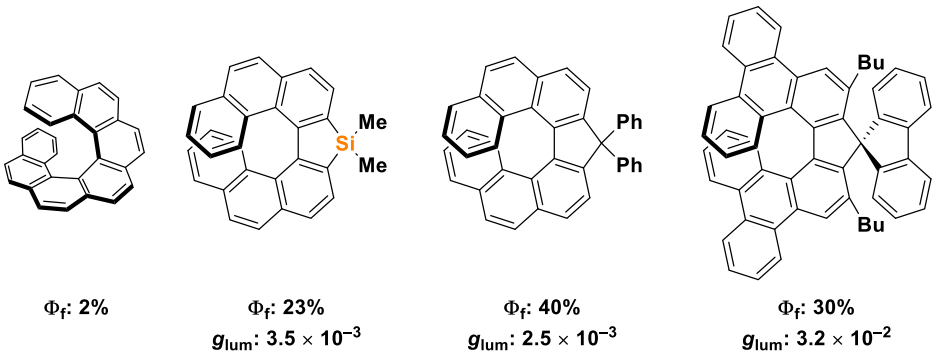

Figure 1.17. Fluorescence and CPL properties of [7]helicene and [7]helicene-like compounds.

which is defined as $g_{lum} = 2(I_L-I_R)/(I_L+I_R)$ (where I_L and I_R are the luminescence intensities of left- and right-handed circularly polarized light).[59] This value indicates the degree of polarization of CPL. The g_{lum} value of the enantiopure silole-fused [7]helicene-like compound was determined to be 3.5×10^{-3} at 470 nm (Figure 1.17),[35] and those of cyclopentadiene-fused [7]helicene-like compounds reported by Nozaki and Tanaka were 2.5×10^{-3} and 3.2×10^{-2}, respectively.[36,38]

1.3.3. Helicene aggregates and helicene oligomers

Molecular assemblies toward any organized aggregates or polymers are important approach to develop functional materials with novel properties. There have been some reports on aggregates of helicenes and helicene-like compounds. A single enantiomer of helicenes or helicene-like compounds forms a columnar structure, exhibiting significant chiroptical properties compared to those from a single molecule. Therefore, self-assembly approach has been considered as an important strategy to develop helicene-based chiral materials.

Katz and coworkers reported the synthesis of helicenebisquinones and their supramolecular organization.[60,61] The non-racemic form of the helicenebisquinones organizes into long fibers which is clearly visible by an optical microscope (Figure 1.18a). The fibers are indicated to consist of columnar aggregates of the helicenebisquinones. This fibrous aggregates of helicenebisquinones exhibited a very intense circular dichroism (CD) response, a large optical rotation, and a large second-order nonlinear optical response than a single helicenebisquinone molecule.

Tanaka and coworkers reported the nanowire composed of the helicene-like

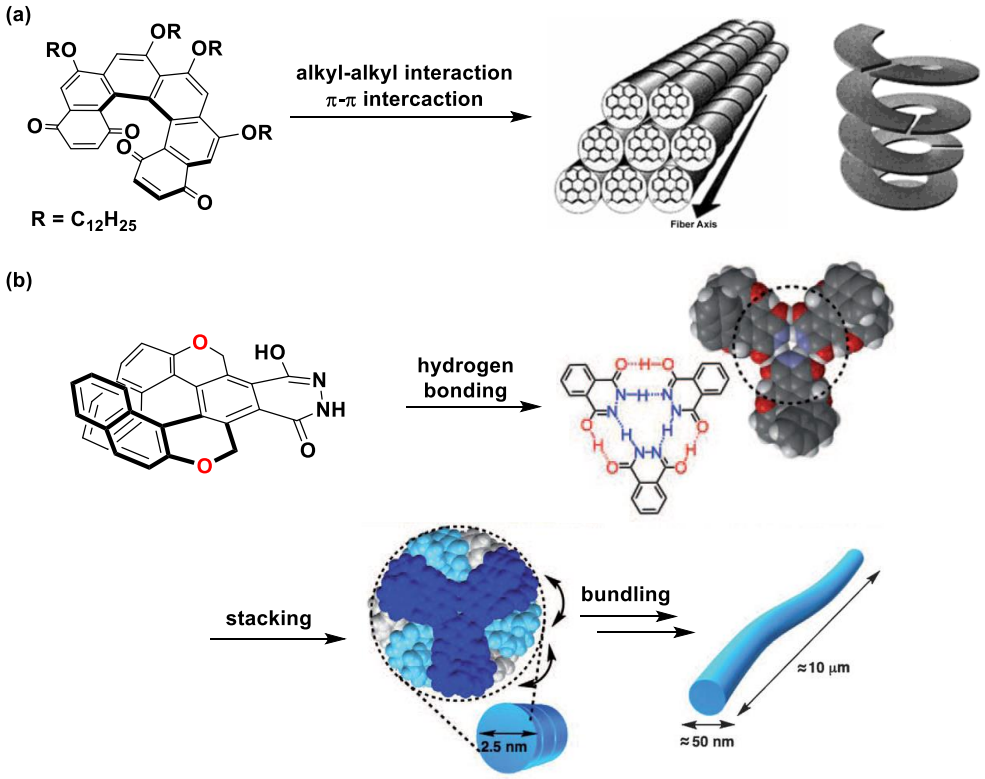

Figure 1.18. Aggregates of helicene-like compounds.

compound (Figure 1.18b).[62] The helicene-like compound has a phthalhydrazide moiety which enable the helicene-like compound to form a trimeric disk structure. The trimeric disks self-assemble to form the fibrous structure and are twisted with each other in the fibrous structure due to the complementary interaction between the helical moieties. The resulting fibrous material exhibits superior CPL properties with a g_{lum} value of -3.5×10^{-2} at the CPL signal maximum.

The polymers and oligomers with helicene moieties have also been investigated. Yashima and coworkers reported the synthesis of the polyacethylene with [6]helicene units as side groups by Rh-catalyzed polymerization (Figure 1.19a).[63] The CD analysis revealed that the polyacetylene main chain of the resulting oligomers forms a one-handed

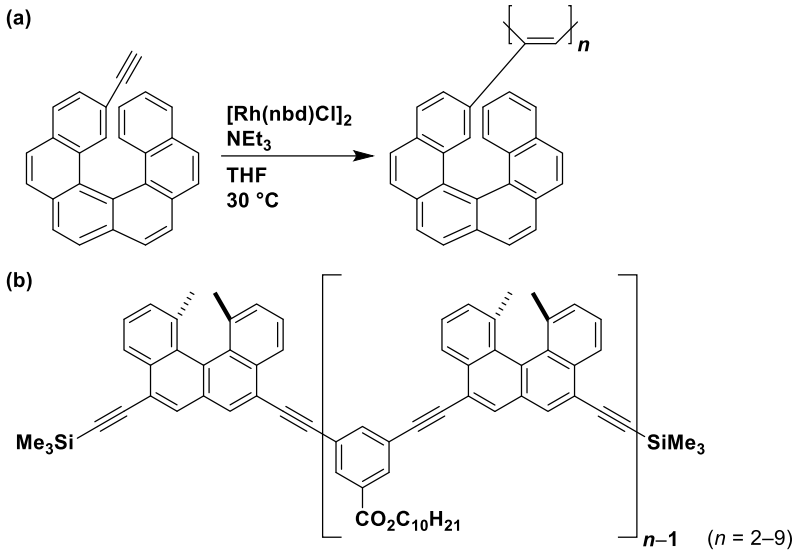

Figure 1.19. Helicene oligomers.

helical conformation induced by the pendant enantiopure [6]helicene units.

Yamaguchi and coworkers reported the synthesis and unique structure of the oligomers containing the twisted benzo[*c*]phenanthrene units (The twisted benzo[*c*]phenanthrene unit is named as helicene in the literature although it consists of only four benzene rings).[64] They synthesized a series of oligomers containing two to nine (*P*)-benzo[*c*]phenanthrene units (Figure 1.19b). In CD spectra, the oligomers containing two to six benzo[*c*]phenanthrene units show a monotonic increase in Δε in accordance with the number of benzo[*c*]phenanthrene units. On the other hand, the oligomers containing seven to nine benzo[*c*]phenanthrene units show significant increase in Δε compared to the others. This result is attributed to the formation of higher-ordered helical structure. Further analysis revealed that two oligomers participate in the formation of a higher-ordered helical structure. In addition, the thermal switching between the helix dimer and two random coil oligomers was observed.[65]

1.4. Summary

As briefly described in this chapter, a variety of synthetic methodologies for helicenes and helicene-like compounds have been developed. With the progress in the synthetic methodologies, various types of helicenes and helicene-like compounds have been synthesized and it has been revealed that they demonstrate unique and novel properties. The number and the type of fused rings have significant impact on their properties. Therefore, in order to develop helicene-based organic functional materials, it is important to elucidate the relationship between molecular structures and their properties. For that reason, there is still a tremendous need for developing more diversity-oriented synthetic methodologies.

Based on these backgrounds, the author has developed new synthetic routes to helicenes and helicene-like compounds. The key concept is the late-stage diversification starting from a common synthetic precursor. In particular, the author focused on the reaction of the biaryl dianions with carbon- or heteroatom-centered dielectrophiles to form the corresponding diareno-fused five-membered rings (Figure 1.20). By changing the dielectrophiles, a series of helicenes and helicene-like

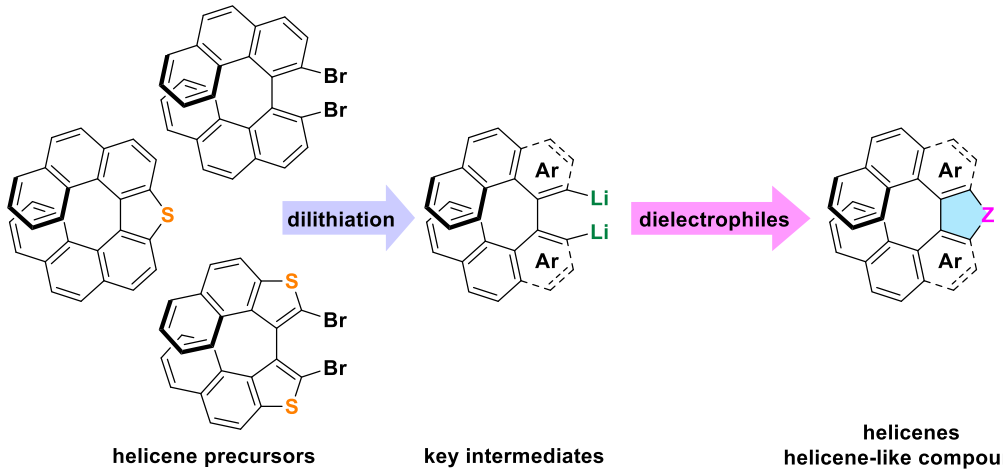

Figure 1.20. Diversity-oriented synthesis of helicenes and helicene-like compounds.

compounds with a different five-membered ring can be prepared. Therefore, this methodology enables the systematic and diversity-oriented synthesis of helicenes and helicene-like compounds.

In Chapter 2, the convenient synthesis of [7]helicenes and [7]helicene-like compounds composed of two phenanthrene units and one five-membered ring is described. The author first focused on 3,3'-dibromo-4,4'-biphenanthrene as a precursor for the dianion species and successfully synthesized it, while its synthesis required lengthy multistep sequence. The author also focused on thia[7]helicene as a common precursor and achieved its transformation to [7]helicene-like compounds via desulfurative dilithiation and the subsequent trapping with dielectrophiles (Figure 1.21). In addition, thia[7]helicene *S*,*S*-dioxide was successfully transformed to the cyclopentadiene-fused [7]helicene-like compound and aza[7]helicenes.

In Chapter 3, the synthesis and properties of spiro-fused double helicene-like compounds with a silicon spiro atom are described. The dianion prepared from 3,3'-dibromo-4,4'-biphenanthrene reacted with $SiCl_4$ to give the spiro-double helicene-like

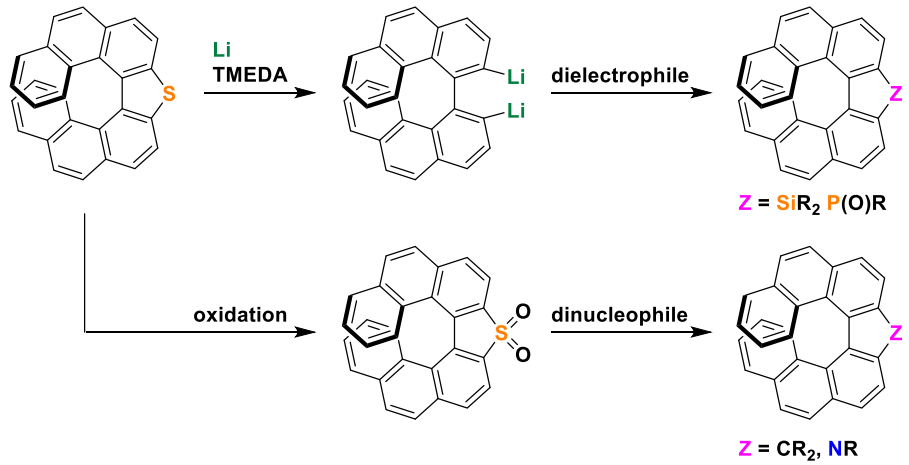

Figure 1.21. Synthesis of helicenes and helicene-like compounds from thia[7]helicene.

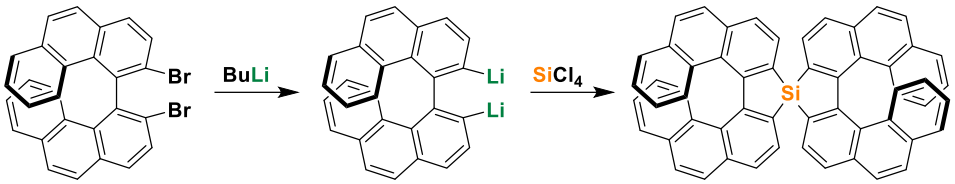

Figure 1.22. Synthesis of the spiro-double helicene-like compound from 3,3'-dibromo-4,4'-biphenanthrene.

compounds (Figure 1.22). The combination of the silicon-centered spiro fusion and the π-extended helical structure were found to offer unique optical properties attributable to the LUMO spiro-conjugation between the two silole-fused [7]helicene-like units.

In Chapter 4, the synthesis of 1,1'-binaphtho[2,1-*b*]thiophene and its transformation to [7]helicenes and [7]helicene-like compounds are described. Lithiation at the α-position of thiophene rings and the following reaction with a variety of electrophiles gave a series of helical compounds (Figure 1.23). The photophysical properties of the synthesized compounds were also evaluated.

General conclusion of this thesis is summarized in Chapter 5.

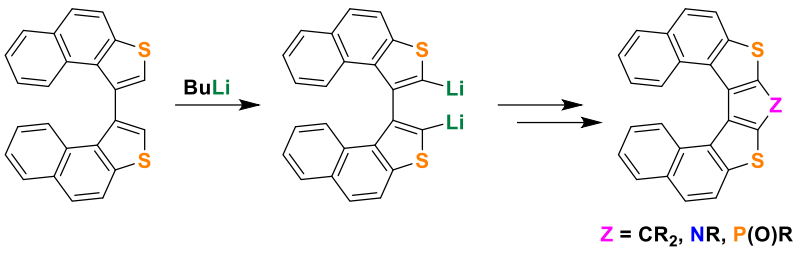

Figure 1.23. Synthesis of helicenes and helicene-like compounds from 1,1'-binaphtho[2,1-*b*]thiophene.

1.5. References

(1) Shen, Y.; Chen, C.F. *Chem. Rev.* **2012**, *112*, 1463–1535.

(2) Gingras, M. *Chem. Soc. Rev.* **2013**, *42*, 968–1006.

(3) Gingras, M.; Félix, G.; Peresutti, R. *Chem. Soc. Rev.* **2013**, *42*, 1007–1050.

(4) Gingras, M. *Chem. Soc. Rev.* **2013**, *42*, 1051–1095.

(5) Moss, G. P.; Smith, P. A. S. *Pure Appl. Chem.* **1995**, *67*, 1307–1375.

(6) Cahn, R. S.; Ingold, C.; Prelog, V. *Angew. Chem. Int. Ed.* **1966**, *5*, 385–415.

(7) Meisenheimer, J.; Witte, K. *Ber. Dtsch. Chem. Ges.* **1903**, *36*, 4153–4164.

(8) Weitzenböck, R.; Klingler, A. *Monatsh. Chem.* **1918**, *39*, 315–323.

(9) Newman, M. S.; Lutz, W. B.; Lednicer, D. *J. Am. Chem. Soc.* **1955**, *77*, 3420–3421.

(10) Flammang-Barbieux. M.; Nasielski, J.; Martin, R. H. *Tetrahedron Lett*. **1967**, *8*, 743–744.

(11) Mori, K.; Murase, T.; Fujita, M. *Angew. Chem. Int. Ed.* **2015**, *54*, 6847–6851.

(12) Moradpour, A.; Nicoud, J. F.; Balavoine, G.; Kagan, H.; Tsoucaris, G. *J. Am. Chem. Soc.* **1971**, *93*, 2353–2354.

(13) Willmore, N. D.; Liu, L. B.; Katz, T. J. *Angew. Chem. Int. Ed.* **1992**, *31*, 1093–1095.

(14) Katz, T. J.; Liu, L. B.; Willmore, N. D.; Fox, J. M.; Rheingold, A. L.; Shi, S. H.; Nuckolls, C.; Rickman, B. H. *J. Am. Chem. Soc.* **1997**, *119*, 10054–10063.

(15) Carreno, M. C.; Hernandez-Sanchez, R.; Mahugo, J.; Urbano, A. *J. Org. Chem.* **1999**, *64*, 1387–1390.

(16) Carreno, M. C.; Garcia-Cerrada, S.; Urbano, A. *Chem. Commun.* **2002**, 1412–1413.

(17) Dreher, S. D.; Weix, D. J.; Katz, T. J. *J. Org. Chem.* **1999**, *64*, 3671–3678.

(18) Phillips, K. E. S.; Katz, T. J.; Jockusch, S.; Lovinger, A. J.; Turro, N. J. *J. Am. Chem. Soc.* **2001**, *123*, 11899–11907.

(19) Ichikawa, J.; Yokota, M.; Kudo, T.; Umezaki, S. *Angew. Chem. Int. Ed.* **2008**, *47*, 4870–4873.

(20) Fuchibe, K.; Jyono, H.; Fujiwara, M.; Kudo, T.; Yokota, M.; Ichikawa, J. *Chem. Eur. J.* **2011**, *17*, 12175–12185.

(21) Pieters, G.; Gaucher, A.; Prim, D.; Marrot, J. *Chem. Commun.* **2009**, 4827–4828.

(22) Morrison, D. J.; Trefz, T. K.; Piers, W. E.; McDonald, R.; Parvez, M. *J. Org. Chem.* **2005**,*70*, 5309–5312.

(23) Dore, A.; Fabbri, D.; Gladialia, S.; Lucchi, O. D. *J. Chem. Soc., Chem. Commun*. **1993**, 1124–1125.

(24) Hoshi, T.; Nakamura, T.; Suzuki, T.; Ando, M.; Hagiwara, H. *Organometallics* **2000**, *19*, 4483–4487.

(25) Yasuike, S.; Iida, T.; Okajima, S.; Yamaguchi, K.; Seki, H.; Kurita, J. *Tetrahedron Lett.* **2001**, *57*, 10047–10053.
(26) Rajca, A.; Miyasaka, M.; Pink, M.; Wang, H.; Rajca, S. *J. Am. Chem. Soc.* **2004**, *126*, 15211–15222.
(27) Miyasaka, M.; Pink, M.; Rajca, S.; Rajca, A. *Angew. Chem. Int. Ed.* **2009**, *48*, 5954 –5957.
(28) Stará, I. G.; Starý, I. *Acc. Chem. Res.* **2020**, *53*, 144–158.
(29) Stará, I. G.; Starý I.; Kollárovič. A.; Teplý, F.; Šaman, D.; Tichý, M. *J. Org. Chem.* **1998**, *63*, 4046–4050.
(30) Sehnal, P.; Stará, I. G.; Šaman, D.; Tichý, M.; Míšek, J.; Cvačka, J.; Rulíšek, L.; Chocholoušová, J.; Vacek, J.; Goryl, G.; Szymonski, M.; Císařová, I.; Starý, I. *Proc. Natl. Acad. Sci. U.S.A.* **2009**, *106*, 13169–13174.
(31) Stará, I. G.; Starý, I.; Kollárovič, A.; Teplý, F.; Vyskočil, Š.; Šaman, D. *Tetrahedron Lett.* **1999**, *40*, 1993–1996.
(32) Tanaka, K.; Kamisawa, A.; Suda, T.; Noguchi, K.; Hirano, M. *J. Am. Chem. Soc.* **2007**, *129*, 12078–12079.
(33) Shibata, Y.; Tanaka, K. *Synthesis* **2012**, 323–350.
(34) Storch, J.; Sýkora, J.; Čermák, J.; Karban, J.; Císařová, I.; Růžička, A. *J. Org. Chem.* **2009**, *74*, 3090–3093.
(35) Oyama, H.; Nakano, K.; Harada, T.; Kuroda, R.; Naito, M.; Nobusawa, K. Nozaki, K. *Org. Lett.* **2013**, *15*, 2104–2107.
(36) Oyama, H.; Akiyama, M.; Nakano, K.; Naito, M.; Nobusawa, K.; Nozaki, K. *Org. Lett.* **2016**, *18*, 3654–3657.
(37) Tanaka, K.; Fukawa, N.; Suda, T.; Noguchi, K. *Angew. Chem. Int. Ed.* **2009**, *48*, 5470–5473.
(38) Sawada, Y.; Furumi, S.; Takai, A.; Takeuchi, M.; Noguchi, K.; Tanaka, K. *J. Am. Chem. Soc.* **2012**, *134*, 4080–4083.
(39) Collins, S. K.; Grandbois, A.; Vachon, M. P.; Cote, J. *Angew. Chem. Int. Ed.* **2006**, *45*, 2923–2926.
(40) Grandbois, A.; Collins, S. K. *Chem. Eur. J.* **2008**, *14*, 9323–9329.
(41) Nozaki, K.; Takahashi, K.; Nakano, K.; Hiyama, T.; Tang, H.; Fujiki, M.; Yamaguchi, S.; Tamao, K. *Angew. Chem. Int. Ed.* **2003**, *42*, 2051–2053.
(42) Kuwahara, A.; Nakano, K.; Nozaki, K. *J. Org. Chem.* **2005**, *70*, 413–419.
(43) Nakano, K.; Hidehira, Y.; Takahashi, K.; Hiyama, T.; Nozaki, K. *Angew. Chem. Int. Ed.* **2005**, *44*, 7136–7138.
(44) Nakano, K.; Oyama, H.; Nishimura, Y.; Nakasako, S.; Nozaki, K. *Angew. Chem. Int.*

Ed. **2012**, *51*, 695–699.
(45) Reetz, M. T.; Beuttenmiiller, E. W.; Goddard, R. *Tetrahedron Lett.* **1997**, *38*, 3211–3214.
(46) Nakano, D.; Yamaguchi, M. *Tetrahedron Lett.* **2003**, *44*, 4969–4971.
(47) Dreher, S. D.; Katz, T. J.; Lam, K.; Rheingold, A. L. *J. Org. Chem.* **2000**, *65*, 815–822.
(48) Nakazaki, M.; Yamamoto, K.; Ikeda, T.; Kitsuki, T.; Okamoto, Y. *J. Chem. Soc., Chem. Commun.* **1983**, 787–788.
(49) Yamamoto, K.; Ikeda, T.; Kitsuki, T.; Okamoto, Y.; Chikamatsu, H.; Nakazaki, M. *J. Chem. Soc. Perkin Trans.* **1990**, 271-276.
(50) Vander Donckt, E.; Nasielski, J.; Greenleaf, J. R.; Birks, J. B. *Chem. Phys. Lett.* **1968**, *2*, 409–410.
(51) Birks, J. B.; Birch, D. J. S.; Cordemans, E.; Vander Donckt, E. *Chem. Phys. Lett.* **1976**, *43*, 33–36.
(52) Sapir, M.; Donckt, E. V. *Chem. Phys. Lett.* **1975**, *36*, 108–110.
(53) Kubo, H.; Hirose, T.; Matsuda, K. *Org. Lett.* **2017**, *19*, 1776–1779.
(54) Kubo, H.; Hirose, T.; Shimizu, D.; Matsuda, K. *Chem. Lett.* **2021** *50*, 804–807.
(55) Kubo, H.; Hirose, T.; Nakashima, T.; Kawai, T.; Hasegawa, J.; Matsuda, K. *J. Phys. Chem. Lett.* **2021**, *12*, 686–695.
(56) Yamamoto, Y.; Sakai, H.; Yuasa, J.; Araki, Y.; Wada, T.; Sakanoue, T. Takenobu, T.; Kawai, T.; Hasobe, T. *J. Phys. Chem. C* **2016**, *120*, 7421–7427.
(57) Sánchez-Carnerero, E. M.; Agarrabeitia, A. R.; Moreno, F.; Maroto, B. L.; Muller, G.; Ortiz, M. J.; De La Moya, S. *Chem. Eur. J.* **2015**, *21*, 13488–13500.
(58) Tanaka, H.; Inoue, Y.; Mori, T. *ChemPhotoChem* **2018**, *2*, 386–402.
(59) Riehl, J. P.; Richardson, F. S. *Chem. Rev.* **1986**, *86*, 1–16.
(60) Verbiest, T.; Elshocht, S. V.; Kauranen, M.; Hellemans, L.; Snauwaert, J.; Nuckolls, C.; Katz, T. J.; Persoons, A. *Science*, **1998**, *282*, 913–915.
(61) Lovinger, A. J.; Nuckolls, C.; Katz, T. J. *J. Am. Chem. Soc*. **1998**, *120*, 264–268.
(62) Kaseyama, T.; Furumi, S.; Zhang, X.; Tanaka, K.; Takeuchi, M. *Angew. Chem. Int. Ed.* **2011**, *50*, 3684–3687.
(63) Anger, E.; Iida, H.; Yamaguchi, T.; Hayashi, K.; Kumano, K.; Crassous, J.; Vanthuyne, N.; Rousselc. C.; Yashima, E. *Polym. Chem.* **2014**, *5*, 4909–4914.
(64) Sugiura, H.; Nigorikawa, Y.; Saiki, Y.; Nakamura, K.; Yamaguchi, M. *J. Am. Chem. Soc.* **2004**, *126*, 14858–14864.
(65) Sugiura, H.; Yamaguchi, M. *Chem. Lett.* **2007**, *36*, 58–59.

Chapter 2

Transformation of Thia[7]helicene to Aza[7]helicenes and [7]Helicene-like Compounds via Aromatic Metamorphosis

The [7]helicenes and [7]helicene-like compounds were successfully synthesized from the thia[7]helicene as a common precursor. The silole- and phosphole-fused [7]helicene-like compounds were synthesized by desulfurative dilithiation of thia[7]helicene and the subsequent reaction with silicon and phosphorus dielectrophiles, respectively. The cyclopentadiene-fused [7]helicene-like compound and the aza[7]helicenes were also synthesized by the inter/intra-S_NAr reaction between the thia[7]helicene *S*,*S*-dioxide and the carbon and nitrogen dinucleophiles, respectively. The thia[7]helicene *S*,*S*-dioxide and the silole-fused [7]helicene-like compound emitted bright blue light, while the cyclopentadiene-fused [7]helicene-like compound and the aza[7]helicenes emitted violet light. Aza[7]helicene single enantiomers exhibited circularly polarized luminescence with dissymmetry factors of 4.2–4.4 × 10^{-3}. 3,3'-Dibromo-4,4'-biphenanthrene was also prepared as a promising precursor for synthesizing [7]helicenes and [7]helicene-like compounds.

2.1. Introduction

Dibenzoheteroles[1] (dibenzothiophene, carbazole, dibenzosilole, etc.) and spirocyclic fluorenes (spiro[fluorene-9,9'-xanthene], etc.) have been important modules for organic functional materials because they showed excellent electronic, optoelectronic, and emission properties, which offers them applications in a variety of fields, such as light-emitting diodes and organic field-effect transistors.[2–5] Until now, a variety of synthetic methodologies have been developed for each class of dibenzoheteroles and spirocyclic fluorenes. For example, carbazoles can be prepared through Fischer–Borsche synthesis,[6] Cadgan cyclization of nitrobiaryls,[7] palladium-catalyzed double *N*-arylation reaction of dihalobiaryls,[8] transition metal-free intramolecular oxidative C–H amination of aminobiaryls with hypervalent iodine reagents,[9] and so on (Figure 2.1a). The classical yet practical synthetic route to dibenzosiloles is the lithiation of dihalobiaryls and the subsequent reaction of the resulting dianions with a silicon dielectrophile such as dichlorodiorganosilane (Figure 2.1b).[10] Transition metal-catalyzed cyclization and radical cyclization pathways have also been developed for the dibenzosilole synthesis.[11,12] Undoubtedly, the development of the synthetic methodology has greatly contributed to a recent progress in the fields of organic chemistry and organic materials chemistry.

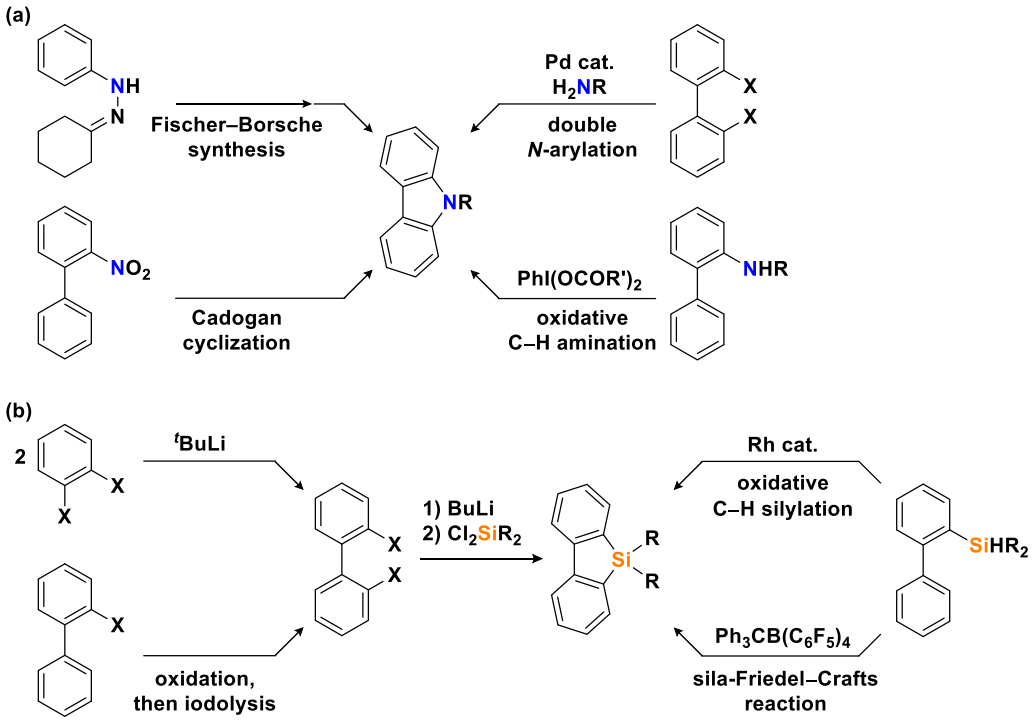

Figure 2.1. Synthetic routes to carbazoles and dibenzosiloles.

Recently, it has been reported that the dibenzothiophene skeleton can be transformed into various ring systems such as dibenzosilole, dibenzophosphole, fluorene, and carbazole (Figure 2.2).[13–17] The reaction of dibenzothiophene with lithium metal generates 2,2'-dianions via desulfurative dilithiation. Then, the dibenzosiloles and dibenzophospholes are obtained by the reaction of the generated 2,2'-dianion with silicon and phosphorus dielectrophiles, respectively. Fluorenes and carbazoles are successfully synthesized from the oxidized compound of dibenzothiophene. The oxidized compound, dibenzothiophene *S*,*S*-dioxide, is converted to fluorenes and carbazoles via successive intermolecular and intramolecular S_NAr reactions with carbon and nitrogen dinucleophiles. As many compounds containing the dibenzothiophene unit have been reported, this methodology, named "aromatic metamorphosis", would be a useful

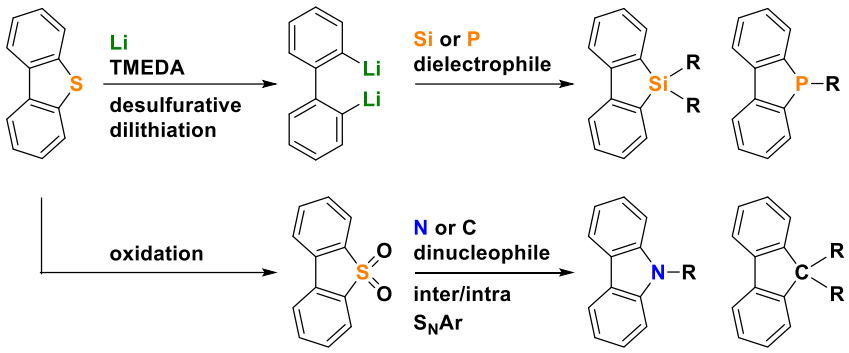

Figure 2.2. Aromatic metamorphosis of dibenzothiophene.

synthetic approach for the synthesis of a variety of π-extended compounds. In fact, the conversion of dithia[8]helicene to its carbazole and fluorene analogues has been reported using this method as well as the synthesis of [8]circulenes and spiro π-conjugated compounds.[18–21]

In this context, the author envisaged that a series of silole-, phosphole-, and cyclopentadiene-fused [7]helicene-like compounds and pyrrole-fused aza[7]helicenes are possible to be synthesized from (i) 3,3'-dibromo-4,4'-biphenanthrene (**1**)[22] (Figure 2.3) or (ii) thia[7]helicene **7**, diphenanthro[3,4-*b*:4',3'-*d*]thiophene (Figure 2.4),[23,24] as a common precursor.

The halogen–lithium exchange reaction of **1** with an organolithium reagent would give the corresponding dianion **2**. Then, the reaction of the resulting dianion **2** with silicon (Cl_2SiR_2), phosphorus (Cl_2PR), and carbon ($ClCO_2Me$) dielectrophiles is expected to afford the silole-, phosphole-, and cyclopentadienone-fused [7]helicene-like compounds **3**–**5**, respectively. Aza[7]helicenes **6** would also be synthesized by the double *N*-arylation of **1** with a primary amine.

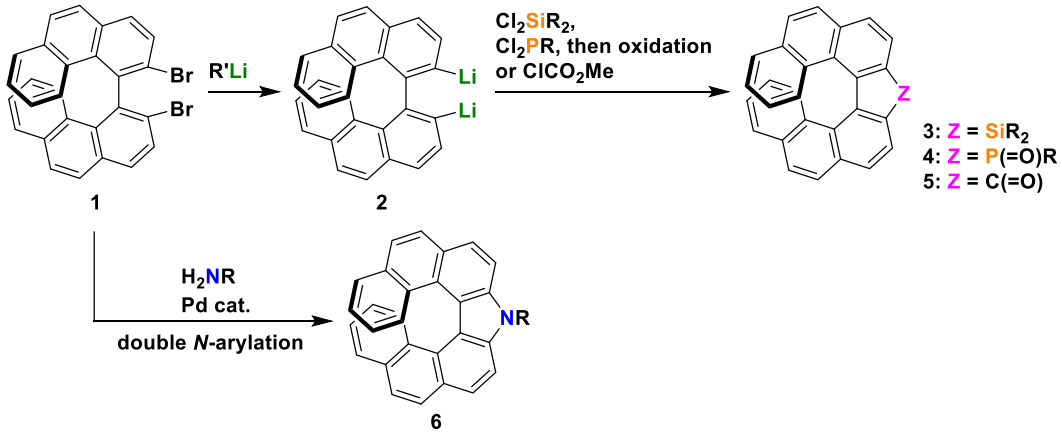

Figure 2.3. Possible synthetic routes to [7]helicenes and [7]helicene-like compounds from 3,3'-dibromo-4,4'-biphenanthrene (**1**).

When thia[7]helicene **7** is used as a common precursor, the dianion **2** would be prepared by desulfurative dilithiation of thia[7]helicene **7** and react with silicon (Cl_2SiR_2), phosphorus (Cl_2PR), and carbon ($ClCO_2Me$) dielectrophiles to afford the corresponding [7]helicene-like compounds **3**–**5**. In addition, it is possible to produce aza[7]helicenes **6** and cyclopentadiene-fused [7]helicene-like compounds **9** by the reaction of thia[7]helicene *S*,*S*-dioxide **8** with the nitrogen and carbon dinucleophiles, respectively.

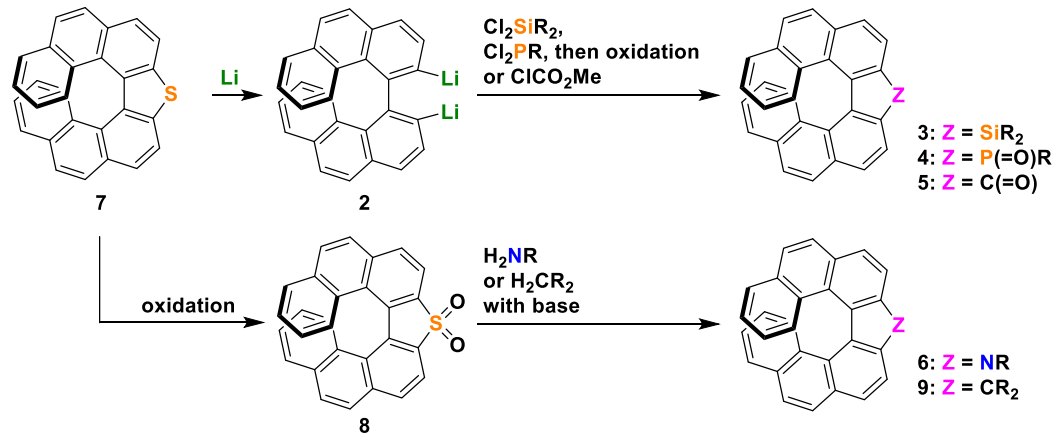

Figure 2.4. Possible synthetic routes to [7]helicenes and [7]helicene-like compounds from thia[7]helicene **7**.

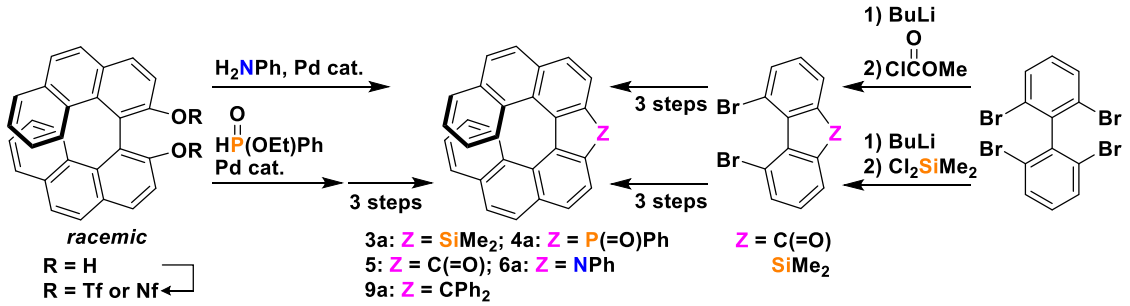

Figure 2.5. Aromatic metamorphosis of dibenzothiophene.

The synthesis of silole-, phosphole-, cyclopentadienone-, and cyclopentadiene-fused [7]helicene-like compounds **3a**, **4a**, **5**, and **9a** and the aza[7]helicene **6a** has already been reported (Figure 2.5),[25–28] but the proposed synthetic routes in Figures 2.3 and 2.4 could allow more efficient synthesis. In the previous literatures, [7]helicene-like compounds **3a**, **4a**, **5**, and **9a** require the introduction of each heteroatom and the bridging carbon atom at the early stage in the synthetic sequence. In contrast, the proposed synthetic routes allow the introduction of each heteroatom and the bridging carbon atom at the late stage of the synthetic sequences. Furthermore, the proposed synthetic routes employ no transition metal catalyst, while the previous syntheses need to use costly transition metal catalysts in the cyclization steps.

In this chapter, the author investigated the synthesis of 3,3'-dibromo-4,4'-biphenanthrene (**1**). Although compound **1** was successfully synthesized, the synthesis required the lengthy multistep sequence. Therefore, aromatic metamorphosis of thia[7]helicene **7** was applied to the synthesis of [7]helicenes and [7]helicene-like compounds. The optical properties of the synthesized compounds were evaluated and compared with those of the related compounds in the previous literatures.

2.2. Synthesis

2.2.1. Synthesis of 3,3'-dibromo-4,4'-biphenanthrene

It has been reported that 3,3'-dibromo-4,4'-biphenanthrene (**1**) can be prepared by a one-step bromination of [4,4'-biphenanthrene]-3,3'-diol.[22] The author tried its preparation according to the literature, but fail to obtained it most likely due to the difficulty of controlling the high temperature condition (230–250 °C). Therefore, the new synthetic route was designed as shown in Scheme 2.1. The biphenyl **10**, which was synthesized in 81% yield by the Suzuki–Miyaura cross-coupling reaction of 2,6-dimethoxyphenylboronic acid and iodobenzene, was treated with BBr_3. One of the methoxy groups was dealkylated to give compound **11** in 73% yield. The hydroxy group in compound **11** was converted to a triflate group to give compound **12**. Then, the Miyaura–Ishiyama borylation reaction with the resulting triflate **12** and pinacol borane in the presence of a palladium catalyst gave the borylated compound **13** in 94% yield. The Suzuki–Miyaura cross-coupling of compounds **12** and **13** with $Pd(PPh_3)_4$ afforded compound **14** in 87% yield. The resulting compound **14** was treated with bromine, and the following reaction with an excess amount of BBr_3 gave compound *rac*-**16** in 62% yield (in 2 steps). The hydroxy groups of *rac*-**16** was triflated with Tf_2O to give compound *rac*-**17** in 74% yield. The triflate groups of *rac*-**17** was selectively converted to (trimethylsilyl)ethynyl groups to give compound *rac*-**18** in 77% yield. Deprotection (92% yield) and the following $PtCl_2$-catalyzed double cyclization (38% yield) gave the target compound **1**. Although compound **1** can be synthesized in a pure form, this synthetic sequence requires 10 steps and the total yield is about 6%. Therefore, the author concluded that compound **1** is not a suitable precursor for diversity-oriented synthesis of [7]helicenes and [7]helicene-like compounds in this thesis.[29]

Scheme 2.1. Synthesis of 3,3'-Dibromo-4,4'-biphenanthrene (**1**)

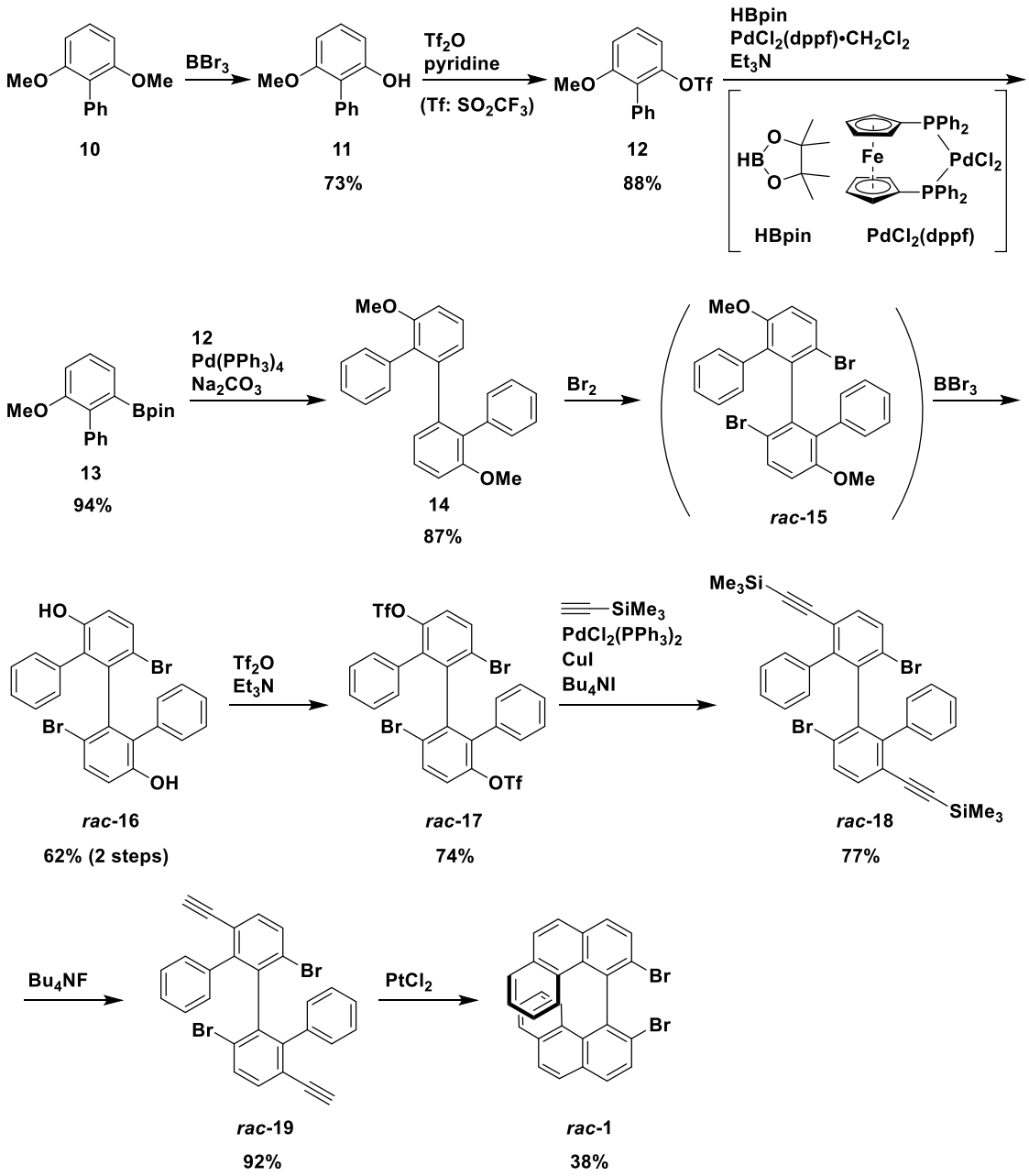

2.2.2. Aromatic metamorphosis of thia[7]helicene

Next, the aromatic metamorphosis approach shown in Figure 2.4 was investigated. The desulfurative dilithiation of thia[7]helicene **7** by lithium metal has already been

discussed.[24] In the previous report, the trapping with MeI after the desulfurative dilithiation gave not the desired methylated compound, but the reduced compound, 4,4'-biphenanthrene, as the main product. Nevertheless, based on the recent progress in aromatic metamorphosis,[17] the reaction of compound **7** with lithium metal was carried out under the optimized conditions reported for the desulfurative dilithiation of dibenzothiophene. The reaction of **7** with 5 equivalents of lithium metal in the presence of 2 equivalents of *N*,*N*,*N*',*N*'-tetramethylethylenediamine (TMEDA) in THF was carried out at room temperature (Scheme 2.2). Then, the silicon dielectrophile, Cl_2SiMe_2, was added to the resulting dark purple solution to give the desired product **3a** in 48% yield. This result clearly demonstrates that the desulfurative dilithiation of thia[7]helicene **7** gives the dianion **2** which can react with dielectrophiles. Encouraged by this result, other dielectrophiles were tested for trapping the dianion species. The reaction with Cl_2SiPh_2 under the same conditions gave the new silole-fused [7]helicene-like compound **3b** in 41% yield. It was also found that phosphorus dielectrophiles could be applied. The reaction of the dianion with Cl_2PPh followed by oxidation afforded the phosphole-fused [7]helicene-like compound **4a**.

Scheme 2.2. Synthesis of Compounds **3** and **4a**

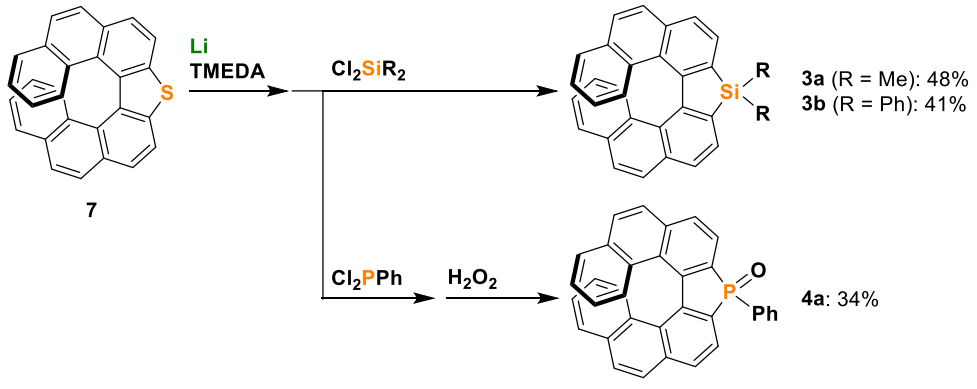

Scheme 2.3. Synthesis of Compounds **9b** and **6**

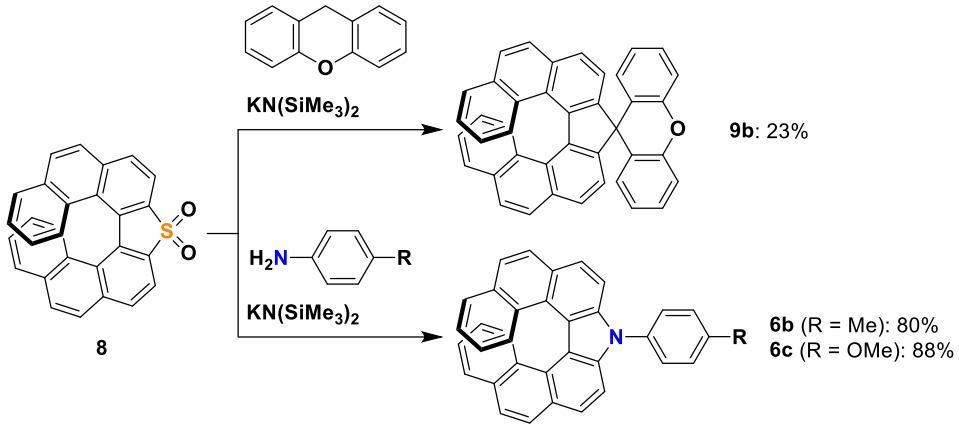

The transformation of thia[7]helicene *S*,*S*-dioxide **8**, which can be prepared by oxidation of **7**, was also investigated (Scheme 2.3). According to the literature procedure,[15] the reaction of **8** with xanthene, a commercially available carbon dinucleophile, was carried out with $KN(SiMe_3)_2$ as a base. The desired spirocyclic carbo[7]helicene-like compound **9b** was obtained in 23% yield. In the same way, the conversion of **8** to aza[7]helicenes **6** was examined. Arylamines bearing an electron-donating group, such as *p*-toluidine and *p*-anisidine, reacted with **8** to give the corresponding aza[7]helicenes **6b** and **6c** in high yields, respectively (80% for **6b** and 88% for **6c**). In contrast, aza[7]helicenes were not formed in reactions with electron-deficient arylamines, such as *p*-(trifluoromethyl)aniline and 4-aminobenzonitrile. This result is caused by low nucleophilicity of these arylamines.[13]

2.2.3. Optical resolution of aza[7]helicenes

The optical resolution of aza[7]helicenes **6b** and **6c** by chiral HPLC was achieved. Moreover, the absolute configuration of the single enantiomer of **6c** was clearly identified by single crystal X-ray analysis (Figure 2.6 and Table 2.1). The practical condition for the optical resolution of other newly synthesized [7]helicene-like compounds has not been obtaiend yet.

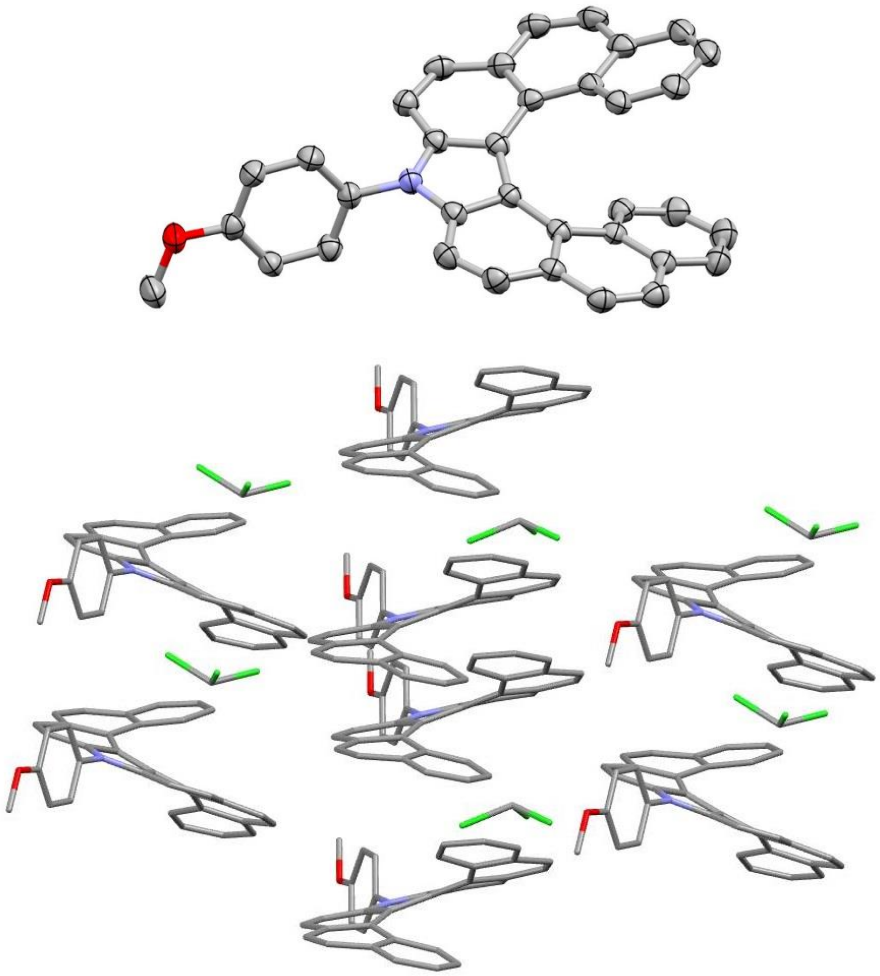

Figure 2.6. ORTEP drawing of (*M*)-**6c** with thermal ellipsoids at 50% probability [All hydrogen atoms and the crystal solvent molecule ($CHCl_3$) are omitted for clarity] and its packing structure.

Table 2.1. Crystallographic Data and Structure Refinement Details for (*M*)-**6c**

formula	$(C_{35}H_{23}NO)\bullet(CHCl_3)$	
formula weight	592.91	
temperature	193(2) K	
wavelength	1.54187 Å	
crystal system	monoclinic	
space group	$P2_1$	
unit cell dimensions	a = 8.25287(15) Å	α = 90°
	b = 18.2292(3) Å	β =110.7590(8)°
	c = 10.12564(18) Å	γ = 90°
volume	1424.44(5) Å^3	
Z	2	
density (calculated)	1.382 g/cm^3	
absorption coefficient	3.152 mm^{-1}	
F(000)	612	
crystal size	0.60 × 0.40 × 0.10 mm^3	
theta range for data collection	4.670 to 68.238°	
index ranges	–9<=h<=9, –21<=k<=21, –12<=l<=12	
reflections collected	22925	
independent reflections	4954 [R_{int} = 0.0676]	
completeness to theta	99.7%	
max. and min. transmission	0.730 and 0.234	
refinement method	full-matrix least-squares on F^2	
data / restraints / parameters	4954 / 1 / 370	
goodness-of-fit on F^2	1.045	
Flack parameter	0.003(10)	
final R indices [I>2σ(I)]	R_1 = 0.0536, wR_2 = 0.1365	
R indices (all data)	R_1 = 0.0584, wR_2 = 0.1458	
largest diff. peak and hole	0.429 and –0.456 e/Å^3	

2.3. Photophysical properties

2.3.1. Absorption and fluorescence properties

By applying aromatic metamorphosis, new [7]helicene-like compounds **3b** and **9b** and aza[7]helicenes **6b** and **6c** were obtained. Therefore, the UV–vis absorption and photoluminescence (PL) spectra of them were measured to elucidate their optical properties (Figure 2.7). Although thia[7]helicene **7** and its *S*,*S*-dioxide **8** are known compounds, only the absorption property of **7** in cyclohexane has been reported. Therefore, their absorption and PL spectra in CH_2Cl_2 were also measured. The photophysical properties are summarized in Table 2.2. The photophysical data of compounds **3a**, **9a**, and **6a**, which have already been reported, are also included in Table 2.2 as comparison.

Thia[7]helicene **7** exhibits a longest absorption maximum (λ_{abs}) at 401 nm and an emission maximum (λ_{em}) at 417 nm with a shoulder at 435 nm (Figure. 2.7a). The absolute quantum yield (Φ_f) was estimated to be less than 1%. Compared to **7**, the oxidized compound **8** showed a slightly red-shifted absorption band with a shoulder at

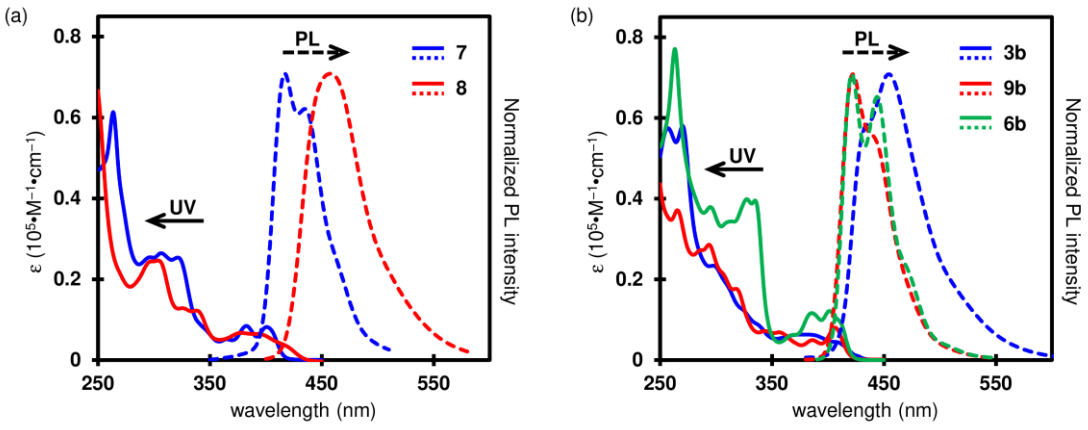

Figure 2.7. UV–vis absorption (solid line) and PL (broken line) spectra of (a) **7** and **8** in CH_2Cl_2 (1.0×10^{-5} M) and (b) **3b**, **9b**, and **6b** in CH_2Cl_2 (1.0×10^{-5} M). The spectra of **6c** are omitted since they are almost the same as those of **6b**.

415 nm and the significantly red-shifted emission maximum at 458 nm. The absolute quantum yield was improved to 4%, and a bright blue emission was observed.

The silole-fused [7]helicene-like compound **3b** showed a broad absorption spectrum with a shoulder at 411 nm and an absorption edge at 434 nm (Figure 2.7b). These characteristics were almost the same as those of the dimethyl derivative **3a** (λ_{abs}: 412 nm; absorption edge: 431 nm).[27] The compound **3b** exhibited a bright blue emission, but with a lower absolute quantum yield (11%) than **3a** (23%).

The UV–vis absorption and PL spectra of the cyclopentadiene-fused [7]helicene-like compound **9b** and aza[7]helicenes **6b** and **6c** were almost the same as those of their analogues **9a** and **6a**, respectively (Figure 2.7b). All of these compounds showed a violet emission at 421–422 nm. Thus, the replacement of the two phenyl groups in **9a** with oxybis(2,1-phenylene) group and the introduction of an electron-donating group at the para-position of the *N*-phenyl group in **6a** have little impact on their photophysical properties.

Table 2.2. Photophysical Properties of [7]Helicene-like Compounds and Aza[7]helicenes

	λ_{abs} (nm)[a]	λ_{em} (nm)[b]	Φ_f[c]
7	401	417, 435 (sh) (265)	< 1
8	395, 415 (sh)	458 (300)	4
3b	389, 411 (sh)	434 (sh), 454 (325)	11
9b	406	422, 441 (sh) (294)	31
6b	401	421, 444 (335)	17
6c	401	422, 445 (335)	16
3a[d]	412	450 (320)	23
9a[e]	408	421, 441 (sh) (340)	40
6a[f]	400	418, 442 (330)	17

[a]The longest absorption maximum in CH_2Cl_2. sh: shoulder. [b]Emission maximum in CH_2Cl_2. Excitation wavelength in parenthesis. [c]Absolute quantum yield in CH_2Cl_2. [d]Reference 27. [e]Reference 28. [f]Reference 25.

2.3.2. Chiroptical properties

The chiroptical properties of **6b** and **6c** were characterized by CD and CPL spectroscopies (Figure 2.8). Both **6b** and **6c** exhibited mirror image CD spectra showing the Cotton effects in the longest absorption region of thier absorption spectrum. The *P*-isomer of **6c** exhibited a negative Cotton effect at its longest absorption band and two positive Cotton effects at around 340 nm and 280 nm. The observed characteristics of the CD spectrum of (*P*)-**6c** are identical to that of (*P*)-**6a** reported previously.[25] Based on these results, the absolute configuration of the single enantiomer of **6b**, which showed a negative Cotton effect at around 410 nm, was determined to be *P*. The dissymmetry factors in absorption (g_{abs}) at the maximum of the first Cotton effects of (*P*)-**6b** and (*P*)-**6c** were estimated to be 3.8×10^{-3} and 4.0×10^{-3}, respectively. In the CPL spectra, the sign of the *P*-isomers of **6b** and **6c** is negative. The dissymmetry factors of the emission (g_{lum}) of (*P*)-**6b** and (*P*)-**6c** were 4.2×10^{-3} (429 nm) and 4.4×10^{-3} (432 nm), respectively, similar to those of previously reported chiral organic small molecules.[30]

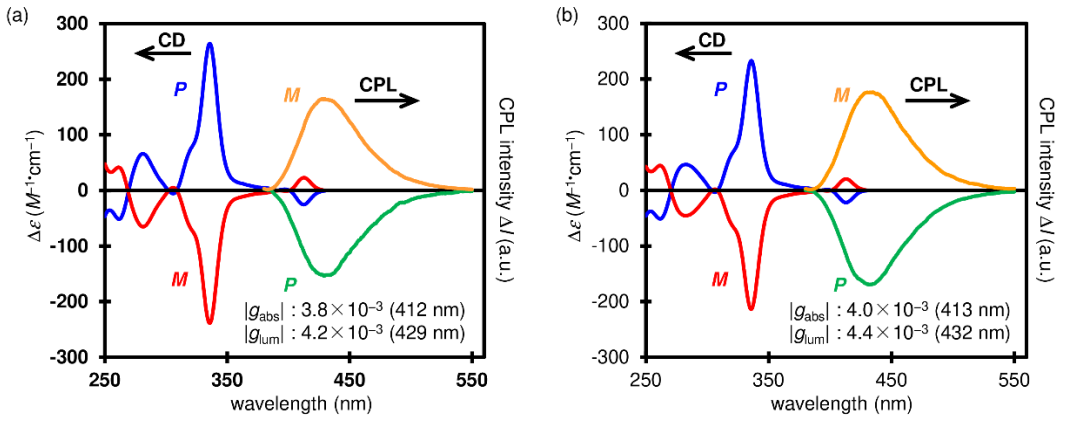

Figure 2.8. CD (in CH_2Cl_2) and CPL (in 2-Me-THF) spectra of (a) **6b** and (b) **6c**. The g_{abs} and g_{lum} values were calculated at the longest CD maximum and the CPL maximum, respectively. Wavelength for the calculated g_{abs} and g_{lum} values in parentheses.

2.4. Theoretical calculations

In order to understand the experimental photophysical properties, theoretical calculations with density functional theory (DFT) and time-dependent (TD) DFT methods were conducted at the B3LYP/6-31G (d) level of theory.

The longest absorption wavelength of thia[7]helicene **7** and its *S*,*S*-dioxide **8** were estimated to be 387 nm and 406 nm, respectively, well demonstrating a slight red shift of the experimental absorption band of **8** (Table 2.3). The energy levels of the HOMO and HOMO–1 of **7** are almost identical (−5.42 eV and −5.45 eV) (Figure 2.8), and the HOMO–1 → LUMO transition mainly contributes to the longest-wavelength absorption band of **7**. On the other hand, the HOMO → LUMO transition is the main contribution to the longest-wavelength absorption band of **8**. The HOMOs of thia[7]helicene **7** and its oxidized compound **8** are delocalized over entire skeltons, while no contribution was observed over the sulfur atoms (Figure 2.9). The HOMO energy level of **8** is 0.40 eV lower than that of **7**, which would be caused by the electron-withdrawing effect of the *S*,*S*-dioxide moiety. The LUMOs of **7** and **8** is delocalized over the entire skeletons including the sulfur atoms. It was observed that the difference in the LUMO energy levels between **7** and **8** (0.62 eV) was larger than that in the HOMO energy levels. The reason for this observation may be due to the effective σ*–π* conjugation between the exocyclic S–O σ* orbital and the endocyclic butadiene π* orbital of the thiophene unit, which lowers the LUMO energy level of **8**.[31]

Table 2.3. The Selected Absorption of (*P*)-**7**, **8**, and **3** Calculated by TD−DFT Method at the B3LYP/6-31G(d) Level of Theory

	excited state	transition energy (eV)	wavelength (nm)	main transition configuration (CI expansion coefficient)	oscillator strength *f*
(*P*)-**7**	1	3.207	387	HOMO−1 → LUMO (0.66493)	0.0251
	2	3.262	380	HOMO → LUMO (0.67382)	0.1264
	3	3.539	350	HOMO−2 → LUMO (0.67854)	0.0331
	4	3.881	320	HOMO−1 →LUMO+1 (0.68263)	0.1434
	5	3.907	317	HOMO−3 → LUMO (0.54000)	0.0094
	6	3.931	315	HOMO → LUMO+1 (0.52264)	0.0303
(*P*)-**8**	1	3.053	406	HOMO → LUMO (0.68689)	0.0714
	2	3.289	377	HOMO−1 → LUMO (0.62341)	0.0373
	3	3.388	366	HOMO−2 → LUMO (0.66097)	0.0319
	4	3.624	342	HOMO → LUMO+1 (0.61182)	0.1261
	5	3.721	333	HOMO−3 → LUMO (0.65739)	0.0000
	6	3.962	313	HOMO → LUMO+2 (0.62412)	0.0862
(*P*)-**3a**	1	3.162	392	HOMO → LUMO (0.68088)	0.1156
	2	3.307	375	HOMO−1 → LUMO (0.54443)	0.0068
	3	3.524	352	HOMO−2 → LUMO (0.54443)	0.0092
	4	3.589	345	HOMO → LUMO+1 (0.52768)	0.0802
	5	3.848	322	HOMO → LUMO+2 (0.45264)	0.0287
	6	3.895	318	HOMO−3 → LUMO (0.47198)	0.0357
(*P*)-**3b**	1	3.133	396	HOMO → LUMO (0.68486)	0.0982
	2	3.276	378	HOMO−1 → LUMO (0.53879)	0.0041
	3	3.510	353	HOMO−2 → LUMO (0.60686)	0.0112
	4	3.553	349	HOMO → LUMO+1 (0.52515)	0.0929
	5	3.824	324	HOMO−3 → LUMO (0.46782)	0.0330
	6	3.872	320	HOMO → LUMO+2 (0.45741)	0.0586

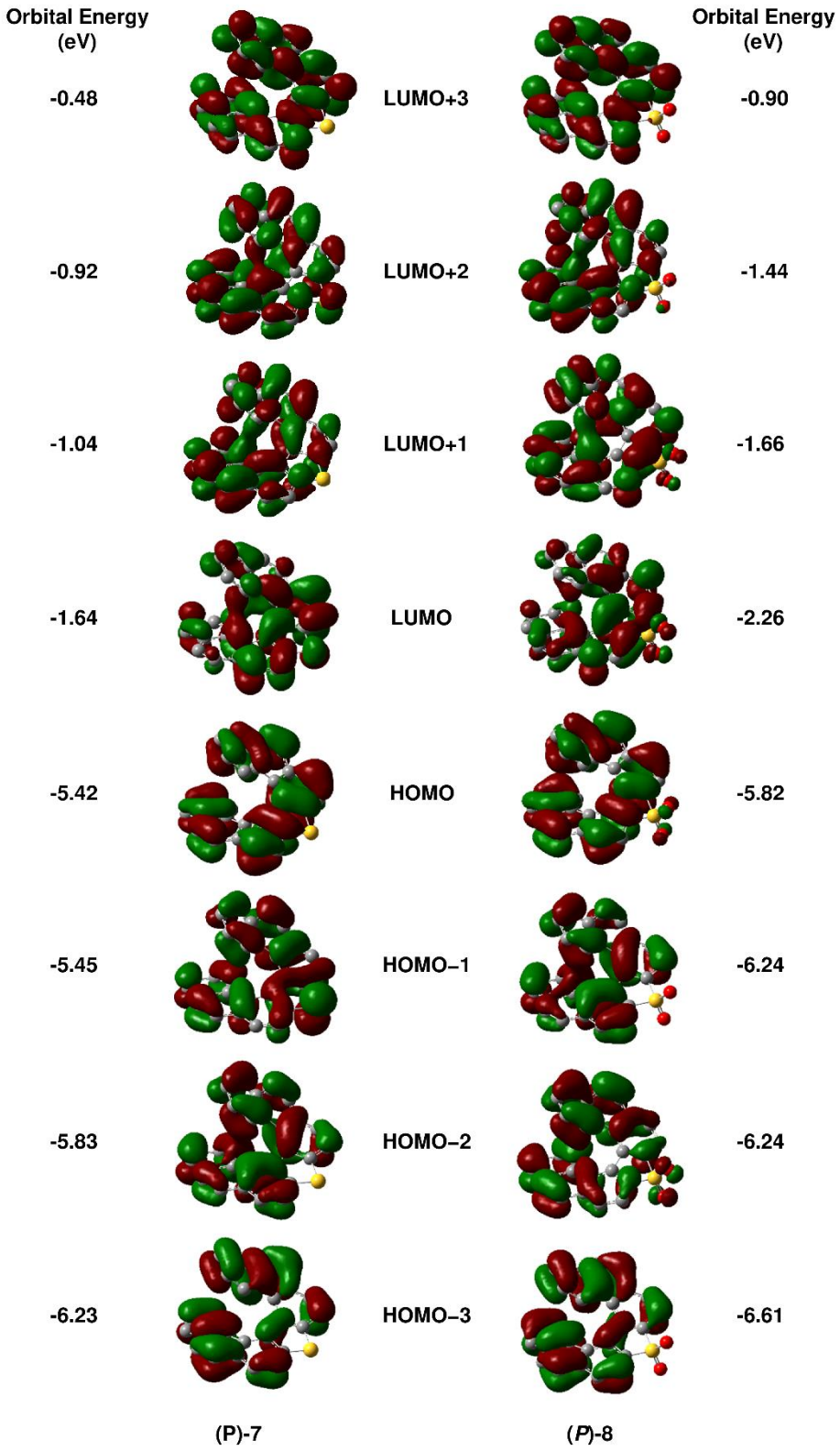

Figure 2.9. Molecular orbitals of (*P*)-**7** and (*P*)-**8** calculated by DFT method at the B3LYP/6-31G(d) level of theory.

The longest absorption wavelength of silole-fused [7]helicene-like compound **3b** is estimated to be 396 nm (Table 2.3), which is in agreement with the experimental absorption characteristics. As observed in **3a**, the features of a silole unit in **3b** can be understood by focusing on the LUMO (Figure 2.10). The LUMO of **3b** is distributed over the silicon atom. It is due to the σ*–π* conjugation between Si–C(phenyl) σ* orbitals and the butadiene π* orbital of the silole unit. On the other hand, no obvious contribution from the phenyl group could be identified. Therfore, the difference in the substituents on the silicon atom (Me or Ph) does not affect the frontier molecular orbitals, and the HOMOs and LUMOs of **3a** and **3b** show almost the same molecular orbital distribution, affording a similar absorption properties.

The molecular orbitals of the cyclopentadiene-fused [7]helicene-like compound **9b** and the aza[7]helicenes **6b** and **6c** are shown in Figures 2.11–2.13. The oxybis(2,1-phenylene) unit in compound **9b** does not contribute to the frontier orbitals. Therefore, molecular orbital distributions of the frontier orbitals of compounds **9a** and **9b** are almost the same, which well explains the similar absorption properties of these compounds. The compound **9b** contains a spirocyclic structure, but a through-space orbital interaction known as spiroconjugation[32–34] between the 4,4'-biphenanthrene and oxybis(2,1-phenylene) units is not observed. The electron-donating groups of the aza[7]helicenes **6b** and **6c** also do not affect the frontier orbitals, and thus all of aza[7]helicenes **6a**–**6c** showed similar photophysical properties.

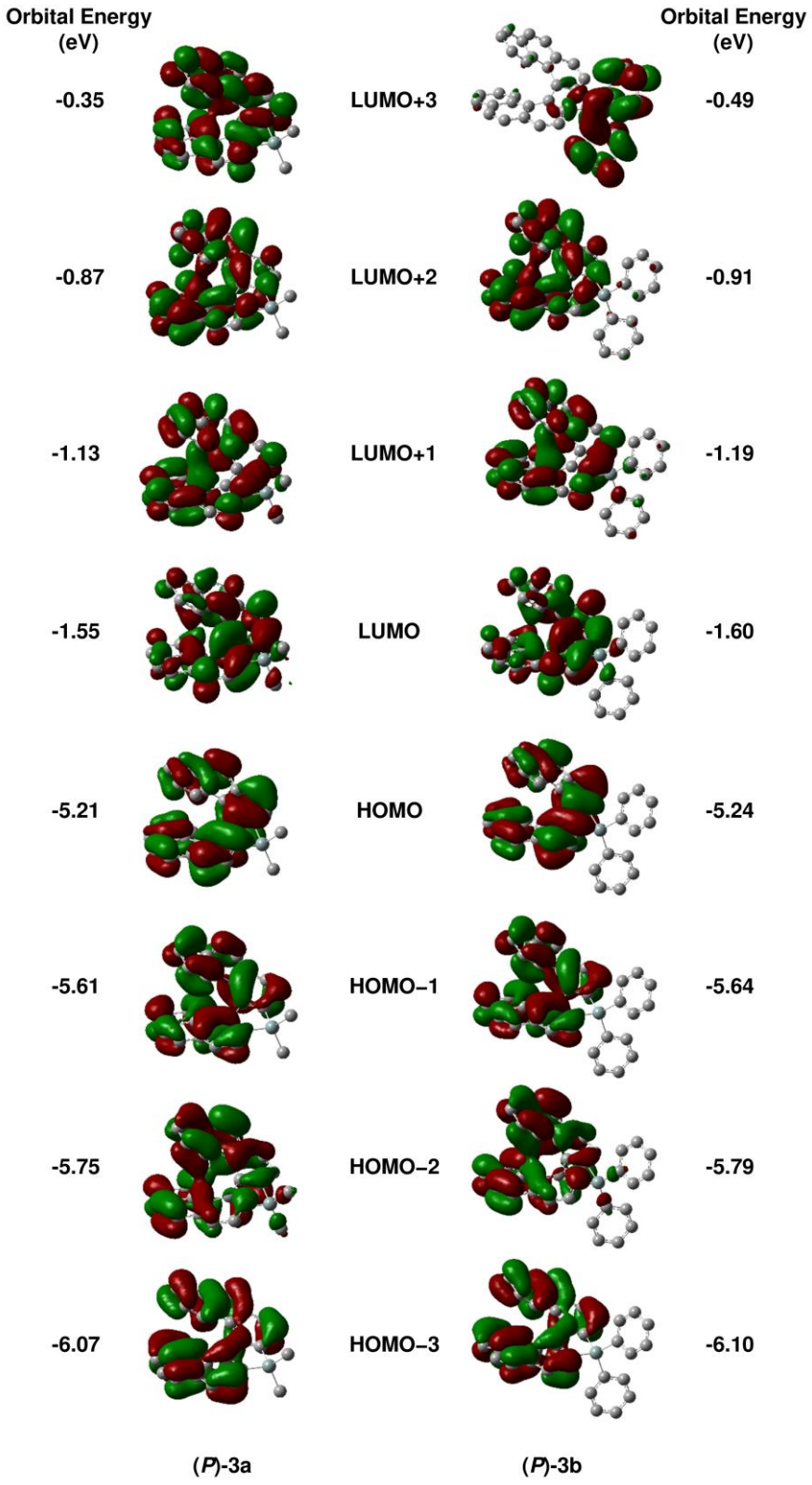

Figure 2.10. Molecular orbitals of (*P*)-**3a** and (*P*)-**3b** calculated by DFT method at the B3LYP/6-31G(d) level of theory.

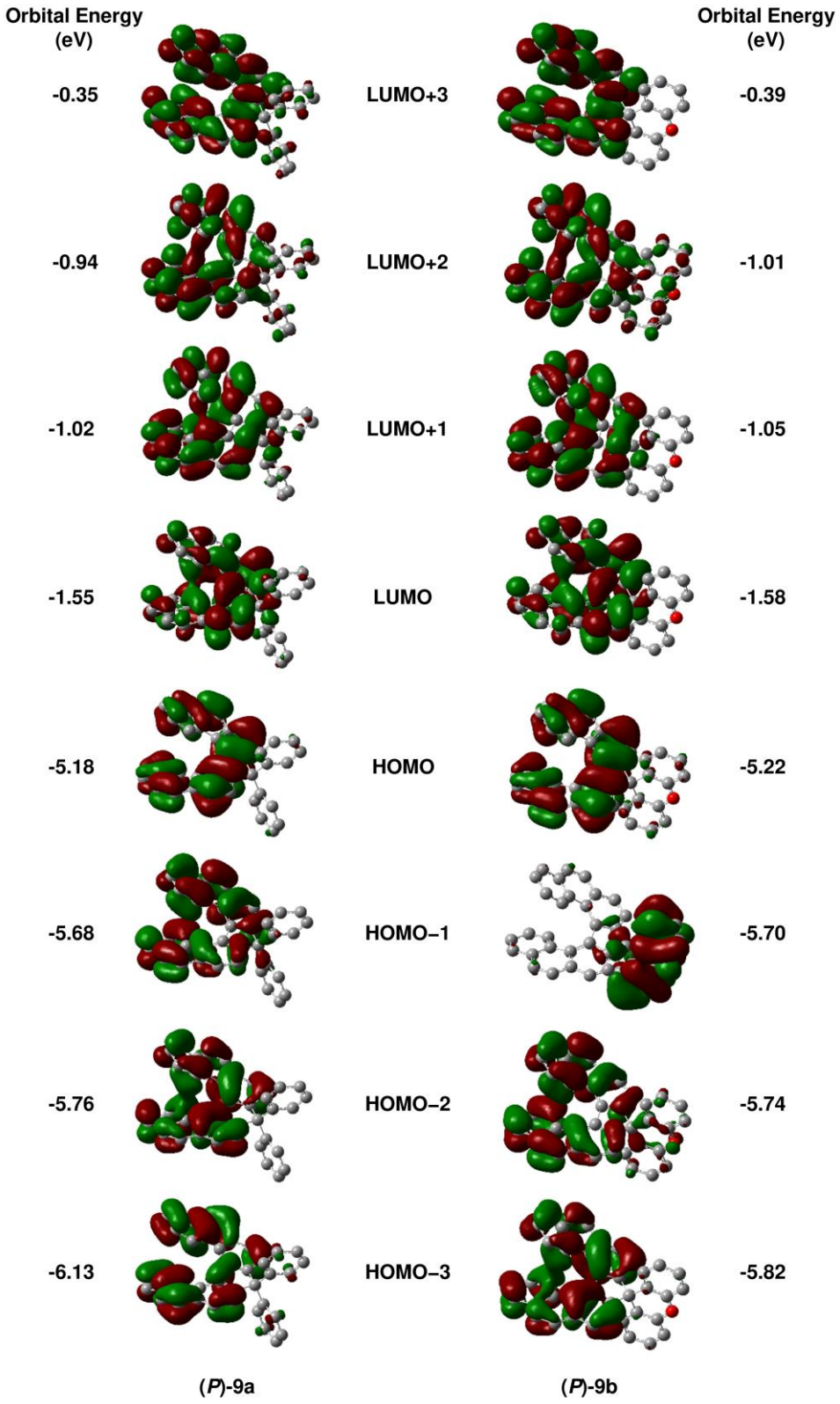

Figure 2.11. Molecular orbitals of (*P*)-**9a** and (*P*)-**9b** calculated by DFT method at the B3LYP/6-31G(d) level of theory

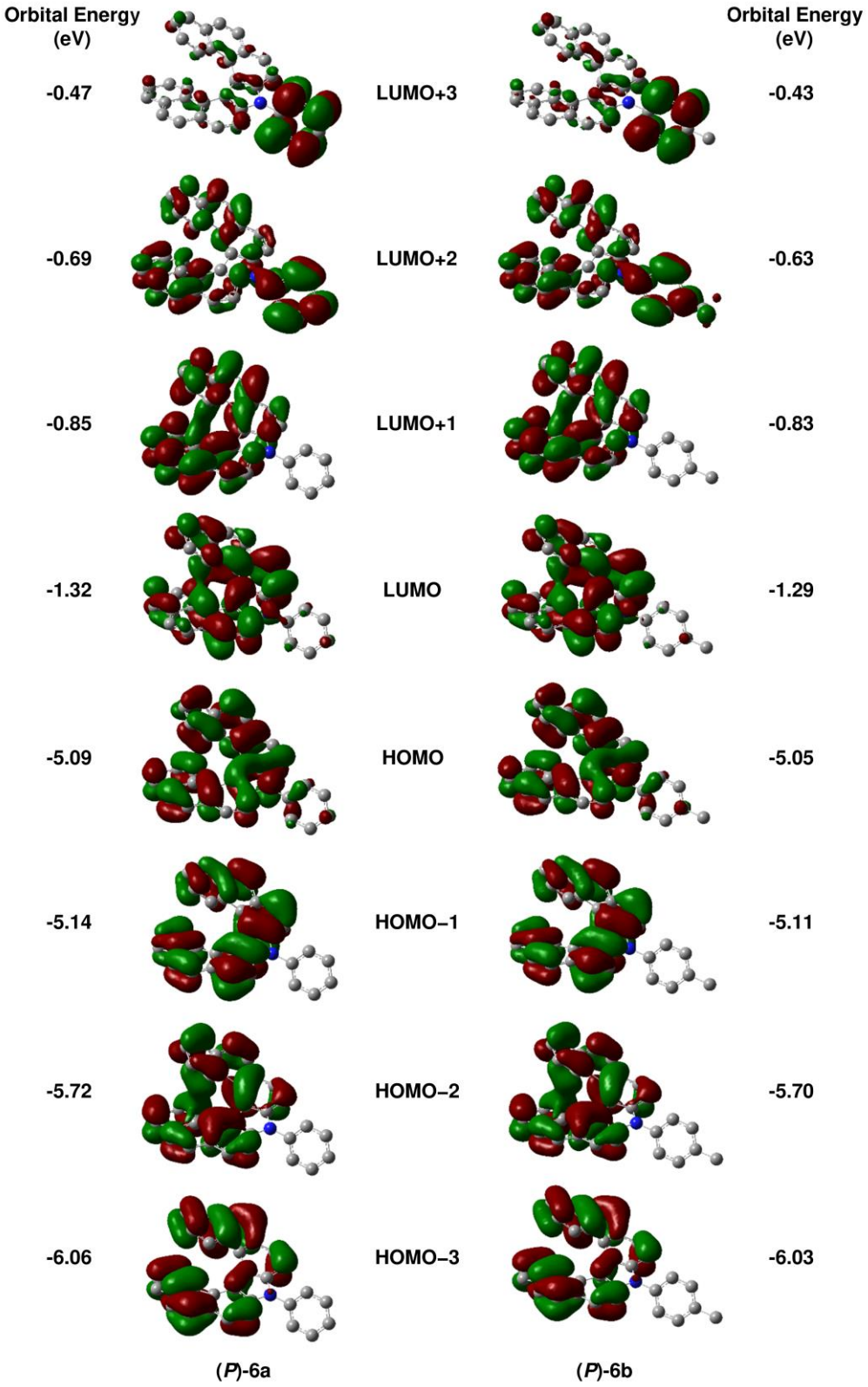

Figure 2.12. Molecular orbitals of (*P*)-**6a** and (*P*)-**6b** calculated by DFT method at the B3LYP/6-31G(d) level of theory

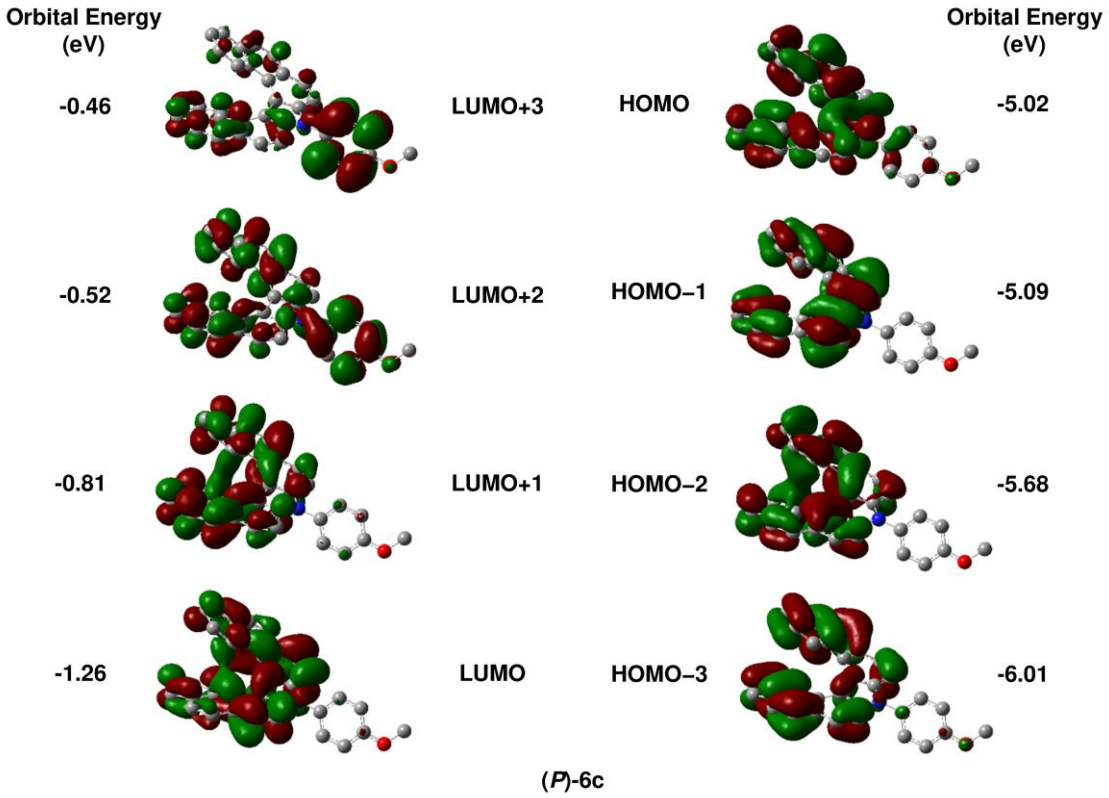

Figure 2.13. Molecular orbitals of (*P*)-**6c** calculated by DFT method at the B3LYP/6-31G(d) level of theory

Table 2.4. The Selected Absorption of (*P*)-**9** and **6** Calculated by TD–DFT Method at the B3LYP/6-31G(d) Level of Theory

	excited state	transition energy (eV)	wavelength (nm)	main transition configuration (CI expansion coefficient)	oscillator strength *f*
(*P*)-**9a**	1	3.157	393	HOMO → LUMO (0.68058)	0.1447
	2	3.470	357	HOMO−1 → LUMO (0.59219)	0.0073
	3	3.478	356	HOMO−2 → LUMO (0.49445)	0.0191
	4	3.724	333	HOMO−2 → LUMO (0.49463)	0.0587
	5	3.837	323	HOMO → LUMO+2 (0.56369)	0.1570
	6	3.974	312	HOMO−3 → LUMO (0.60105)	0.0567
(*P*)-**9b**	1	3.171	391	HOMO → LUMO (0.67747)	0.1447
	2	3.484	356	HOMO−2 → LUMO (0.54038)	0.0009
	3	3.504	354	HOMO → LUMO+1 (0.48680)	0.0205
	4	3.557	349	HOMO−1 → LUMO (0.66521)	0.0056
	5	3.748	331	HOMO−3 → LUMO (0.51075)	0.0678
	6	3.825	324	HOMO → LUMO+2 (0.56366)	0.1836
(*P*)-**6a**	1	3.187	389	HOMO → LUMO (0.66109)	0.0409
	2	3.296	376	HOMO−1 → LUMO (0.64999)	0.1036
	3	3.760	330	HOMO−2 → LUMO (0.53834)	0.1176
	4	3.780	328	HOMO → LUMO+1 (0.59701)	0.1755
	5	3.843	323	HOMO → LUMO+2 (0.63485)	0.0217
	6	3.882	319	HOMO−1 →LUMO+1 (0.58640)	0.2091
(*P*)-**6b**	1	3.184	389	HOMO → LUMO (0.66146)	0.0425
	2	3.295	376	HOMO−1 → LUMO (0.64832)	0.1008
	3	3.765	329	HOMO → LUMO+1 (0.56690)	0.2748
	4	3.779	328	HOMO−2 → LUMO (0.52395)	0.0246
	5	3.854	322	HOMO → LUMO+2 (0.47594)	0.0030
	6	3.892	319	HOMO → LUMO+2 (0.46655)	0.2407
(*P*)-**6c**	1	3.183	389	HOMO → LUMO (0.66137)	0.0393
	2	3.297	376	HOMO−1 → LUMO (0.64605)	0.0973
	3	3.760	330	HOMO → LUMO+1 (0.65072)	0.2990
	4	3.797	327	HOMO−2 → LUMO (0.63461)	0.0113
	5	3.857	321	HOMO−1 →LUMO+1 (0.60073)	0.0705
	6	3.943	314	HOMO → LUMO+2 (0.56263)	0.1081

2.5. Conclusion

The transformation of thia[7]helicene to aza[7]helicenes and [7]helicene-like compounds was achieved via aromatic metamorphosis. The dianion **2** obtained by desulfurative dilithiation of thia[7]helicene **7** can react with dielectrophiles to give the corresponding [7]helicene-like compounds, thus avoiding the use of transition metal catalysts. The dianion can be prepared from 3,3′-dibromo-4,4′-biphenanthrene (see chapter 3), but the synthesis of the parent dibromide **1** requires lengthy multiple steps and the total yield is low. In addition, the present aromatic metamorphosis approach accepts not only dielectrophiles but also dinucleophiles and enables to introduce a variety of heteroatoms and a carbon atom into the helical skeleton at the final stage of synthetic sequence. Therefore, the present synthetic method is a more convenient way to construct the helicene structure. Application of this method to other thiophene-fused thiahelicenes, electrophiles, and nucleophiles will contribute to the development of novel helicenes and helicene-like compounds with unique properties.

2.6. Experimental section

2.6.1. General

All manipulations involving air- and/or moisture-sensitive compounds were carried out with the standard Schlenk technique under argon. Analytical thin-layer chromatography was performed on a glass plate coated with 0.25-mm 230–400-mesh silica gel containing a fluorescent indicator. Column chromatography was performed by using silica gel (spherical neutral, particle size: 63–210 μm). The recycling preparative HPLC was performed with YMC-GPC T–2000 and T–4000 columns (chloroform as an eluent). Most of reagents were purchased from commercial suppliers, such as Sigma-Aldrich Co. LLC, Tokyo Chemical Industry Co., Ltd., and Kanto Chemical Co., Inc., and used without further purification unless otherwise specified. Commercially available anhydrous solvents were used for air- and/or moisture sensitive reactions. Diphenanthro[3,4-*b*:4',3'-*d*]thiophene (**7**) and diphenanthro[3,4-*b*:4',3'-*d*]thiophene *S*,*S*-dioxide (**8**) were prepared according to the literature.[23]

NMR spectra were recorded in $CDCl_3$ or acetone-d_6,on a JEOL ECX400 spectrometer (^{1}H 400 MHz; ^{13}C 101 MHz) or JEOL ECA500 spectrometer (^{1}H 500 MHz; ^{13}C 126 MHz). Chemical shifts are reported in ppm relative to the internal standard signal (0 ppm for Me_4Si in $CDCl_3$) or the solvent residual signal (2.05 ppm for acetone-d_6) for ^{1}H and the deuterated solvent signal (77.16 ppm for $CDCl_3$ and 206.26 ppm for acetone-d_6) for ^{13}C. Data are presented as follows: chemical shift, multiplicity (s = singlet, d = doublet, t = triplet, m = multiplet and/or multiple resonances), coupling constant in hertz (Hz), and signal area integration in natural numbers. High resolution mass spectra are taken with a Bruker Daltonics micrOTOF-QII mass spectrometer by atmospheric pressure chemical ionization-time-of-flight (APCI–TOF) method. UV–Vis absorption spectra were recorded on a JASCO V–650 spectrophotometer. Photoluminescence spectra were recorded on a JASCO FP–6500 spectrofluorometer. Absolute quantum yields were determined by absolute quantum yield measurement system with a JASCO ILF–533 integrating sphere. HPLC analyses and optical resolution were carried out using a DAICEL CHIRALPAK® IA-3 column (4.6 mm × 250 mm) and a DAICEL CHIRALPAK® IA column (20 mm × 250 mm), respectively. CD spectra were recorded on a JASCO J–725 spectrometer. CPL spectra were measured by using a JASCO CPL–300 spectrometer.

2.6.2. Synthetic procedure

2,6-Dimethoxy-1,1'-biphenyl (10). A mixture of (2,6-dimethoxyphenyl)boronic acid (10 g, 55 mmol), $Pd(PPh_3)_4$ (1.6 g, 1.4 mmol), Cs_2CO_3 (53 g, 0.16 mol), iodobenzene (6.2 mL, 55 mmol), methanol (50 mL), and toluene (50 mL) was placed in a 500-mL three-necked flask under Ar and degassed by three freeze-pum-thaw cycles. After stirred at 100 °C for 3 h, the solvent was removed under reduced pressure. To the residue were added $CHCl_3$ (300mL) and aqueous HCl (1 M, 300 mL), and the resulting mixture was stirred to dissolve the crude residue. After the organic layer was separated, the aqueous layer was extracted with $CHCl_3$ (300 mL × 2). The combined organic layers were dried over anhydrous Na_2SO_4, filtered, and concentrated under reduced pressure. The resulting crude residue was purified by silica-gel column chromatography with hexane/CH_2Cl_2 (5/2 R_f = 0.40) as an eluent to give **10** as a colorless solid (9.5 g, 44 mmol, 81%). The ^{1}H NMR data were identical with those in the literature.[35]

6-Methoxy[1,1'-biphenyl]-2-ol (11). To a solution of **10** (6.5 g, 31 mmol) in CH_2Cl_2 (60 mL), boron tribromide (1.0 M in CH_2Cl_2, 16 mL, 16 mmol) was slowly added at −78 °C under Ar. After stirred at ambient temperature for 17.5 h, water (50 mL) was added to the reaction mixture at 0 °C. The organic layer was separated, and the aqueous layer was extracted with CH_2Cl_2 (100 mL × 3). The combined organic layers were washed with saturated aqueous $NaHCO_3$, dried over anhydrous Na_2SO_4, filtered, and concentrated under reduced pressure. The resulting crude residue was purified by silica-gel column chromatography with hexane/CH_2Cl_2 (2/1 R_f = 0.25) as an eluent to give **11** as a colorless solid (4.5 g, 22 mmol, 73%). The ^{1}H and ^{13}C NMR data were identical with those in the literature.[36]

6-Methoxy[1,1'-biphenyl]-2-yl trifluoromethanesulfonate (12). A mixture of **11** (10 g, 51 mmol) and pyridine (13 mL, 153 mmol), and CH_2Cl_2 (150 mL) was placed in a 300 mL three-necked flask under Ar. To the solution was added trifluoromethanesulfonic anhydride (10 mL, 61 mmol) slowly at 0 °C. After stirred at ambient temperature for 17 h, aqueous HCl (1 M, 150 mL) was added to the reaction mixture. The organic layer was separated, and the aqueous layer was extracted with CH_2Cl_2 (200 mL × 3). The combined organic layers were dried over anhydrous Na_2SO_4, filtered, concentrated under reduced pressure. The resulting crude residue was purified by silica-gel column chromatography with hexane/ethyl acetate (4/1 R_f = 0.60) as an eluent to give **12** as a colorless solid (15 g, 45 mmol, 88%): ^{1}H NMR (400 MHz, $CDCl_3$) δ 7.47–7.32 (m, 6H), 7.01 (d, J = 8.7, 1H), 7.00 (d, J = 8.2, 1H), 3.79 (s, 3H); ^{13}C NMR

(126 MHz, $CDCl_3$) δ 158.3, 147.7, 131.2, 130.8, 129.3, 128.2, 128.1, 125.1, 118.4 (q, J_{C-F} = 320.3 Hz), 113.7, 110.9, 56.2; ^{19}F NMR (471 MHz, $CDCl_3$) δ −74.2; HRMS–APCI$^+$ (*m*/*z*) calcd for $C_{14}H_{11}F_3O_4S^+$ (M^+) 332.0325, found 332.0332.

2-(6-Methoxy[1,1'-biphenyl]-2-yl)-4,4,5,5-tetramethyl-1,3,2-dioxaborolane (13). A mixture of **12** (8.1 g, 24 mmol), $PdCl_2(dppf)\cdot CH_2Cl_2$ (0.61 g, 0.74 mmol), 1,4-dioxane (70 mL), Et_3N (12 mL, 86 mmol), and HBpin (12 mL, 83 mmol) was placed in a 300-mL three-necked flask under Ar and degassed by three freeze-pump-thaw cycles. The reaction mixture was stirred at 100 °C for 17 h under Ar, and then concentrated under reduced pressure. The resulting crude residue was purified by silica-gel column chromatography with hexane/ethyl acetate (4/1, R_f = 0.63) as an eluent to give **13** as a white solid (7.2 g, 23 mmol, 94%). ^1H NMR (500 MHz, acetone-d_6) δ 7.36–7.25 (m, 7H), 7.10 (d, *J* = 8.0 Hz, 1H), 3.70 (s, 3H), 1.12 (s, 12H); ^{13}C NMR (126 MHz, acetone-d_6) δ 157.0, 140.2, 136.5, 131.1, 128.7, 127.9, 127.1, 126.6, 113.5, 84.0, 55.7, 24.8; HRMS–APCI$^+$ (*m*/*z*) calcd for $C_{19}H_{23}BO_3^+$ (M^+) 310.1735, found 310.1760.

3'',6'-dimethoxy-1,1':2',1'':2'',1'''-quaterphenyl (14). A mixture of **12** (6.8 g, 21 mmol), **13** (8.1 g, 26 mmol), and $Pd(PPh_3)_4$ (948 mg, 0.82 mmol) were placed in a 300-mL three-necked flask under Ar. To the mixture were added DME (108 mL) and aqueous Na_2CO_3 solution (2 *M*, 82 mL), and the resulting mixture was degassed by three freeze-pump-thaw cycles, and then stirred at 70 °C for 55 h under Ar. After adding H_2O (50 mL), the resulting mixture was extracted with CH_2Cl_2 (100 mL × 3). The combined organic layers were washed with aqueous HCl (1 *M*, 300 mL) and brine (200 mL), dried over anhydrous Na_2SO_4, filtered, and concentrated under reduced pressure. The resulting crude residue was washed with hexane/CH_2Cl_2 (10/1) to give **14** as a colorless solid (6.8 g, 20 mmol, 88%): ^1H NMR (400 MHz, $CDCl_3$) δ 7.15 (t, *J* = 7.8 Hz, 2H), 7.12-7.07 (m, 6H), 6.84 (d, *J* = 7.3Hz, 2H), 6.82–6.77 (m, 6H), 3.64 (s, 6H); ^{13}C NMR (101 MHz, $CDCl_3$) δ 156.5, 142.0, 136.3, 131.4, 130.1, 127.2, 127.0, 126.2, 124.5, 109.7, 55.8; HRMS–APCI$^+$ (*m*/*z*) calcd for $C_{26}H_{23}O_2^+$ ([M+H]$^+$) 367.1693, found 367.1685.

3',6''-Dibromo[1,1':2',1'':2'',1'''-quaterphenyl]-3'',6'-diol (16). A mixture of **14** (5.9 g, 16 mmol) and $CHCl_3$ (420 mL) was placed in a 1-L three-necked flask under Ar. To the solution was added bromine (3.8 mL, 74 mmol) at ambient temperature. After stirred at ambient temperature for 19 h, saturated aqueous $Na_2S_2O_3$ (300 mL) was added to the reaction mixture. The organic layer was separated, and the aqueous layer was extracted with CH_2Cl_2 (200 mL × 3). The combined organic layers were washed

with saturated aqueous $Na_2S_2O_3$ (300 mL) and concentrated under reduced pressure. The resulting crude residue, which contained **15**, was used in the next step without separation since the unidentified by-products could not be separated.

The obtained crude residue was dissolved in CH_2Cl_2 (180 mL) in a 500-mL three-necked flask. To the solution was added BBr_3 (1.0 M in CH_2Cl_2, 56 mL) dropwise at 0 °C, and the resulting mixture was warmed to ambient temperature and stirred for 15 h. After adding water (200 mL) at 0 °C, the organic layer was separated. The aqueous layer was extracted with CH_2Cl_2 (100 mL × 3), and the combined organic layers were washed with saturated aqueous $NaHCO_3$ (200 mL), dried over Na_2SO_4, filtered, and concentrated under reduced pressure. The crude residue was purified by silica-gel column chromatography with hexane/CH_2Cl_2 (1/1, R_f = 0.13) as an eluent to give **16** as a colorless solid (4.8 g, 9.7 mmol, 61%): ^{1}H NMR (400 MHz, acetone-d_6) δ 8.02 (brs, 2H), 7.44 (d, J = 8.7 Hz, 2H), 7.15–7.11 (m, 6H), 6.84–6.77 (m, 6H); ^{13}C NMR (126 MHz, acetone-d_6) δ 154.5, 141.6, 136.2, 132.3, 131.3, 130.7, 127.6, 127.6, 117.5, 116.7; HRMS–APCI$^+$ (m/z) calcd for $C_{24}H_{16}Br_2O_2^+$ (M^+) 493.9512 (monoisotopic ion), found 493.9514.

3',6''-Dibromo[1,1':2',1'':2'',1'''-quaterphenyl]-3'',6'-diyl bis(trifluoromethanesulfonate) (17). A mixture of **16** (5.5 g, 11 mmol), Et_3N (9.4 mL), and CH_2Cl_2 (110 mL) was placed in a 500-mL three-necked flask under Ar. To the solution was added Tf_2O (4.4 mL, 27 mmol) slowly at 0 °C. After stirred at 0 °C for 1 h, the reaction mixture was warmed to ambient temperature and stirred for 20 h. To the reaction mixture was added aqueous HCl (1 *M*, 300 mL), and the organic layer was separated. The aqueous layer was extracted with CH_2Cl_2 (200 mL × 3), and the combined organic layers were dried over anhydrous Na_2SO_4, filtered, and concentrated under reduced pressure. The resulting crude residue was purified by silica-gel column chromatography with hexane/CH_2Cl_2 (1/1, R_f = 0.73) as an eluent to give **17** as a colorless solid (6.3 g, 8.3 mmol, 74%): ^{1}H NMR (500 MHz, acetone-d_6) δ 7.96 (d, J = 9.2 Hz, 2H), 7.50 (d, J = 8.6 Hz, 2H), 7.32–7.18 (m, 8H), 6.44 (brs, 2H); ^{13}C NMR (126 MHz, acetone-d_6) δ 147.3, 142.1, 137.3, 134.1, 132.7, 132.2, 129.8, 129.6, 128.5, 128.4, 126.9, 124.5, 119.0 (q, $J_{C\text{-}F}$ = 319.9 Hz); ^{19}F NMR (471 MHz, acetone-d_6) δ −75.2; HRMS–APCI$^+$ (m/z) calcd for $C_{26}H_{14}Br_2F_6O_6S_2^+$ (M^+) 757.8498 (monoisotopic ion), found 757.8522.

[(3',6''-Dibromo[1,1':2',1'':2'',1'''-quaterphenyl]-3'',6'-diyl)bis(ethyne-2,1-diyl)]bis(trimethylsilane) (18). A mixture of **17** (101 mg, 0.13 mmol), Et_3N (1.0 mL,

7.1 mmol), and DMF (1.0 mL) was placed in a 30-mL Schlenk tube under Ar and degassed by three freeze-pump-thaw cycles. To the solution was added (trimethylsilyl)acetylene (55 μL, 0.39 mmol), $PdCl_2(PPh_3)_2$ (11 mg, 16 μmol), CuI (9 mg, 49 μmol), tetrabutylammonium iodide (150 mg, 0.41 mmol) under Ar. The resulting mixture was stirred at 40 °C for 18 h, and aqueous HCl (1 *M*, 20 mL) was added to the reaction mixture. The resulting mixture was extracted with Et_2O (10 mL × 3), and the combined organic layers were dried over anhydrous Na_2SO_4, filtered, and concentrated under reduced pressure. The crude residue was purified by silica-gel column chromatography with hexane/CH_2Cl_2 (3/1, R_f = 0.65) as an eluent to give **18** as a colorless solid (66 mg, 0.10 mmol, 77%): ^{1}H NMR (500 MHz, acetone-d_6) δ 7.70 (d, J = 8.6 Hz, 2H), 7.39 (d, J = 8.0 Hz, 2H), 7.25–6.59 (m, 10H), −0.07 (s, 18H); ^{13}C NMR (126 MHz, acetone-d_6) δ 146.0, 140.7, 138.4, 134.2, 132.3, 128.5, 127.9, 127.7, 123.7, 104.3, 99.5, −0.5; HRMS–APCI$^+$ (*m*/*z*) calcd for $C_{34}H_{32}Br_2Si_2^+$ (M^+) 654.0404 (monoisotopic ion), found 654.0394.

3',6''-Dibromo-3'',6'-diethynyl-1,1':2',1'':2'',1'''-quaterphenyl (19). A mixture of **18** (89 mg, 0.14 mmol) and THF (1.0 mL) was placed in a 30-mL Schlenk tube under Ar. To the solution was added Bu_4NF (1.0 *M* THF solution, 1.0 mmol) under Ar. The resulting mixture was stirred at rt for 20 min, and water (20 mL) was added to the reaction mixture. The resulting mixture was extracted with CH_2Cl_2 (10 mL × 3), and the combined organic layers were dried over anhydrous Na_2SO_4, filtered, and concentrated under reduced pressure. The crude residue was purified by silica-gel column chromatography with hexane/CH_2Cl_2 (3/1, R_f = 0.45) as an eluent to give **19** as a colorless solid (64 mg, 0.12 mmol, 92%): ^{1}H NMR (400 MHz, acetone-d_6) δ 7.72 (d, J = 8.2 Hz, 2H), 7.46 (d, J = 8.7 Hz, 2H), 7.24–6.57 (m, 10H), 3.45 (s, 2H); ^{13}C NMR (101 MHz, acetone-d_6) δ 145.8, 140.8, 138.2, 135.1, 132.3, 128.6, 128.1, 127.8, 122.9, 83.5, 82.5; HRMS–APCI$^+$ (*m*/*z*) calcd for $C_{28}H_{16}Br_2^+$ (M^+) 509.9614 (monoisotopic ion), found 509.9611.

3,3'-Dibromo-4,4'-biphenanthrene (1). A mixture of **19** (37 mg, 72 μmol), $PtCl_2$ (1.9 mg, 7.1 μmol), and toluene (2.0 mL) was placed in a 20-mL Schlenk tube under Ar and degassed by three freeze-pump-thaw cycles. The resulting mixture was refluxed for 39 h and concentrated under reduced pressure. The resulting crude residue was purified by silica-gel column chromatography with hexane/ethyl acetate (9/1, R_f = 0.45) as an eluent to give **3** as a colorless solid (14 mg, 27 μmol, 38%): ^{1}H NMR (500 MHz, $CDCl_3$) δ 7.99–7.93 (m, 4H), 7.89–7.82 (m, 6H), 7.79 (d, J = 8.5 Hz, 2H), 7.39 (t, J = 7.5

Hz, 2H), 6.93 (t, J = 8.0 Hz, 2H); ^{13}C NMR (126 MHz, $CDCl_3$) δ 141.1, 133.4, 133.0, 131.8, 131.2, 130.5, 130.2, 128.8, 128.6, 127.3, 126.8, 126.6, 125.6, 124.7; HRMS–APCI$^+$ (m/z) calcd for $C_{28}H_{16}Br_2^+$ (M^+) 509.9614 (monoisotopic ion), found 509.9625.

9,9-Dimethyl-9*H*-diphenanthro[3,4-*b*:4′,3′-*d*]silole (3a). Lithium (7 mg, 1.0 mmol), THF (1.0 mL) andTMEDA (60 μL, 0.40 mmol) was placed in a 20-mL Schlenk tube under argon atmosphere. After the mixture was stirred at room temperature for 10 min, diphenanthro[3,4-*b*:4',3'-*d*]thiophene (**7**) (77 mg, 0.20 mmol) was added. The resulting mixture was stirred vigorously at room temperature for 4 h, and then cooled to −78 °C. After adding Cl_2SiMe_2 (48 μL, 0.40 mmol) under argon atmosphere, the resulting mixture was stirred at −78 °C for 15 min and at room temperature for an additional 1 h. The reaction was quenched with water at 0 °C, and the resulting mixture was extracted with AcOEt (10 mL × 3). The combined organic layers were washed with brine, dried over Na_2SO_4, filtered, and concentrated under reduced pressure. The crude residue was purified by silica-gel column chromatography (hexane as an eluent) and then by recycling preparative HPLC to give the title compound **3a** as a yellow solid (39 mg, 48% yield). The ^{1}H NMR data was identical to that reported in the literature.[27]

9,9-Diphenyl-9*H*-diphenanthro[3,4-*b*:4′,3′-*d*]silole (3b). The crude product was obtained by using lithium (14 mg, 2.0 mmol), THF (4 mL), TMEDA (0.12 mL, 0.80 mmol), diphenanthro[3,4-*b*:4',3'-*d*]thiophene (**7**) (154 mg, 0.40 mmol), and Cl_2SiPh_2 (0.17 mL, 0.80 mmol) at room temperature for 19 h. Purification by silica-gel column chromatography (CH_2Cl_2/hexane = 7/3 as an eluent; R_f = 0.82) and then by recycling preparative HPLC gave the title compound **3b** as a yellow solid (88 mg, 41% yield): ^{1}H NMR (400 MHz, $CDCl_3$) δ 7.95 (d, J = 7.3 Hz, 2H), 7.79 (d, J = 7.3 Hz, 2H), 7.77–7.75 (m, 4H), 7.65 (d, J = 8.7 Hz, 2H), 7.52 (d, J = 8.7 Hz, 2H), 7.43–7.35 (m, 8H), 7.32 (d, J = 7.8 Hz, 2H), 6.94 (t, J = 7.8 Hz, 2H), 6.37 (t, J = 8.2 Hz, 2H); ^{13}C NMR (101 MHz, $CDCl_3$) δ 149.0, 136.6, 135.8, 134.6, 132.8, 132.1, 130.4, 130.3, 130.0, 129.1, 128.4, 128.1, 127.6, 126.7, 126.5, 126.2, 125.1, 123.1; HRMS–APCI$^+$ (m/z) calcd for $C_{40}H_{27}Si^+$ ($[M+H]^+$) 535.1877, found 535.1876.

9-Phenylnaphtho[1,2-*e*]phenanthro[3,4-*b*]phosphindole 9-oxide (4a). Lithium (7 mg, 1.0 mmol), THF (2.0 mL), and *N*,*N*,*N*′,*N*′-tetramethylethylenediamine (TMEDA) (60 μL, 0.40 mmol) was placed in a 20-mL Schlenk tube under argon atmosphere. After the mixture was stirred at room temperature for 10 min, diphenanthro[3,4-*b*:4',3'-*d*]thiophene (**7**) (77 mg, 0.20 mmol) was added. The resulting

mixture was stirred vigorously at room temperature for 4 h, and then cooled to −78 °C. After adding Cl_2PPh (54 μL, 0.40 mmol) under argon atmosphere, the resulting mixture was stirred at −78 °C for 10 min and at room temperature for an additional 30 min. The reaction mixture was concentrated under reduced pressure. The resulting residue was dissolved with CH_2Cl_2 (10 mL) and passed through a short pad of neutral alumina under argon atmosphere. The alumina pad was washed with CH_2Cl_2 (5 mL), and the combined filtrates were concentrated under reduced pressure. The resulting residue was dissolved in CH_2Cl_2 (5 mL), and H_2O_2 (0.40 mL, 35% aqueous solution) was added in one portion. After the resulting mixture was stirred at room temperature for 30 min, saturated aqueous $Na_2S_2O_3$ (5 mL) was added slowly to the reaction mixture. Organic layer was separated, and the aqueous layer was extracted with AcOEt (10 mL × 2). The combined organic layers were dried over Na_2SO_4, filtered, and concentrated under reduced pressure. The resulting residue was purified by silica-gel column chromatography (CH_2Cl_2/AcOEt = 4/1 as an eluent, R_f = 0.25) and then by recycling preparative HPLC to give the title compound **4a** as a yellow solid (32 mg, 34% yield). The ^{1}H NMR data was identical to that reported in the literature.[26]

Spiro[cyclopenta[1,2-*c*:4,3-*c*′]diphenanthrene-9,9′-xanthene] (9b). Diphenanthro[3,4-*b*:4',3'-*d*]thiophene *S*,*S*-dioxide (**8**) (50 mg, 0.12 mmol), xanthene (27 mg, 0.18 mmol), and 1,4-dioxane (2.5 mL) was placed in a 20-mL Schlenk tube under argon atmosphere. A solution of $KN(SiMe_3)_2$ (0.5 M in toluene, 0.60 mL, 0.30 mmol) was added to the mixture at an ambient temperature. The resulting solution was stirred at 80 °C for 16 h. After the reaction was quenched with saturated aqueous NH_4Cl (3 mL), the resulting mixture was extracted with CH_2Cl_2 (10 mL × 3). The combined organic layers were dried over Na_2SO_4, filtered, and concentrated under reduced pressure. The crude residue was dissolved in CH_2Cl_2 and passed through a short pad of silica gel. The filtrate was concentrated, and the resulting crude residue was purified by recycling preparative HPLC to give the title compound **9b** as a pale-yellow solid (15 mg, 23% yield): ^{1}H NMR (500 MHz, $CDCl_3$) δ 7.81 (d, *J* = 7.5 Hz, 2H), 7.76–7.71 (m, 6H) 7.65 (d, *J* = 8.0 Hz, 2H), 7.47 (d, *J* = 8.0 Hz, 2H), 7.30 (dd, *J* = 8.0, 1.2 Hz, 2H), 7.23–7.20 (m, 2H), 7.14 (t, *J* = 7.5 Hz, 2H), 6.73–6.70 (m, 2H), 6.52 (dd, *J* = 7.7, 1.2 Hz, 2H), 6.36–6.33 (m, 2H); ^{13}C NMR (101 MHz, $CDCl_3$) 156.3, 152.0, 136.7, 132.6, 131.8, 131.0, 129.6, 128.5, 128.27, 127.7, 127.6, 127.0, 126.9, 126.8, 126.6, 123.7, 123.5, 123.4, 117.2, 54.49; HRMS–APCI$^+$ (*m*/*z*) calcd for $C_{41}H_{25}O^+$ ($[M+H]^+$) 533.1900, found 533.1900.

9-(4-Methylphenyl)-9*H*-dinaphtho[2,1-*c*:1′,2′-*g*]carbazole (6b). Diphenanthro[3,4-*b*:4',3'-*d*]thiophene *S*,*S*-dioxide (**8**) (50 mg, 0.12 mmol), *p*-toluidine (32 mg, 0.30 mmol), and 1,4-dioxane (2.5 mL) was placed in a 20-mL Schlenk tube under argon atmosphere. A solution of $KN(SiMe_3)_2$ (0.5 M in toluene, 0.90 mL, 0.45 mmol) was added to the mixture at an ambient temperature. The resulting solution was stirred at 80 °C for 15 h. After the reaction was quenched with saturated aqueous NH_4Cl solution (2 mL), the resulting mixture was extracted with AcOEt (10 mL × 3). The combined organic layers were washed with brine (10 mL), dried over Na_2SO_4, filtered, and concentrated under reduced pressure. The crude residue was purified by silica-gel column chromatography (hexane/AcOEt = 10/1 as an eluent; R_f = 0.40) to give the title compound **6b** as a pale-yellow solid (55 mg, 80% yield). The compound **6b** can be separated into enatiomerically pure (*P*)-**6b** and (*M*)-**6b** by HPLC equipped with a DAICEL CHIRALPAK® IA-3 column (4.6 mm × 250 mm) [t_R = 4.24 min for (*P*)-**6b** and 5.23 min for (*M*)-**6b** (flow rate: 1.0 mL; eluent: hexane/$CHCl_3$ = 7/3)]: ^{1}H NMR (500 MHz, $CDCl_3$) δ 8.03 (d, *J* = 8.6 Hz, 2H), 8.01 (d, *J* = 8.6, 2H), 7.844 (d, *J* = 8.6 Hz, 2H), 7.835 (d, *J* = 7.5 Hz, 2H), 7.78 (d, *J* = 8.6 Hz, 2H), 7.63–7.61 (m, 2H), 7.53 (d, *J* = 8.0 Hz, 2H), 7.50 (d, *J* = 8.6 Hz, 2H), 7.22–7.18 (m, 2H), 6.28–6.25 (m, 2H); ^{13}C NMR (126 MHz, $CDCl_3$) δ 140.4, 138.7, 134.6, 131.5, 130.9, 130.5, 128.5, 128.3, 127.4, 127.1, 126.9, 126.8, 126.4, 126.1, 124.6, 122.8, 117.2, 110.9, 21.5; HRMS–APCI$^+$ (*m*/*z*) calcd for $C_{35}H_{24}N^+$ ($[M+H]^+$) 458.1903, found 458.1904.

9-(4-Methoxyphenyl)-9*H*-dinaphtho[2,1-*c*:1′,2′-*g*]carbazole (6c). The crude product was obtained by using diphenanthro[3,4-*b*:4',3'-*d*]thiophene *S*,*S*-dioxide (**8**) (42 mg, 0.10 mmol), *p*-anisidine (25 mg, 0.20 mmol), 1,4-dioxane (1.5 mL), and $KN(SiMe_3)_2$ (0.5 M in toluene, 0.60 mL, 0.30 mmol) at 80 °C for 19 h according to the procedure for **6b**. Purification by silica-gel column chromatography with hexane/AcOEt = 5/1 as an eluent (R_f = 0.48) gave the title compound **6c** as a pale-yellow solid (42 mg, 88% yield). The compound **6c** can be separated into enatiomerically pure (*P*)-**6c** and (*M*)-**6c** by HPLC equipped with a DAICEL CHIRALPAK® IA-3 column (4.6 mm × 250 mm) [t_R = 5.02 min for (*P*)-**6c** and 6.18 min for (*M*)-**6c** (flow rate: 1.0 mL; eluent: hexane/$CHCl_3$ = 7/3)]: ^{1}H NMR (400 MHz, $CDCl_3$) δ 8.02 (d, *J* = 8.2 Hz, 2H), 8.01 (d, *J* = 8.7, 2H), 7.84 (d, *J* = 8.7 Hz, 2H), 7.83 (d, *J* = 7.6 Hz, 2H), 7.73 (d, *J* = 8.2 Hz, 2H), 7.63–7.59 (m, 2H), 7.50 (d, *J* = 8.2 Hz, 2H), 7.23–7.18 (m, 4H), 6.29–6.25 (m, 2H); ^{13}C NMR (101 MHz, $CDCl_3$) δ 159.8, 140.7, 131.5, 130.5, 129.9, 129.8, 128.4, 127.4, 127.1, 126.94, 126.86, 126.4, 126.1, 124.6, 122.8, 117.1, 115.4, 110.9, 55.9; HRMS–APCI$^+$ (*m*/*z*) calcd for $C_{35}H_{24}NO^+$ ($[M+H]^+$) 474.1852, found 474.1861.

2.6.3. X-ray crystallography

For X-ray crystallographic analysis, a suitable single crystal was selected under ambient conditions, mounted using a nylon loop filled with paraffin oil, and transferred to the goniometer of a RIGAKU R–AXIS RAPID diffractometer with a graphite-monochromated Cu–Kα irradiation (α = 1.54187 Å). The structure was solved by a direct method (SIR 2008[37]) and refined by full-matrix least-squares techniques against F^2 (SHELXL–2014[38,39]). The intensities were corrected for Lorentz and polarization effects. All non-hydrogen atoms were refined anisotropically. Hydrogen atoms were placed using AFIX instructions.

2.6.4. Theoretical calculations

The DFT and TD–DFT calculations were performed by using the Gaussian 16 program[40] at the B3LYP/6–31G(d) level with workstation at Research Center for Computational Science, National Institutes of Natural Sciences, Okazaki, Japan. The starting molecular models for DFT geometry optimizations were built and optimized with MMFF molecular mechanics by using the Spartan ’08 package (Wavefunction, Inc., Irvine, CA, USA). Twelve singlet states were calculated in TD–DFT calculations. The visualization of the molecular orbitals was performed using GaussView 5 (Gaussian, Inc., Wallingford, CT, USA).

2.7. References

(1) Chen, R. F.; Zheng, C.; Fan, Q. L.; Huang, W. *J. Comput. Chem.* **2007**, *28*, 2091–2101.

(2) King, S. M.; Perepichka, I. I.; Perepichka, I. F.; Dias, F. B.; Bryce, M. R.; Monkman, A. P. *Adv. Funct. Mater.* **2009**, *19*, 586–591.

(3) Chen, R.-F.; Xie, G.-H.; Zhao, Y.; Zhang, S.-L.; Yin, J.; Liu, S.-Y.; Huang, W. *Org. Electron.* **2011**, *12*, 1619–1624.

(4) Chen, R.-F.; Zhu, R.; Fan, Q.-L.; Huang, W. *Org. Lett.* **2008**, *10*, 2913–2916.

(5) Poriel, C.; Cocherel, N.; Rault-Berthelot, J.; Vignau, L.; Jeannin, O. *Chem. Eur. J.* **2011**, *17*, 12631–12645.

(6) Gilchrist, T. L. *Heterocyclic Chemistry*; Pitman Publishing Ltd.: London, 1985.

(7) Freeman, A. W.; Urvoy, M.; Criswell, M. E. *J. Org. Chem.* **2005**, *70*, 5014–5019.

(8) Nozaki, K.; Takahashi, K.; Nakano, K.; Hiyama, T.; Tang, H. Z.; Fujiki, M.; Yamaguchi, S.; Tamao, K. *Angew. Chen. Int. Ed.* **2003**, *42*, 2051–2053.

(9) Cho, S. H.; Yoon, J.; Chang, S. *J. Am. Chem. Soc.* **2011**, *133*, 5996–6005.

(10) Gilman, H.; Gorsich, R. D. *J. Am. Chem. Soc.* **1958**, *80*, 1883–1886.

(11) Ureshino, T.; Yoshida, T.; Kuninobu, Y.; Takai, K. *J. Am. Chem. Soc.* **2010**, *132*, 14324–14326.

(12) Furukawa, S.; Kobayashi, J.; Kawashima, T. *J. Am. Chem. Soc.* **2009**, *131*, 14192–14193.

(13) Bhanuchandra, M.; Murakami, K.; Vasu, D.; Yorimitsu, H.; Osuka, A. *Angew. Chem. Int. Ed.* **2015**, *54*, 10234–10238.

(14) Yorimitsu, H.; Vasu, D.; Bhanuchandra, M.; Murakami, K.; Osuka, A. *Synlett* **2016**, *27*, 1765–1774.

(15) Bhanuchandra, M.; Yorimitsu, H.; Osuka, A. *Org. Lett.* **2016**, *18*, 384–387.

(16) Kaga, A.; Nogi, K.; Yorimitsu, H. *Chem. Eur. J.* **2019**, *25*, 14780–14784.

(17) Kaga, A.; Iida, H.; Tsuchiya, S.; Saito, H.; Nakano, K.; Yorimitsu, H. *Chem. Eur. J.* **2021**, *27*, 4567–4572.

(18) Nagata, Y.; Kato, S.; Miyake, Y.; Shinokubo, H. *Org. Lett.* **2017**, *19*, 2718–2721.

(19) Takase, K.; Noguchi, K.; Nakano, K. *Bull. Chem.Soc. Jpn.* **2019**, *92*, 1008–1017.

(20) Matsuo, Y.; Tanaka, T.; Osuka, A. *Chem. Lett.* **2020**, *49*, 959–962.

(21) Yanagi, T.; Tanaka, T.; Yorimitsu, H. *Chem. Sci.* **2021**, *12*, 2784–2793.

(22) Iwakura, K.; Minamii, M. JP07118282, 1995.

(23) Dore, A.; Fabbri, D.; Gladiali, S.; Valle, G. *Tetrahedron: Asymmetry* **1995**, *6*, 779–788.

(24) Cossu, S.; De Lucchi, O.; Fabbri, D.; Valle, G.; Painter, G. F.; Smith, R. A. J. *Tetrahedron* **1997**, *53*, 6073–6084.

(25) Nakano, K.; Hidehira, Y.; Takahashi, K.; Hiyama, T.; Nozaki, K. *Angew. Chem. Int. Ed.* **2005**, *44*, 7136–7138.
(26) Nakano, K.; Oyama, H.; Nishimura, Y.; Nakasako, S.; Nozaki, K. *Angew. Chem. Int. Ed.* **2012**, *51*, 695–699.
(27) Oyama, H.; Nakano, K.; Harada, T.; Kuroda, R.; Naito, M.; Nobusawa, K.; Nozaki, K. *Org. Lett.* **2013**, *15*, 2104–2107.
(28) Oyama, H.; Akiyama, M.; Nakano, K.; Naito, M.; Nobusawa, K.; Nozaki, K. *Org. Lett.* **2016**, *18*, 3654–3657.
(29) During this study, the more efficient synthesis of **1** was reported, see: Terada, N.; Uematsu, K.; Higuchi, R.; Tokimaru, Y.; Sato, Y.; Nakano, K.; Nozaki, K. *Chem. Eur. J.* **2021**, *27*, 9342–9349.
(30) Sanchez-Carnerero, E.M.; Agarrabeitia, A.R.; Moreno, F.; Maroto, B.L.; Muller, G.; Ortiz, M.J.; de la Moya, S. *Chem. Eur. J.* **2015**, *21*, 13488–13500.
(31) Fukui, N.; Osuka, A. *Bull. Chem. Soc. Jpn.* **2018**, *91*, 1131–1137.
(32) Simmons, H.E.; Fukunaga, T. *J. Am. Chem. Soc.* **1967**, *89*, 5208–5215.
(33) Schweig, A.; Weulner, U.; Hellwinkel, D.; Krapp, W. *Angew. Chem. Int. Ed.* **1973**, *12*, 310–311.
(34) Dürr, H.; Gleiter, R. *Angew. Chem. Int. Ed.* **1978**, *17*, 559–569.
(35) Greig, L. M.; Slawin, A. M. Z.; Smith, M. H.; Philp, D. *Tetrahedron* **2007**, *63*, 2391–2403.
(36) Phipps, R. J.; Toste, F. D. *J. Am. Chem. Soc.* **2013**, *135*, 1268–1271.
(37) Burla, M.C.; Caliandro, R.; Camalli, M.; Carrozzini, B.; Cascarano, G.L.; De Caro, L.; Giacovazzo, C.; Polidori, G.; Siliqi, D.; Spagna, R. *J. Appl. Crystallogr.* **2007**, *40*, 609–613.
(38) Sheldrick, G.M. *Acta Crystallogr. A* **2008**, *64*, 112–122.
(39) Sheldrick, G.M. *Acta Crystallogr. C Struct. Chem.* **2015**, *C71*, 3–8.
(40) Frisch, M. J.; Trucks, G. W.; Schlegel, H. B.; Scuseria, G. E.; Robb, M. A.; Cheeseman, J. R.; Scalmani, G.; Barone, V.; Petersson, G. A.; Nakatsuji, H.; Li, X.; Caricato, M.; Marenich, A. V.; Bloino, J.; Janesko, B. G.; Gomperts, R.; Mennucci, B.; Hratchian, H. P.; Ortiz, J. V.; Izmaylov, A. F.; Sonnenberg, J. L.; Williams; Ding, F.; Lipparini, F.; Egidi, F.; Goings, J.; Peng, B.; Petrone, A.; Henderson, T.; Ranasinghe, D.; Zakrzewski, V. G.; Gao, J.; Rega, N.; Zheng, G.; Liang, W.; Hada, M.; Ehara, M.; Toyota, K.; Fukuda, R.; Hasegawa, J.; Ishida, M.; Nakajima, T.; Honda, Y.; Kitao, O.; Nakai, H.; Vreven, T.; Throssell, K.; Montgomery Jr., J. A.; Peralta, J. E.; Ogliaro, F.; Bearpark, M. J.; Heyd, J. J.; Brothers, E. N.; Kudin, K. N.; Staroverov, V. N.; Keith, T. A.; Kobayashi, R.; Normand, J.; Raghavachari, K.; Rendell, A. P.; Burant, J. C.; Iyengar, S. S.; Tomasi,

J.; Cossi, M.; Millam, J. M.; Klene, M.; Adamo, C.; Cammi, R.; Ochterski, J. W.; Martin, R. L.; Morokuma, K.; Farkas, O.; Foresman, J. B.; Fox, D. J. *Gaussian 16 Rev. C.01*, Gaussian Inc. Wallingford, CT, 2016.

Chapter 3

Synthesis and Properties of Spiro-Double Silole-fused [7]Helicene-like Compound

A spiro-double helicene-like compound with a silicon atom at the spiro center was successfully synthesized from 3,3'-dibromo-4,4'-biphenanthrene. Its characteristic structure was revealed by single crystal X-ray analysis. The spiro and helical skeletons cuase (*P*,*P*), (*M*,*M*), and (*P*,*M*) isomers. This is the first example of the synthesis of an optically resolvable spiro-double helicene-like compound. The twisted spiro-conjugation by the helical skeleton was found to induce the lower-lying LUMO for the spiro-double silole-fused [7]helicene-like compound compared to that of the mono silole-fused [7]helicene-like compound.

3.1. Introduction

Recently, multiple helicenes, in which two or more helicene units are combined in one polycyclic aromatic skeleton, have attract growing interest owing to their higher curved π-conjugated surfaces compared to those of mono helicenes. The higher-order helicenes have been reported to form unique three-dimensional structures and show intermolecular electronic interactions between the helicene units. Among the multiple helicenes ever reported, double helicenes composed of two helicene units have been well investigated. The structures of the representative double helicenes and double helicene-like compounds **20**–**25** are shown in Figure 3.1.[1–6] In almost all double helicenes and double helicene-like compounds, two helical units share a π-conjugated unit. Therefore, the π-conjugation spread over the entire molecules, giving planar structures. In such planar structures, the two helical axes of the two helicene substructures are aligned in approximately parallel manner.

On the other hand, when two helicene units share a spiro atom, the structure of the resulting double helicenes is drastically different from those of the conventional double helicenes. The two helical axes of the two helicene substructures would be aligned perpendicularly to each other. Indeed, this approach has been reported by Wang and coworkers in 2015.[7] They synthesized compound **26** with two thia[7]helicene-like units which share a silicon atom as a spiro linker (Figure 3.1). However, this compound does not maintain a stable helical structure and thus does not exhibit chiral character because the terminal thiophene rings are too far to induce a stable helical structure by steric repulsion.

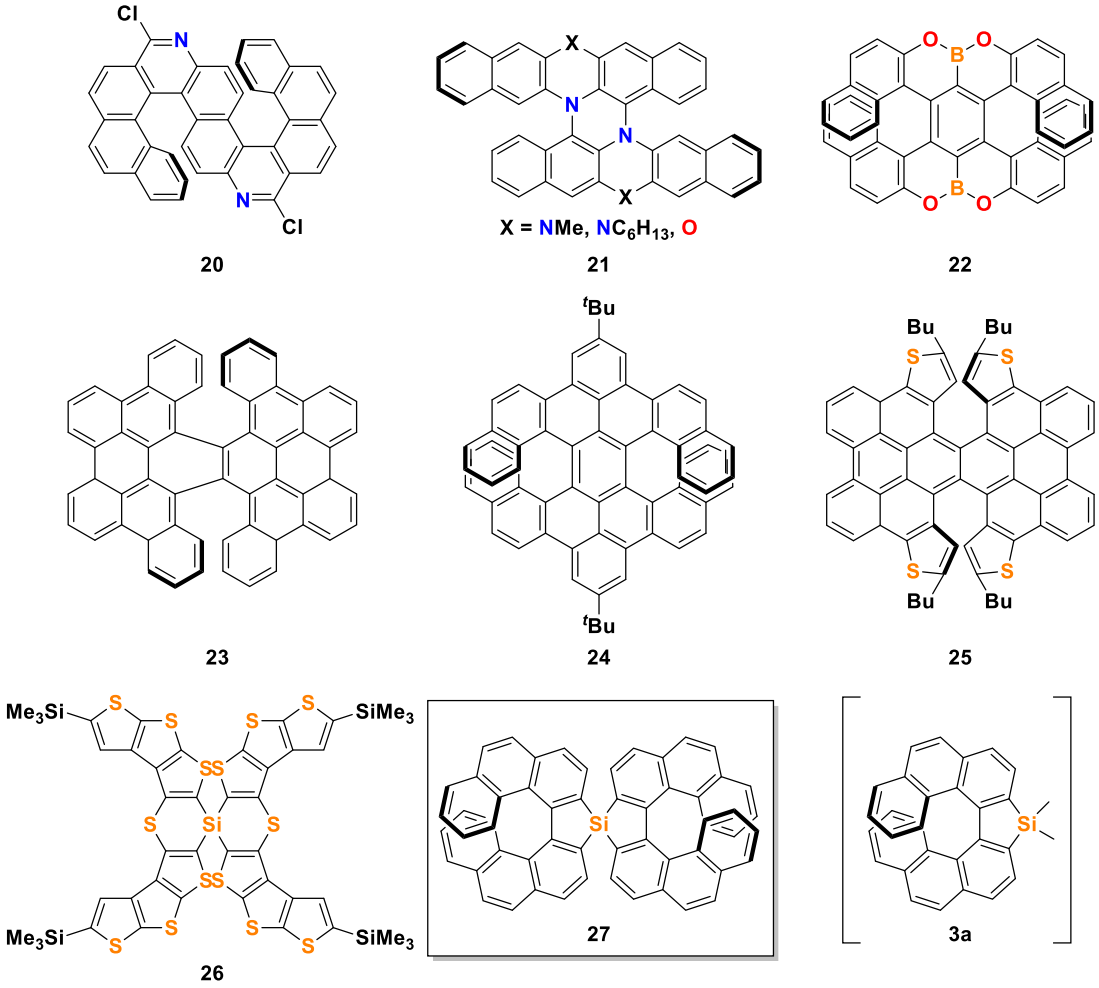

Figure 3.1. Reported double helicenes and the spiro-double silole-fused [7]helicene-like compound in this thesis.

In this context, the author envisaged that the trapping of 4,4'-biphenanthrene-3,3'-diyldilithium (**2**), the dianion species discussed in Chapter 2, with tetrachlorosilane would give the spiro-double helicene-like compound **27** in which two silole-fused [7]helicene-like skeletons are linked through a spiro silicon atom. This compound is expected to maintain the helical structure and show chiral character. The two helicene-like skeletons are arranged symmetrically [D_2-symmetry for (*P*,*P*)- and (*M*,*M*)-**27**; S_4-symmetry for (*P*,*M*)-**27**] and nearly perpendicularly. Different from conventional double helicenes,

the π-conjugation is apparently separated by the spiro silicon atom. In this chapter, the author synthesized a spiro-double helicene-like compound **27** from 3,3'-dibromo-4,4'-biphenanthrene (**1**) and evaluated its photophysical properties through comparison with the previously reported mono silole-fused [7]helicene-like compound **3a**[8] and the related spiro compounds with a silicon spiro atom.

3.2. Synthesis

The spiro-double silole-fused [7]helicene-like compound **27** was synthesized using racemic 3,3'-dibromo-4,4'-biphenanthrene (*rac*-**1**) as a starting material (Scheme 3.1). The dilithiation of the dibromide with BuLi and the following reaction with half equivalent of $SiCl_4$ gave a mixture of racemic [(*P*,*P*)-**27** and (*M*,*M*)-**27**] and meso [(*P*,*M*)-**27**] spiro-double silole-fused [7]helicene-like compounds each in 18% yield. Each isomer of (*P*,*P*)-**27**, (*M*,*M*)-**27**, and (*P*,*M*)-**27** was obtained in pure form by optical resolution with recycling preparative HPLC on a chiral stationary phase (DAICEL

Scheme 3.1. Synthesis of the Spiro-double [7]Helicene-like Compound **27**

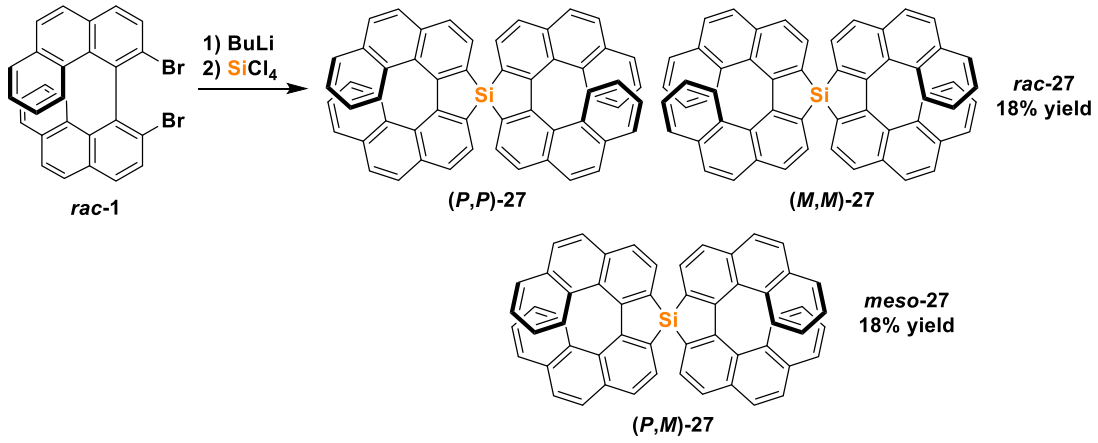

CHRALPAK® IF column). Based on the results discussed in Chapter 2, the preparation of compound **27** via desulfurative dilithiation of thia[7]helicene **7** and the subsequent trapping with $SiCl_4$ was also investigated. The target compound **27** was seemingly formed in a low yield, but its isolation was found to be difficult due to inseparable by-products.

3.3. X-ray crystallographic analysis

The absolute configuration and solid-state structure of each isomer of **27** were identified by single crystal X-ray crystallographic analysis (Figure 3.2 and Table 3.1). Single crystals of each enantiomer [(*P*,*P*) and (*M*,*M*)] of *rac*-**27** were successfully obtained by recrystallization from THF/hexane, and those of (*P*,*M*)-**27** were obtained from $CHCl_3$/hexane. The absolute configuration of the isomer with the shorter HPLC retention time was determined to be (*P*,*P*) by the Flack parameter refinement (data collected by Cu Kα radiation). The degree of torsion of the helical skeleton of each isomer was evaluated by the sum of five dihedral angles [∠C1–C2–C3–C4, ∠C2–C3–C4–C5, ∠C3–C4–C5–C6, ∠C4–C5–C6–C7, and ∠C5–C6–C7–C8]. The total value was found to be 104.2° for each enantiomer (*P*,*P*)-**27** and (*M*,*M*)-**27** and 107.3° for meso isomer (*P*,*M*)-**27**. These values are larger than those of the previously reported [7]helicenes and [7]helicene-like compounds with cyclopentadiene (80.9°–97.8°),[9,10] cyclopentadienone (82.8°–90.7°),[9,10] pyrrole (83.6°),[11] furan (78.9°),[11] phosphole oxide (95.2°–99.6°),[12] or sulfur (88.3°),[13] and almost the same as that of their substructure unit, the silole-fused [7]helicene-like compound **3a** (103.5°).[8] The large helical distorsion would offer high racemization barrier. Indeed, thermal isomerization of **27** did not occur

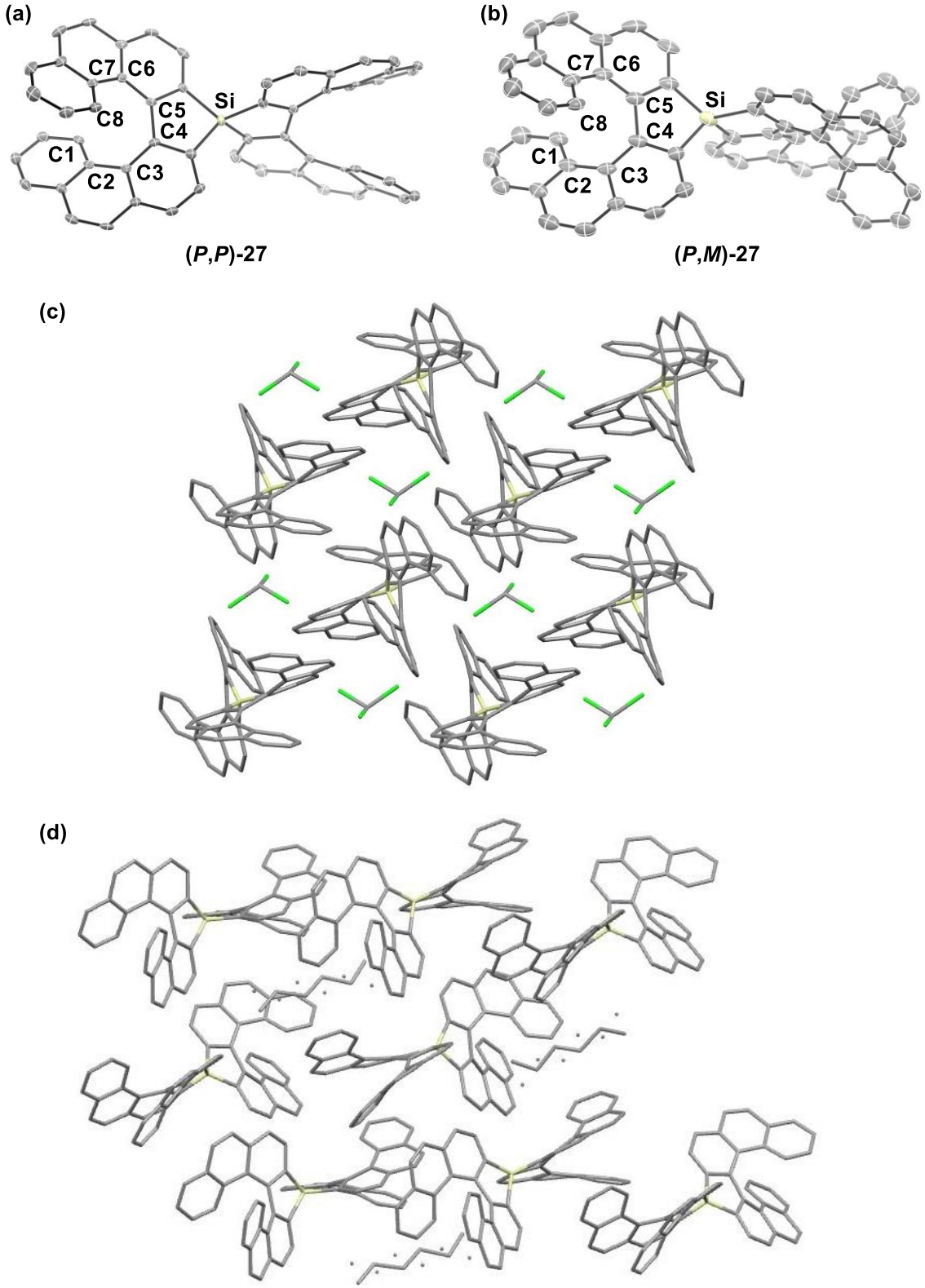

Figure 3.2. ORTEP drawings of (a) (*P,P*)-**27** and (b) (*P,M*)-**27** with thermal ellipsoids at 50% probability (All hydrogen atoms and the crystal solvent molecule are omitted for clarity) and packing structures of (c) *rac*-**27** and (d) (*P,M*)-**27**.

Table 3.1. Crystallographic Data and Structure Refinement Details for **27**

		rac-**27**	(*P*,*M*)-**27**
molecular formula		$C_{56}H_{32}Si{\cdot}CHCl_3$	$C_{56}H_{32}Si{\cdot}0.5C_6H_{14}$
formula weight		852.27	775.99
temperature (K)		93	93
wavelength (Å)		0.71073	0.71073
crystal system		triclinic	monoclinic
space group		$P\bar{1}$	$P2_1/c$
unit cell dimensions	*a* (Å)	10.5082(2)	22.4074(14)
	b (Å)	12.1417(3)	15.1660(8)
	c (Å)	17.2598(5)	24.1554(17)
	α (°)	91.337(2)	90
	β (°)	98.018(2)	92.330(6)
	γ (°)	96.874(2)	90
volume (Å^3)		2163.14(9)	8202.0(9)
Z		2	8
density (calculated) (mg·m^{-3})		1.309	1.257
absorption coefficient (mm^{-3})		0.279	0.099
F(000)		880	3256
theta range for data collection (°)		2.8540 to 28.8060	2.367 to 27.500
index ranges		–13<=*h*<=13	–28<=*h*<=27
		–15<=*k*<=12	–19<=*k*<=19
		–22<=*l*<=22	–31<=*l*<=31
reflections collected		31594	89949
independent reflections		9621	18482
R(int)		0.0546	0.1584
data / restraints / parameters		9621 / 0 / 550	18482 / 76 / 1138
goodness-of-fit on F^2		1.179	1.131
final *R* indices [$I>2\sigma(I)$]	R_1	0.0979	0.1190
	wR_2	0.2174	0.2039
R indices (all data)	R_1	0.1132	0.2070
	wR_2	0.2225	0.2339
largest diff. peak and hole (e/Å^3)		1.126, –1.382	1.096, –0.314

after heating at 200 °C for 48 h in chlorobenzene, and compound **27** perfectly decomposed by further heating. The C–Si bond lengths within the silole rings of **27** are slightly shorter than those of the related silole-fused compounds **3a**[8] and **28**–**30**[14,15] (Table 3.2). The shortening of C–Si bonds in compound **27** is seemingly attributed to the helical torsion which is induced by angular annulation of the silole and benzene rings.

Moreover, DFT caluculations indicates that the s-character of C–Si bond in **27** (24.99%, on Si atom) is larger than that of **3a** (23.67%), affording the shorter C–Si bonds in **27** (Table 3.3).

Table 3.2. Selected Bond Lengths and Angles for **27**, **3a**, and **28**–**30**

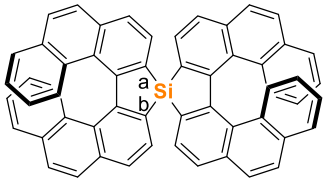

(*P,P*)-27

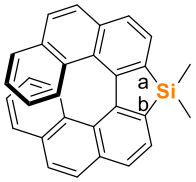

3a

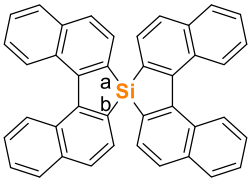

28

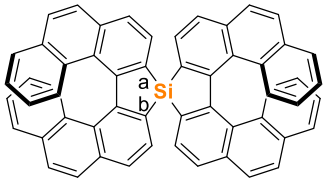

(*P,M*)-27

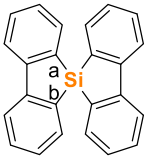

29

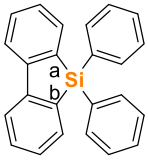

30

	Si–C(a)[a] (Å)	Si–C(b)[a] (Å)	∠C(a)–Si–C(b)[a] (°)
(*P*,*P*)-**27**	1.853(4), 1.857(5)	1.847(5), 1.857(5)	92.9(2), 91.5(2)
(*P*,*M*)-**27**	1.851(5), 1.858(5)	1.857(5), 1.852(5)	91.8(2), 92.1(2)
3a[b]	1.881(7)	1.890(7)	91.5(3)
28[c]	1.866, 1.869	1.866, 1.869	91.1, 91.8
29[d]	1.869, 1.880	1.869, 1.880	92.09, 92.09
30[d]	1.874(1)	1.872(1)	91.56(6)

[a]C(a) and C(b) refer the carbon atoms adjacent to the silicon atom in the silafluorene moiety. [b]Reference 8. [c]Reference 14. [d]Reference 15

Table 3.3. Hybridizations of Selected Bonds of (*P,P*)-**27** and (*P*)-**3a** Calculated at the M06/6-31G(d,p) Level of Theory

	bond	length (Å)	atom	s-character (%)	p-character (%)	d-character (%)
(*P*,*P*)-**27**	C–Si	1.867	Si	24.99	73.90	1.11
			C	30.76	69.23	0.02
(*P*)-**3a**	C(Ar)–Si	1.874	Si	23.67	75.07	1.26
			C	31.31	68.67	0.02
	C(Me)–Si	1.877	Si	26.34	72.57	1.09
			C	29.62	70.36	0.02

3.4. Photophysical properties

3.4.1. Absorption and fluorescence properties

The photophysical properties of **27** were evaluated by UV–vis absorption and PL spectroscopies (Figure 3.3). The longest absorption maxima for (*P*,*P*)-**27**, (*P*,*M*)-**27**, and **3a** in CH_2Cl_2 were almost the same (415 nm, 414 nm, and 412 nm, respectively). On the other hand, the absorption edge of both isomers of **27** (445 nm) are slightly red-shifted compared to that of **3a** (431 nm). The PL maxima were observed at 469 nm for (*P*,*P*)-**27** and at 464 nm for (*P*,*M*)-**27**, both of which are observed at a noticeably longer wavelength than that of **3a** (450 nm).[8] The absorption bands and emission bands of **27** were slightly red-shifted compared to those of the silole-fused double [5]helicene-like compound **28** and significantly red-shifted compared to those of silabi[fluorene] **29**, owing to the extended π-conjugation of **27**.

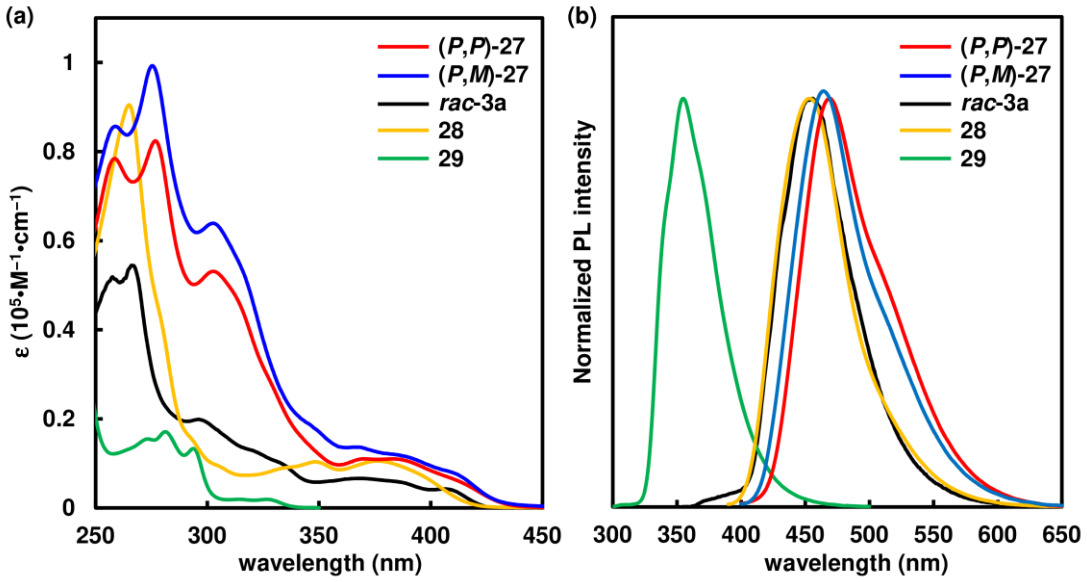

Figure 3.3. (a) UV–Vis absorption and (b) normalized fluorescence spectra of (*P*,*P*)-**27**, (*P*,*M*)-**27**, *rac*-**3a**, **28**, and **29** in CH_2Cl_2.

3.4.2. Chiroptical properties

The specific rotation $[\alpha]_D$ of (*M*,*M*)-**27** is −1250 (*c* = 0.10, $CHCl_3$), of which absolute value is lower than that of (*P*)-**3a** (+2980, *c* = 0.10, $CHCl_3$). The CD and CPL properties were also evaluated (Figure 3.4). The CD spectrum of (*P*,*P*)-**27** exhibited a large positive cotton effect at 339 nm and small and large negative cotton effects at 302 nm and 256 nm, respectively. The dissymmetry factor of absorption (g_{abs}) was determined to be 2.2×10^{-2} at 339 nm, which was double of that of (*P*)-**3a** (1.1×10^{-2} at 331 nm). Enantiopure (*P*,*P*)-**27** and (*M*,*M*)-**27** showed mirror-image CPL signals. The dissymmetry factor (g_{lum}) was also determined to be 2.3×10^{-3} at 486 nm, which was slightly lower than that of **3a** ($g_{lum} = 3.5 \times 10^{-3}$).

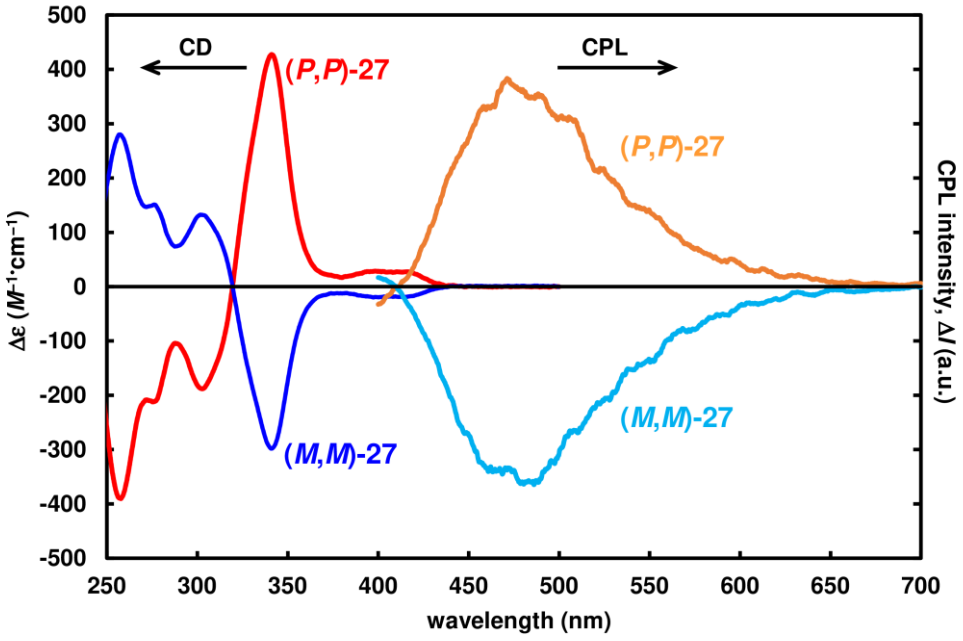

Figure 3.4. CD and CPL spectra of (*P*,*P*)-**27** and (*M*,*M*)-**27**.

3.5. Theoretical calculations

Theoretical calculations were conducted for the spiro-double silole-fused [7]helicene-like compound (*P*,*P*)-**27** and the mono silole-fused [7]helicene-like compounds (*P*)-**3a**, (*P*)-**3b**, (*P*)-**31** with dimethylsilylene, diphenylsilylene, and silafluorenylene moieties, respectively, to compare their HOMO and LUMO energy levels (Figure 3.5). For these compounds, the HOMO distributions and energy levels were almost the same [−5.51 eV for (*P*,*P*)-**27**, −5.48 eV for (*P*)-**3a**, −5.51 eV for (*P*)-**3b**, and −5.56 eV for (*P*)-**31**]. In contrast, the LUMO energy levels of (*P*,*P*)-**27** was ≥0.16 eV lower than those of (*P*)-**3a**, (*P*)-**3b**, and (*P*)-**31** (−1.70 vs −1.40, −1.51, and −1.54 eV, respectively). Therefore, the HOMO–LUMO energy gap of (*P*,*P*)-**27** (ΔE_{calc}: 3.81 eV) was smaller than that of (*P*)-**3a** (ΔE_{calc}: 4.07 eV), which agree well with the experimental

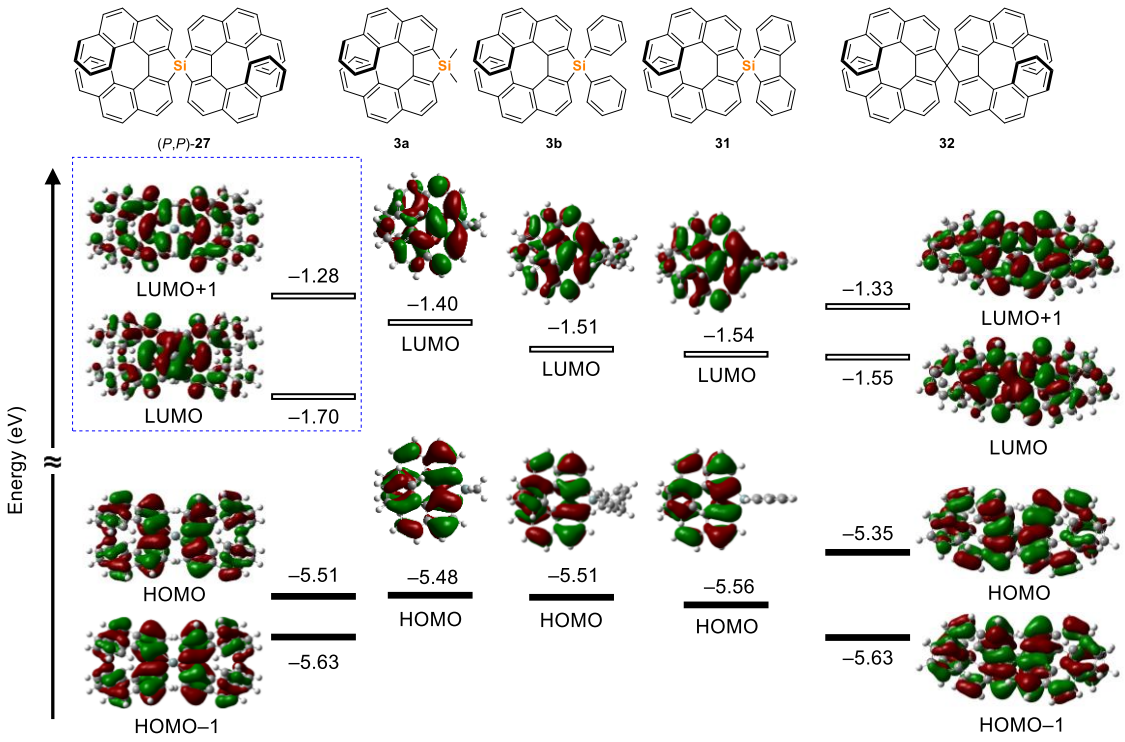

Figure 3.5. Molecular orbitals and their energies of (*P,P*)-**27**, (*P*)-**3a**, (*P*)-**3b**, (*P*)-**31**, and (*P,P*)-**32** based on DFT calculations at th M06/6-31G(d,p) level.

HOMO–LUMO energy gaps estimated from the absorption edges [ΔE_{exp}: 2.78 eV for (*P,P*)-**27** and 2.88 eV for **3a**].

The difference in LUMO energy levels between the silole-fused spiro-double [7]helicene-like compound (*P*,*P*)-**27**, mono [7]helicene-like compounds (*P*)-**3a**, (*P*)-**3b**, and (*P*)-**31** can be explained by the specific effects of spiro compounds.[16,17] The LUMO of (*P*,*P*)-**27** delocalizes over the silafluorene unit through the σ*–π* conjugation between the σ^* orbitals of C–Si bonds and the π* orbitals of the butadiene moieties in the silole units, thus lowering its LUMO energy level.[15] Such effect cannot not be achieved in (*P*)-**3a** and (*P*)-**3b** since they do not contain the second silole moiety. Compound (*P*)-**31** contains a silafluorene moiety like (*P*,*P*)-**27**, but its LUMO energy level is much higher than that of (*P*,*P*)-**27**. Therefore, the lower LUMO energy level of (*P*,*P*)-**27** would further be attributed to the spiro-double helical geometry.

In order to elucidate the characteristics of the LUMO of (*P*,*P*)-**27**, the LUMO and LUMO+1 of (*P*,*P*)-**27** were compared with those of achiral spirosilabi[fluorene] **29** (Figure 3.6). Although the LUMO and LUMO+1 are degenerated in **29**, they split by 0.42 eV in (*P*,*P*)-**27** to afford the lower-lying LUMO in (*P*,*P*)-**27**. This difference would be attributed to the degree of the overlap of the π* orbitals in the spiro-fused silole moieties. As shown in Figure 3.6b, the angle between the two silole units is inclines from vertical owing to the twisting of the helical structure [the angles formed between two straight lines were 96.2° for C(a)–C(b) and C(e)–C(f), 118.2° for C(c)–C(d) and C(g)–C(h)]. This incline stabilizes the combination of the matched sign (LUMO) and destabilizes the combination of the mismatched sign (LUMO+1), affording the LUMO/LUMO+1 splitting.[18] The LUMO/LUMO+1 splitting can also be observed in the related spiro-double helicene-like compound (*P*,*P*)-**32** with a carbon spiro center

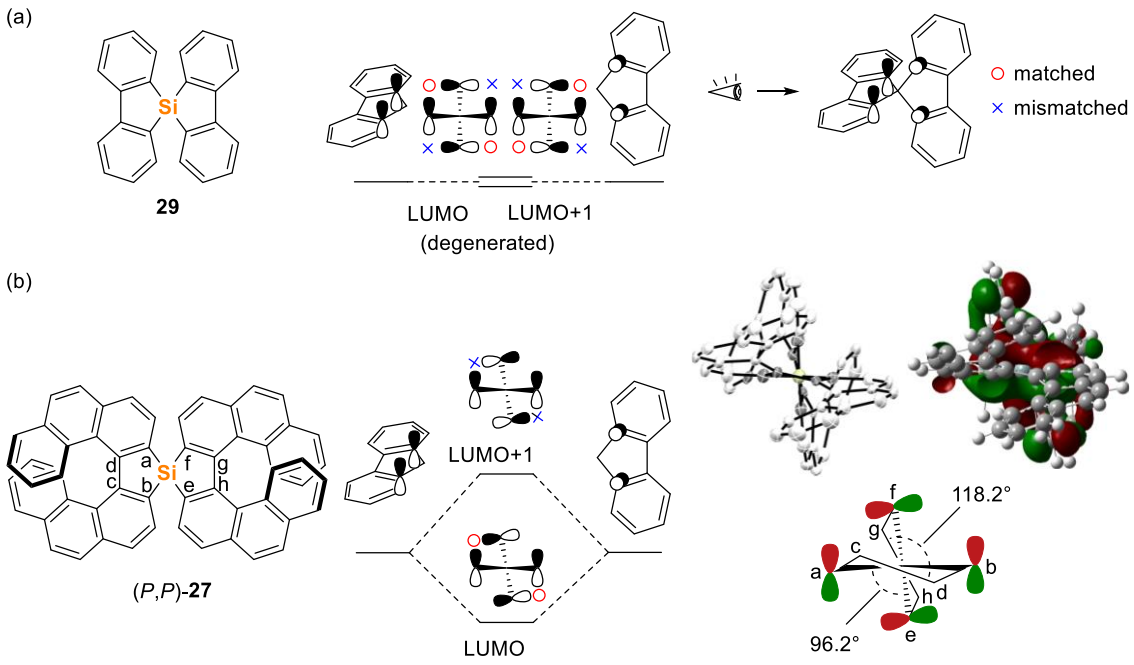

Figure 3.6. (a) Modeling of LUMO and LUMO+1 formed by p orbitals of butadiene moieties of **29**. (b) Modeling of LUMO and LUMO+1, X-ray crystallographic structure, calculated LUMO distributions (those in front of the C(a) and C(b) atoms are omitted), and modeling of geometry of (*P*,*P*)-**27** seen from the same direction.

(Figure 3.5). However, its LUMO–LUMO+1 energy gap (0.22 eV) is much smaller than that of (*P*,*P*)-**27**. Therefore, the stabilizing effect described above also requires participation of not only π* orbitals but also σ* orbitals of the C–Si bonds in (*P*,*P*)-**27**. Furthermore, the splitting of HOMO and HOMO–1 was found to be remarkable for (*P*,*P*)-**32**, which should be due to the shorter spiro-C(sp^3)–C(sp^2) bond lengths of (*P*,*P*)-**32** than spiro-Si(sp^3) –C(sp^2) bond lengths of (*P*,*P*)-**27**. Therefore, the spiro-double helical geometry tunes the LUMO or HOMO energy levels depending on the degree of torsion and the kind of a spiro atom and differs from conventional conjugated double helicenes, which exhibit narrower band gap (higher HOMO and lower LUMO energy levels) when they consist of larger number of fused aromatic rings.

The absorption and emission properties of (*P*,*P*)-**27** can also be explained based on

the TD–DFT calculation results. The longest absorption band at around 400 nm for (*P,P*)-**27** was assigned to the HOMO → LUMO transition (411 nm, f_{calc}: 0.020, 91%) and HOMO−1 → LUMO transition (395 nm, f_{calc}: 0.1262, 82%) (Table 3.4). In the PL spectra (Figure 3.3b), emission maxima were observed at 469 nm for (*P*,*P*)-**27** and at 464 nm for (*P*,*M*)-**27**, which are much longer wavelength than that of **3a** (450 nm). For the lowest excited states (S_1) of (*P,P*)-**27** and (*P*)-**3a**, the frontier orbital distributions in their optimized structures are shown in Figure 3.7. The HOMO–LUMO energy gap of (*P,P*)-**27** (ΔE_{calc}: 3.14 eV) in the S_1 state is smaller than that of (*P*)-**3a** (ΔE_{calc}: 3.22 eV), which is in agreement with the comparatively red-shifted PL spectrum of (*P*,*P*)-**27**.

Table 3.4. The Selected Absorption of (*P*,*P*)-**27** Calculated by TD−DFT Method at the M06/6-31G(d,p) Level of Theory

excited state	transition energy (eV)	wavelength (nm)	main transition configuration (CI expansion coefficient)	oscillator strength, *f*
1	3.0184	411	HOMO → LUMO (0.67628) HOMO−1 → LUMO+1 (0.15410)	0.0200
2	3.1386	395	HOMO−1 → LUMO (0.63852) HOMO → LUMO+1 (0.21413)	0.1262
3	3.2982	376	HOMO−2 → LUMO (0.51456) HOMO → LUMO+3 (–0.29825)	0.0000
4	3.3119	374	HOMO−3 → LUMO (0.40842) HOMO → LUMO+2 (–0.34280)	0.0110
5	3.5122	353	HOMO → LUMO+1 (0.57244) HOMO−1 → LUMO (–0.27452)	0.0105
6	3.5451	350	HOMO−1 → LUMO+1 (0.39559) HOMO → LUMO+3 (–0.35281)	0.0256
7	3.5705	347	HOMO → LUMO+2 (0.44681) HOMO−3 → LUMO (0.46589)	0.0865
8	3.5738	347	HOMO−4 → LUMO (0.57657) HOMO−5 → LUMO+1 (–0.21469)	0.0000
9	3.5980	345	HOMO−5 → LUMO (–0.52666) HOMO−4 → LUMO+1 (–0.26538)	0.0709
10	3.6509	340	HOMO−1 → LUMO+1 (0.50899) HOMO−1 → LUMO+2 (–0.32240)	0.0349

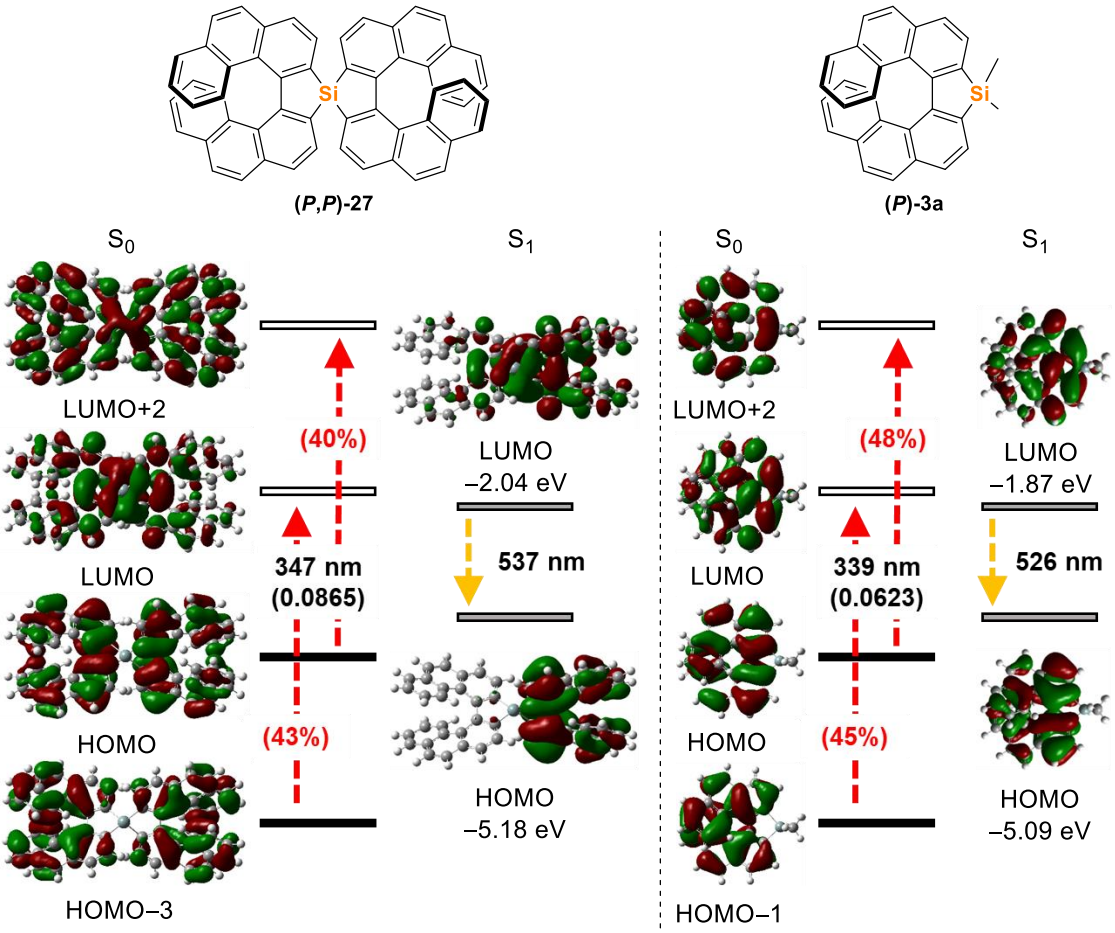

Figure 3.7. Molecular orbitals and energy diagrams of (*P,P*)-**27** (left) and (*P*)-**3a** (right) in the ground state (S_0) and the excited state (S_1) based on TD–DFT calculations at the M06/6-31G(d,p) level. Transitions related to CD and CPL are shown.

The enhancement of g_{abs} value of (*P,P*)-**27** described above can also be explained based on the TD–DFT calculation results. The signals around 350 nm are almost equally contributed by the HOMO → LUMO+2 transition and the HOMO−3 → LUMO transition (347 nm, f_{calc} = 0.0865; Table 3.4 and Figure 3.7). As shown in Figure 3.8, the LUMO and LUMO+2 have a larger distribution on the spiro silicon atom compared to other unoccupied molecular orbitals. Therefore, the CD absorption of **27** is derived from the transition from the π-conjugated orbital of the biphenanthrene unit to the silicon-involved

orbital on both sides of the spiro-double helicene-like skeleton, not just one helicene unit, exhibiting the enhanced g_{abs} value. The frontier orbital distributions of **27** in the S_1 state is localized on a single helicene-like unit (HOMO and LUMO; Figure 3.7). Therefore, the emission of **27** occurs mainly in a single helicene-like unit and show a similar g_{lum} value in CPL to that of the mono helicene-like compound **3a**.

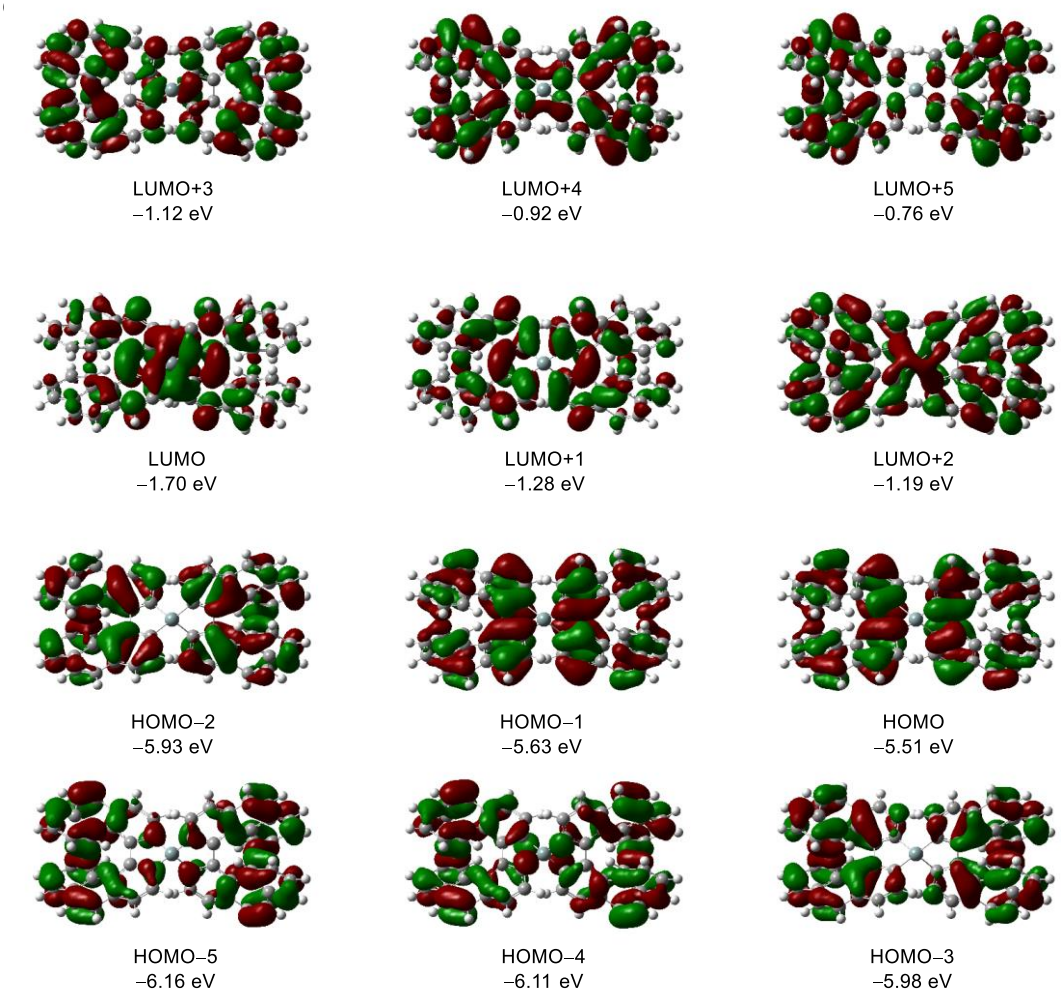

Figure 3.8. Molecular orbitals of (*P,P*)-**27** calculated at the M06/6-31G(d,p) level of theory.

3.6. Conclusion

The spiro-double silole-fused [7]helicene-like compound was successfully synthesized from 3,3'-dibromo-4,4'-biphenanthrene, and photophysical properties were evaluated. This is the first report of a spiro compound with a helicene-like unit which can maintain chiral character. Compared to the previously reported mono silole-fused [7]helicene-like compound, the LUMO energy level is lowered due to the effect of LUMO spiro-conjugation. The helicene-like structure twists the central silole rings, which contributes to stabilization of the LUMO.

3.7. Experimental section

3.7.1. General

All manipulations involving air- and/or moisture-sensitive compounds were carried out with the standard Schlenk technique under argon. Analytical thin-layer chromatography was performed on a glass plate coated with 0.25-mm 230–400-mesh silica gel containing a fluorescent indicator. Column chromatography was performed by using silica gel (spherical neutral, particle size: 63–210 μm). Most of reagents were purchased from commercial suppliers, such as Sigma-Aldrich Co. LLC, Tokyo Chemical Industry Co., Ltd., and Kanto Chemical Co., Inc., and used without further purification unless otherwise specified. Commercially available anhydrous solvents were used for air- and/or moisture sensitive reactions.

NMR spectra were recorded in $CDCl_3$ on a JEOL ECA500 spectrometer (^1H 500 MHz, ^{13}C 126 MHz). Chemical shifts are reported in ppm relative to the internal standard peak (0 ppm for Me_4Si) for ^1H, the deuterated solvent peak (77.16 ppm for $CDCl_3$) for ^{13}C. Data are presented in the following space: chemical shift, multiplicity (d = doublet), coupling constant in hertz (Hz), and signal area integration in natural numbers. High resolution mass spectra are taken with Bruker Daltonics micrOTOF-QII mass spectrometer by atmospheric pressure chemical ionization-time-of-flight (APCI–TOF) method. UV–Vis absorption spectra were recorded on SHIMADZU UV–3150 spectrophotometer or a JASCO V–650 spectrophotometer. Photoluminescence spectra were recorded on JASCO FP–6500 spectrofluorometer. Absolute quantum yields were determined by absolute quantum yield system with a JASCO ILF–533 integrating sphere which were attatched to a JASCO FP–6500 spectrometer. Optical rotations were measured on a JASCO P–1010 spectrometer using a 10 × 10 mm rectangular quartz cell. CD spectra were recorded on a JASCO model J–820 spectrometer. CPL spectra were measured by using a JASCO CPL–300 spectrophotometer. X-ray crystallographic analysis was performed by RIGAKU VariMax Dual with Saturn diffractometer. HPLC analyses were carried out using a DAICEL CHIRALPAK® IA-3 column(4.6 mm × 250 mm), IC column (4.6 mm × 250 mm), and IF column (4.6 mm × 250 mm).

3.7.2. Synthetic procedure

9,9′-Spirobi[biphenanthro[3,4-*b*:4′,3′-*d*]silole]) (27). To a solution of 3,3'-dibromo-4,4'-biphenanthrene (255 mg, 0.50 mmol) in DME (14 mL) was slowly added BuLi (1.57 M solution in hexane, 0.69 mL, 1.08 mmol) at –64 °C and stirred for 2 h.

$SiCl_4$ (0.29 M solution in DME, 0.86 mL, 0.26 mmol) was slowly added to the reaction mixture, and the resulting mixture was warmed to room temperature and stirred for 18 h. Then, the reaction was quenched with water and the mixture was extracted with Et_2O. The combined organic layers were washed with brine, dried over Na_2SO_4, filtered, and concentrated under reduced pressure. The crude residue was purified by silica-gel column chromatography with CH_2Cl_2/hexane (1/4) as an eluent to give *rac*-**27** [(*P,P*)-**27** and (*M,M*)-**27**] and (*P,M*)-**27** (139 mg, 18%, respectively). The mixture of *rac*-**27** and *meso*-**27** were separated into (*P,P*)-**27**, (*M,M*)-**27**, and (*P,M*)-**27** by HPLC with DAICEL CHRALPAK® IF column (4.6 mm × 250 mm) [t_R = 22 min for (*P,P*)-**27**, (*P,M*)-**27** for 24 min, 27 min for (*M,M*)-**27** (flow rate: 5.0 mL/min; solvent: $CHCl_3$/hexane = 1/9]. (*P,P*)-**27** and (*M,M*)-**27**: ^{1}H NMR (500 MHz, $CDCl_3$) δ 7.68 (d, *J* = 7.5 Hz, 4H), 7.65 (d, *J* = 8.5 Hz, 4H), 7.57 (d, *J* = 7.5 Hz, 4H), 7.56 (d, *J* = 7.5 Hz, 4H), 7.55 (d, *J* = 7.5 Hz, 4H), 7.38 (dd, *J* = 8.0, 1.0 Hz, 4H), 7.01 (ddd, *J* = 7.5, 7.5, 1.0 Hz, 4H), 6.45 (ddd, *J* = 8.3, 7.5, 1.4 Hz, 4H); ^{13}C NMR (126 MHz, $CDCl_3$) δ 150.8, 135.1, 134.1, 132.1, 130.3, 130.1, 129.2, 128.1, 127.8, 126.7 126.5, 126.2, 125.1, 123.1; HRMS–APCI$^+$ (*m*/*z*) calcd for $C_{56}H_{32}Si^+$ (M^+) 732.2268, found 732.2285 for (*P*,*P*)-**27**, found 732.2286 for (*M*,*M*)-**27**; (*P,M*)-**27**: ^{1}H NMR (500 MHz, $CDCl_3$) δ 7.73 (d, *J* = 7.5 Hz, 4H), 7.67 (d, *J* = 8.5 Hz, 4H), 7.65 (d, *J* = 7.0 Hz, 4H), 7.58 (d, *J* = 9.0 Hz, 4H), 7.54 (d, *J* = 8.0 Hz, 4H), 7.39 (dd, *J* = 8.0, 1.0 Hz, 4H), 7.01 (ddd, *J* = 7.5, 1.0 Hz, 4H), 6.44 (ddd, *J* = 7.5, 1.4 Hz, 4H); ^{13}C NMR (126 MHz, $CDCl_3$) δ 151.1, 135.2, 133.5, 132.2, 130.3, 130.1, 129.3, 128.3, 127.9, 126.9 126.6, 126.4, 125.3, 123.3; HRMS–APCI$^+$ (*m*/*z*) calcd for $C_{56}H_{32}Si^+$ (M^+) 732.2268, found 732.2275.

3.7.3. Theoretical calculations

DFT calculations were performed using workstation at Research Center for Computational Science, National Institutes of Natural Sciences, Okazaki, Japan. All the calculations were performed by using Gaussian 09 Program, revision E.01.3.[19]

3.8. References

(1) Nakamura, K.; Furumi, S.; Takeuchi, M.; Shibuya, T.; Tanaka, K. *J. Am. Chem. Soc.* **2014**, *136*, 5555–5558.

(2) Sakamaki, D.; Kumano, D.; Yashima, E.; Seki, S. *Angew. Chem. Int. Ed.* **2015**, *54*, 5404–5407.

(3) Fujikawa, T.; Segawa, Y.; Itami, K. *J. Am. Chem. Soc.* **2015**, *137*, 7763–7768.

(4) Wang, X. Y.; Wang, X. C.; Narita, A.; Wagner, M.; Cao, X. Y.; Feng, X.; Müllen, K. *J. Am. Chem. Soc.* **2016**, *138*, 12783–12786.

(5) Hu, Y.; Wang, X. Y.; Peng, P. X.; Wang, X. C.; Cao, X. Y.; Feng, X.; Müllen, K.; Narita, A. *Angew. Chem. Int. Ed.* **2017**, *56*, 3374–3378.

(6) Fujikawa, T.; Segawa, Y.; Itami, K. *J. Org. Chem.* **2017**, *82*, 7745–7749.

(7) Li, C.; Wu, L.; Xu, W.; Song, J.; Shi, J.; Yu, P.; Kan, Y.; Wang, H. *J. Org. Chem.* **2015**, *80*, 11156–11161.

(8) Oyama, H.; Nakano, K.; Harada, T.; Kuroda, R.; Naito, M.; Nobusawa, K.; Nozaki, K. *Org. Lett.* **2013**, *15*, 2104–2107.

(9) Sawada, Y.; Furumi, S.; Takai, A.; Takeuchi, M.; Noguchi, K.; Tanaka, K. *J. Am. Chem. Soc.* **2012**, *134*, 4080–4083.

(10) Oyama, H.; Akiyama, M.; Nakano, K.; Naito, M.; Nobusawa, K.; Nozaki, K. *Org. Lett.* **2016**, *18*, 3654–3657.

(11) Nakano, K.; Hidehira, Y.; Takahashi, K.; Hiyama, T.; Nozaki, K. *Angew. Chem. Int. Ed.* **2005**, *44*, 7136–7138.

(12) Nakano, K.; Oyama, H.; Nishimura, Y.; Nakasako, S.; Nozaki, K. *Angew. Chem. Int. Ed.* **2012**, *51*, 695–699.

(13) Dore, A.; Fabbri, D.; Gladiali, S.; Valle, G. *Tetrahedron: Asymmetry* **1995**, *6*, 779–788.

(14) Russell, A. G.; Spencer, N. S.; Philp, D.; Kariuki, B. M.; Snaith, J. S. *Organometallics* **2003**, *22*, 5589–5592.

(15) Pusztai, E.; Toulokhonova, I. S.; Temple, N.; Albright, H.; Zakai, U. I.; Guo, S.; Guzei, I. A.; Hu, R.; West, R. *Organometallics* **2013**, *32*, 2529–2535.

(16) Lee, S. H.; Jang, B.; Kafafi, Z. H. *J. Am. Chem. Soc.* **2005**, *127*, 9071–9078.

(17) Hamada, H.; Nakamuro, T.; Yamashita, K.; Yanagisawa, H.; Nureki, O.; Kikkawa, M.; Harano, K.; Shang, R.; Nakamura, E. *Bull. Chem. Soc. Jpn.* **2020**, *93*, 776–782.

(18) Zhu, K.; Kamochi, K.; Kodama, T.; Tobisu, M.; Amaya, T. *Chem. Sci.,* **2020**, *11*, 9604–6910.

(19) Frisch, M. J.; Trucks, G. W.; Schlegel, H. B.; Scuseria, G. E.; Robb, M. A.;

Cheeseman, J. R.; Scalmani, G.; Barone, V.; Mennucci, B.; Petersson, G. A.; Nakatsuji, H.; Caricato, M.; Li, X.; Hratchian, H. P.; Izmaylov, A. F.; Bloino, J.; Zheng, G.; Sonnenberg, J. L.; Hada, M.; Ehara, M.; Toyota, K.; Fukuda, R.; Hasegawa, J.; Ishida, M.; Nakajima, T.; Honda, Y.; Kitao, O.; Nakai, H.; Vreven, T.; Montgomery, Jr., J. A.; Peralta, J. E.; Ogliaro, F.; Bearpark, M.; Heyd, J. J.; Brothers, E.; Kudin, K. N.; Staroverov, V. N.; Keith, T.; Kobayashi, R.; Normand, J.; Raghavachari, K.; Rendell, A.; Burant, J. C.; Iyengar, S. S.; Tomasi, J.; Cossi, M.; Rega, N.; Millam, J. M.; Klene, M.; Knox, J. E.; Cross, J. B.; Bakken, V.; Adamo, C.; Jaramillo, J.; Gomperts, R.; Stratmann, R. E.; Yazyev, O.; Austin, A. J.; Cammi, R.; Pomelli, C.; Ochterski, J. W.; Martin, R. L.; Morokuma, K.; Zakrzewski, V. G.; Voth, G. A.; Salvador, P.; Dannenberg, J. J.; Dapprich, S.; Daniels, A. D.; Farkas, O.; Foresman, J. B.; Ortiz, J. V.; Cioslowski, J.; Fox, D. J. Gaussian 09, Revision E.01, Gaussian, Inc., Wallingford CT, **2013**.

Chapter 4

Synthesis and Properties of [7]Helicenes and [7]Helicene-like Compounds with a Cyclopenta[1,2-*b*:4,3-*b*']dithiophene or Dithieno[2,3-*b*:3',2'-*d*]heterole Skeleton

1,1'-Binaphtho[2,1-*b*]thiophene was designed and successfully synthesized as a precursor that can give the dianion species via lithiation. [7]helicenes and [7]helicene-like compounds with a cyclopenta[1,2-*b*:4,3-*b*']dithiophene or dithieno[3,2-*b*:3',2'-*d*]heterole skeleton were successfully synthesized from the precursor. Absorption and fluorescence properties of them were evaluated and compared with those of their benzene analogues. Theoretical calculations were performed to better understand their photophysical properties. In addition, X-ray crystallographic analysis was used to compare the structural difference caused by the five-membered rings between the two thiophene rings.

4.1. Introduction

In order to obtain the helicene structure efficiently, the syntheses utilizing the dianion **2** from thia[7]helicene **7** or 3,3'-dibromo-4,4'-biphenanthrene **1** were investigated in Chapters 2 and 3. For expanding the scope of this strategy, 1,1'-binaphtho[2,1-*b*]thiophene (**33**) was designed as a common precursor in this chapter. The α-position of a thiophene ring is known to be easily lithiated by lithium reagents. Therefore, the author envisaged that the dianion species **34**, which is the thiophene analog of the dionion **2**, would be formed by lithiation of compound **33** and react with dielectrophiles to give the corresponding [7]helicenes and [7]helicene-like compounds (Figure 4.1). The resulting helical compounds are the thiophene analogues of the [7]helicenes and [7]helicene-like compounds ever reported and discussed in Chapter 2. Accordingly, the evaluation of their photophysical properties would lead to a better understanding of structure–property relationship of [7]helicenes and [7]helicene-like compounds.

On the basis of this working hypothesis, the author synthesized 1,1'-binaphtho[2,1-*b*]thiophene (**33**) and applied it to the synthesis of [7]helicenes and [7]helicene-like compounds in this chapter. The solid-state structures of the obtained [7]helicenes and [7]helicene-like compounds were elucidated by X-ray crystallographic analysis. The

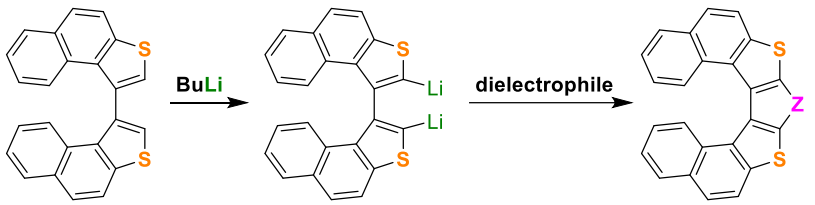

Figure 4.1. Working hypothesis for synthesizing thiophene-fused [7]helicenes and [7]helicene-like compounds from 1,1'-binaphtho[2,1-*b*]thiophene **33**.

photophysical properties were evaluated by UV–vis absorption and PL spectroscopies. Theoretical calculations were also performed to understand the experimental photophysical properties.

4.2. Synthesis

1,1′-Binaphtho[2,1-*b*]thiophene (**33**) used as a common precursor for [7]helicenes and [7]helicene-like compounds was synthesized as shown in Scheme 4.1. First, compound **36** was synthesized by Negishi cross-coupling reaction with 3,4-dibromothiophene and the arylzinc reagent **35** and the subsequent deprotection in 59% yield (2 steps). Then, Wittig reaction with **36** and Ph_3P=CHOMe and the following acid-promoted cyclization gave 1-bromonaphtho[2,1-*b*]thiophene (**37**) in 53% yield (2 steps).[1] Finally, the target compound **33** was obtained by the consecutive palladium-catalyzed borylation and Suzuki–Miyaura coupling reaction in 80% yield.

Scheme 4.1. Synthesis of 1,1′-Binaphtho[2,1-*b*]thiophene (**33**)

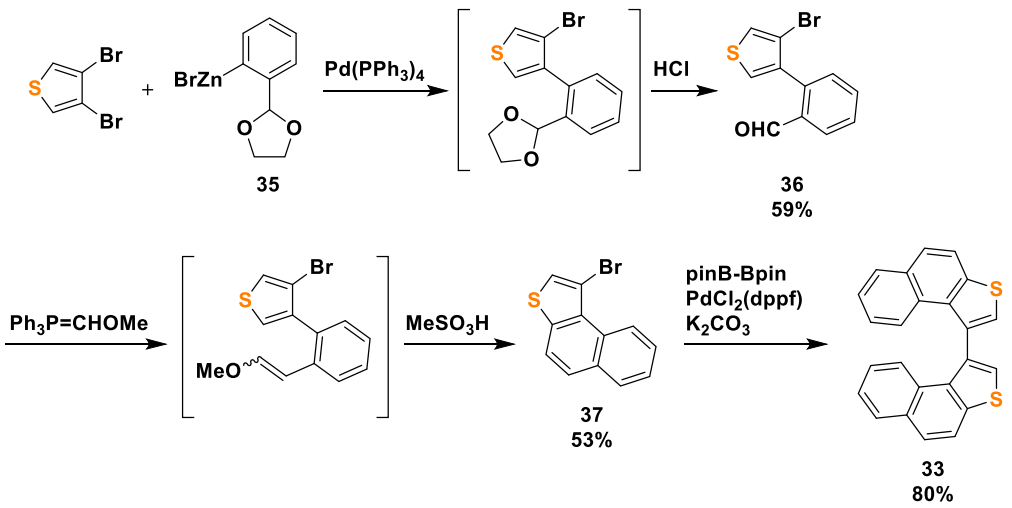

The reaction of the dianion **34** with a dielectrophile was well demonstrated by using dichlorophosphine (Scheme 4.2). Compound **33** was treated with 2.4 equivalnts of BuLi in Et_2O, affording the corresponding dianion species. After the dianion reacted with dichlorophenylphosphine, the resulting phosphole unit was oxidized with H_2O_2 to give the phosphole oxide-fused [7]helicene-like compound **38** in 16% yield.

Next, methyl chloroformate was used as a carbon-centered dielectrophile. The reaction with the dianion **34** with methyl chloroformate was expected to give the cyclopentadienone-fused [7]helicene-like compound, 8*H*-cyclopenta[1,2-*b*:4,3-*b*′]dinaphtho[1,2-*d*:1′,2′-*d*′]dithiophen-8-one (**39**), in one step (Scheme 4.2). However, it was found that one of the thiophene moieties reacted with methyl chloroformate, affording the ester **40** in 79% yield. Therefore, the resulting ester **40** was converted to [7]helicene-like compounds **42** in two steps. First, the tertiary alcohols **41a** and **41b** were synthesized in 87% and 84% yield, respectively, by the reaction with the

Scheme 4.2. Synthesis of [7]Helicene-like Compounds from **33**

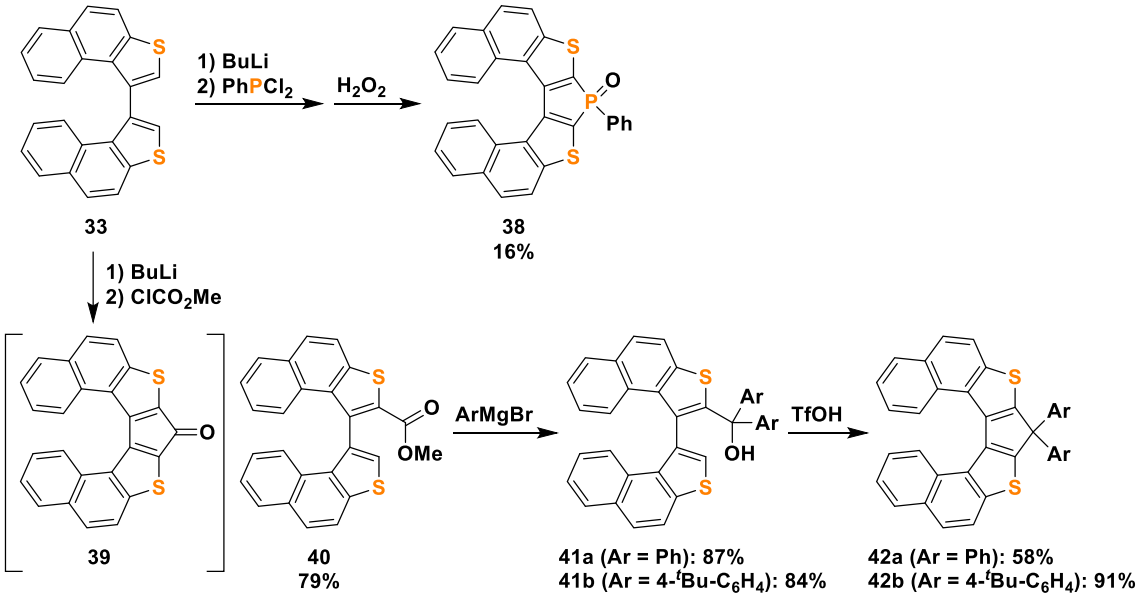

corresponding aryl Grignard reagents. Then, the acid-promoted Friedel–Crafts-type intramolecular cyclization of them provided cyclopentadiene-fused [7]helicene-like compounds **42a** and **42b** in 78% and 91% yield, respectively.[2]

Pyrrole-fused [7]helicenes **45a** and **45b** were also synthesized from the ester **40** (Scheme 4.3). It is difficult to form a pyrrole ring by reaction with the dianion **34** with a nitrogen dielectrophile directly. Therefore, a nitrogen atom was first introduced on one of the thiophene moiety via demethylation of **40** and the subsequent Crutius rearrangement (71% yield). Then, the resulting amine **43** was converted to the carbamate **44a** and the amide **44b**. Finally, pyrrole-fused [7]helicenes **45a** and **45b** were obtained in 11% and 18% yields, respectively, by the palladium-catalyzed intramolecular C–N bond forming reaction.[3]

The optical resolution of **42** and **45** was unsuccessful due to their fast racemization at room temperature. On the other hand, enantiopure **38** was successfully obtained by optical resolution using preparative HPLC on a chiral stationary phase.

Scheme 4.3. Synthesis of Aza[7]Helicenes from **40**

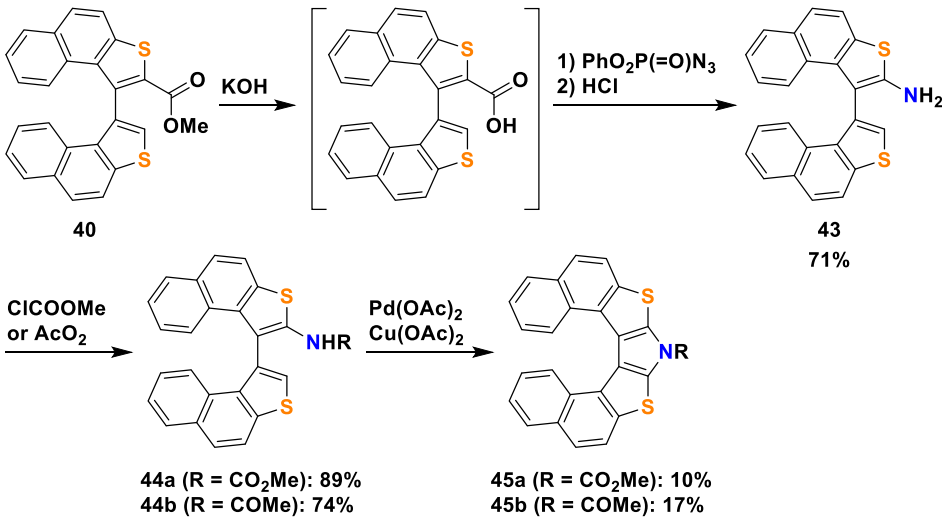

4.3. X-ray crystallographic analysis

The solid-state structures of the obtained [7]helicenes and [7]helicene-like compounds **38**, **42b**, and **45b** were revealed by X-ray crystallographic analysis (Figures 4.2 and 4.3, Table 4.1). All of these compounds were found to form helical structures. The sums of the five dihedral angles derived from the inner C–C bonds [∠C1–C2–C3–C4, ∠C2–C3–C4–C5, ∠C3–C4–C5–C6, ∠C4–C5–C6–C7, and ∠C5–C6–C7–C8], which should be related to the degree of their twisting, are 61.9° (**38**), 56.9° (**42b**), and 57.4° (**45b**). The phosphole oxide-fused helicene-like compound **38** has a more twisted structure than **42b** and **45b**. Such a more twisted structure of **38** would be induced by the larger steric repulsion between the benzene rings at the both edges of the helical skeletons. The longer C–P bond length (1.81 Å) than those of C–C (1.52 Å) and C–N (1.39 Å) bonds within the central five-membered rings would cause such a larger steric repulsion. The higher tolerance of **38** toward racemization should also be attributed to the larger steric repulsion. On the other hand, all of these compounds **38**, **42b**, and **45b** were less distorted than their benzene analogues **4a**,[4] **9a**,[5] and **6a**,[6] respectively (Figure 4.2d). The central dithieno[3,2-*b*:3',2'-*d*]heterole and cyclopenta[1,2-*b*:4,3-*b*']dithiophene skeletons in **38**, **42b**, and **45b** offer smaller curvature than the dibenzoheterole and fluorene skeletons in **4a**, **9a**, and **6a**. As a result, the steric repulsion between the benzene rings at the both edges of the helical skeletons in **38**, **42b**, and **45b** are reduced, resulting in less twisted structures.

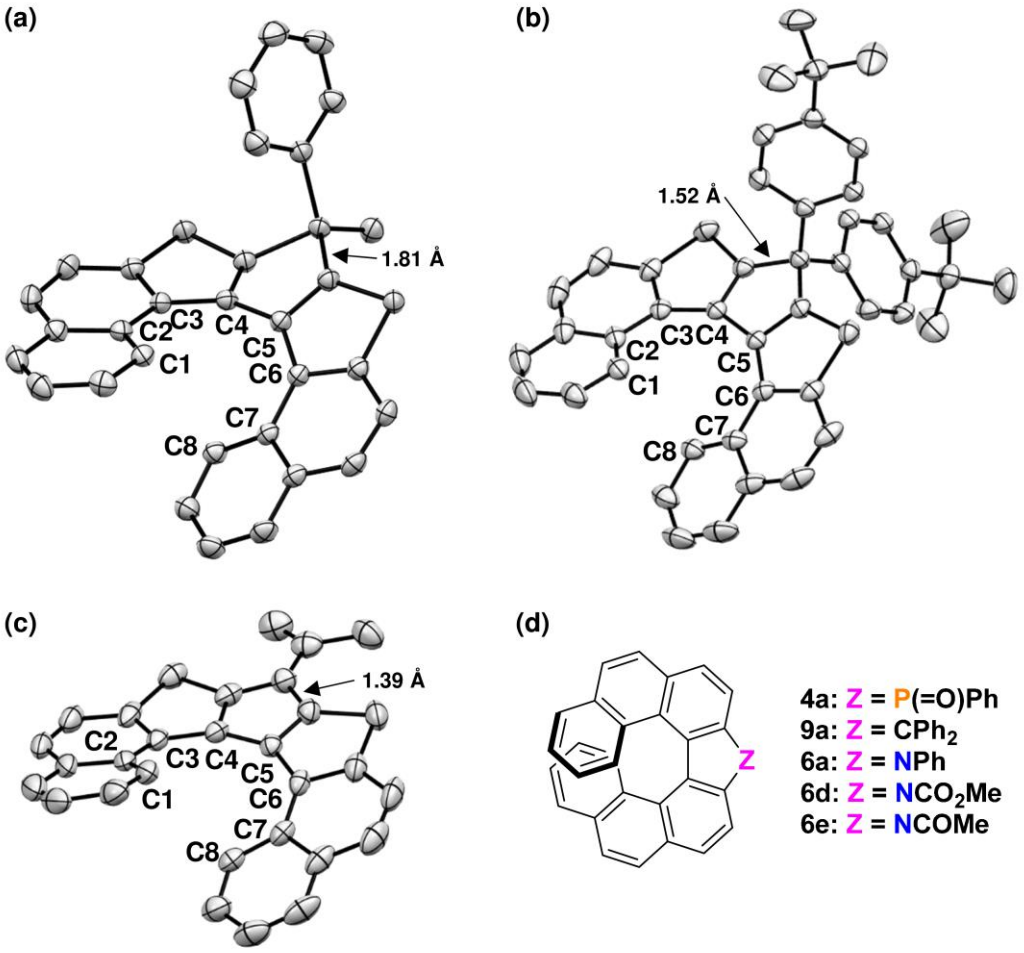

Figure 4.2. ORTEP drawings of (a) **38**, (b) **42b**, and (c) **45b** (50% probability. All hydrogen atoms are omitted for clarity.) and (d) the structures of [7]helicenes and [7]helicene-like compounds **4a**, **9a**, **6a**, **6d**, and **6e**.

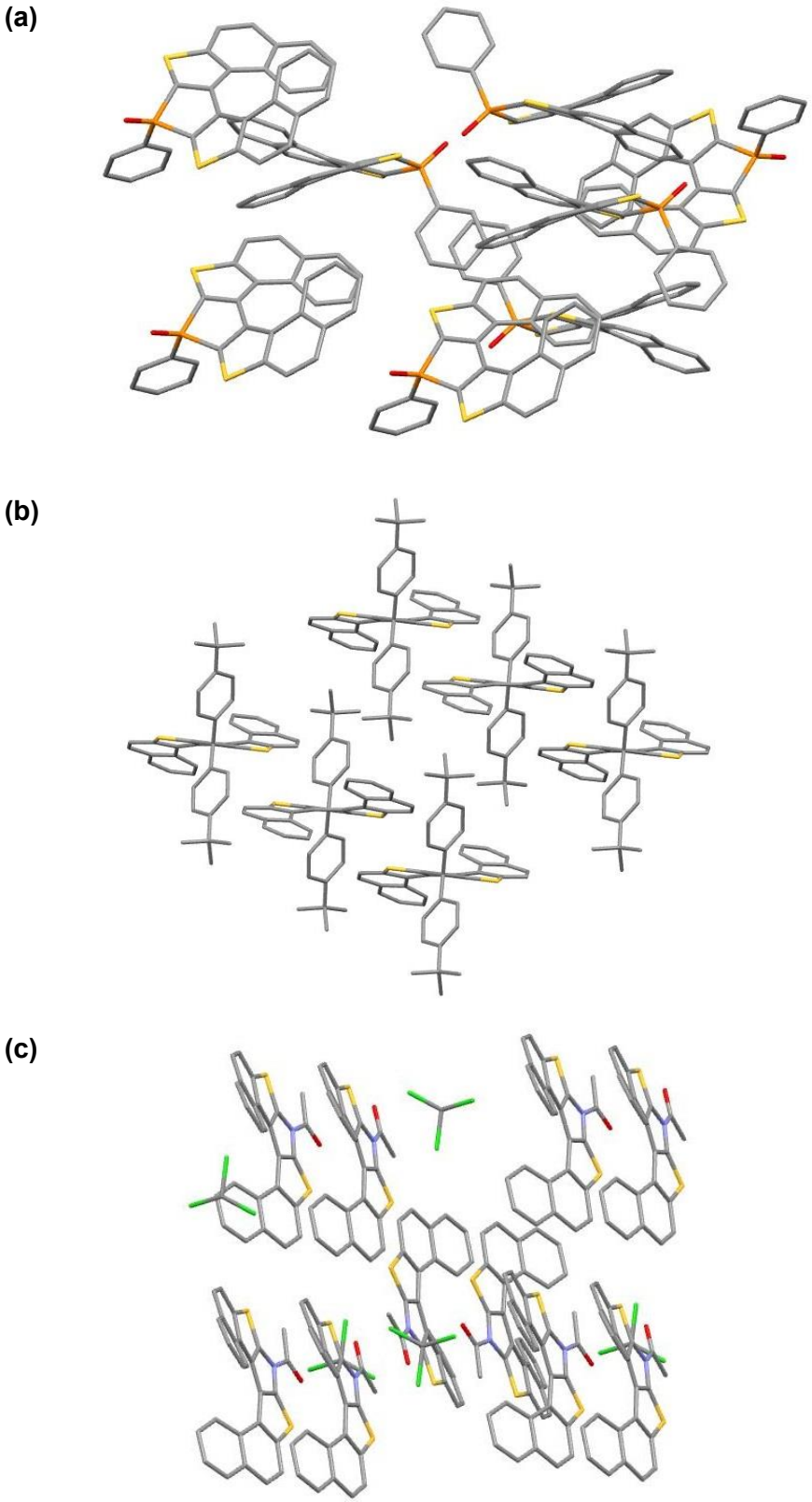

Figure 4.3. Packing structures of (a) **38**, (b) **42b**, and (c) **45b**.

Table 4.1. Crystallographic Data and Structure Refinement Details for **38**, **42b**, and **45b**

compound	**38**	**42b**	**45b**
formula	$C_{30}H_{17}OPS_2$	$C_{45}H_{38}S_2$	$C_{26}H_{15}NOS_2$
formula weight	488.52	642.87	481.19
temperature (K)	193(2) K	193(2)	193(2)
wavelength (Å)	1.54187 Å	1.54187	1.54187
crystal system	orthorhombic	monoclinic	triclinic
space group	$P2_1/n$	$C2/c$	$P\bar{1}$
unit cell dimensions			
a (Å)	12.0140(2)	22.8514(4)	12.1314(2)
b (Å)	9.11776(17)	12.0435(2)	12.3033(2)
c (Å)	21.2612(4)	13.7823(3)	14.3697(3)
α (°)	90	90	83.5273(7)
β (°)	104.4257(7)	115.769(1)	85.5012(7)
γ (°)	90	90	81.3505(7)
volume (Å^3)	2255.54(7)	3415.83(11)	2102.72(7)
Z	4	4	4
density (calculated) (g/cm^3)	1.439	1.250	1.520
absorption coefficient (mm^{-1})	2.985	1.641	4.217
F(000)	1008	1360	988
crystal size (mm^3)	0.50 × 0.40 × 0.15	0.35 × 0.20 × 0.15	0.35 × 0.20 × 0.080
theta range for data collection (°)	3.870 to 68.249°	4.253 to 68.240°	3.101 to 68.229
index ranges	–16<=h<=17	–27<=h<=27	–14<=h<=14
	–9<=k<=10	–14<=k<=14	–14<=k<=14
	–39<=l<=39	–16<=l<=16	–17<=l<=17
reflections collected	40480	29606	39772
independent reflections	4121 [R_{int} = 0.064]	3113 [R_{int} = 0.0174]	7590 [R_{int} = 0.0247]
completeness to theta (%)	100%	99.4%	98.5%
max. and min. transmission	0.220 and 0.639	0.621 and 0.782	0.714 and 0.304
refinement method	full-matrix least-squares on F^2		
data / restraints / parameters	4121/0/307	216/0/3113	7590/0/577
goodness-of-fit on F^2	1.062	1.070	1.088
final R indices [I>2σ(I)]			
R_1, wR_2	0.0344, 0.0924	0.0388, 0.1075	0.0673, 0.1837
R indices (all data)			
R_1, wR_2	0.0352, 0.0931	0.0415, 0.1098	0.0762, 0.1917
largest diff. peak and hole (e/Å^3)	0.361 and –0.254	0.287 and –0.179	1.753 and –0.719

4.4. Photophysical properties

4.4.1. Absorption and fluorescence properties

The absorption and emission properties of **38**, **42a**, **45a**, and **45b** were evaluated by UV–vis absorption and PL spectroscopies. These results were summarized in Table 4.2 and Figures 4.4 and 4.5. A comparison of the longest absorption maxima (λ_{abs}) of **42a** (360 nm), **45a** (318 nm), and **45b** (317 nm) shows that the replacement of the cyclopentadiene ring in **42a** with the pyrrole ring causes a blue-shift. This trend was also confirmed by their absorption edges (λ_{edge}). On the other hand, the phosphole-fused compound **38** exhibited different absorption characteristics. Absorption spectrum of **38** shows a broad absorption band at longer wavelength region. As a result, the red-shifted λ_{edge} compared to those of **42a**, **45a**, and **45b** was observed. These effects of the central five-membered ring on absorption properties were also demonstrated by their benzene analogues **4a**, **9a**, **6d**, and **6e** (Figure 4.2d). In addition, the same trend was observed in the previously reported 4*H*-cyclopenta[2,1-*b*:3,4-*b*′]dithiophene and dithieno[3,2-*b*:2′,3′-*d*]heteroles, the compounds related to **38**, **42a**, **45a**, and **45b**.[7–12] The effects of two thiophene rings were also evaluated. The absorption spectrum of **38**, **42a**, **45a**, and **45b** were blue-shifted from those of their benzene analogues **4a**, **9a**, **6d**, and **6e** (Figure 4.5).[4,5] This result would indicate that the replacement of benzene ring(s) with thiophene ring(s) causes less extended π–conjugation.

Table 4.2. Photophysical Data of Compounds **38**, **42a**, **45a**, and **45b** and Their Benzene Analogues **4a**, **9a**, **6d**, and **6e**

	λ_{abs} (nm)[a]	λ_{edge} (nm)[b]	ε (M^{-1}•cm^{-1})[c]	λ_{em} (nm)[d]	Φ_f (%)[e]
38	331	406	32000	514	0.17
42a	360	382	7100	415	1.8
45a	318	367	17000	393	0.29
45b	317	367	16000	381, 420	0.11
4a[f]	416	435	11000	462	7.8
9a[g]	408	425	7700	421	40
6d	396	406	14000	407	8.4
6e	398	412	14000	410	12

[a]The longest absorption maximum in CH_2Cl_2. [b]Absorption edge in the longer wavelength in CH_2Cl_2. [c]At λ_{abs}. [d]Emission maximum in CH_2Cl_2. [e]Absolute quantum yield determined by a calibrated integrating sphere system. [f]Reference 4. [g]Reference 5.

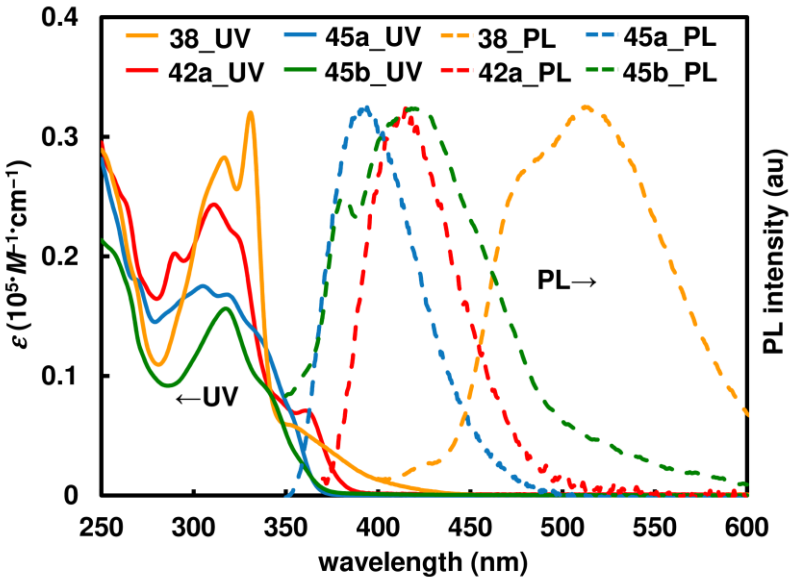

Figure. 4.4. UV-vis absorption and PL spectra of compounds **38**, **42a**, **45a**, and **45b**.

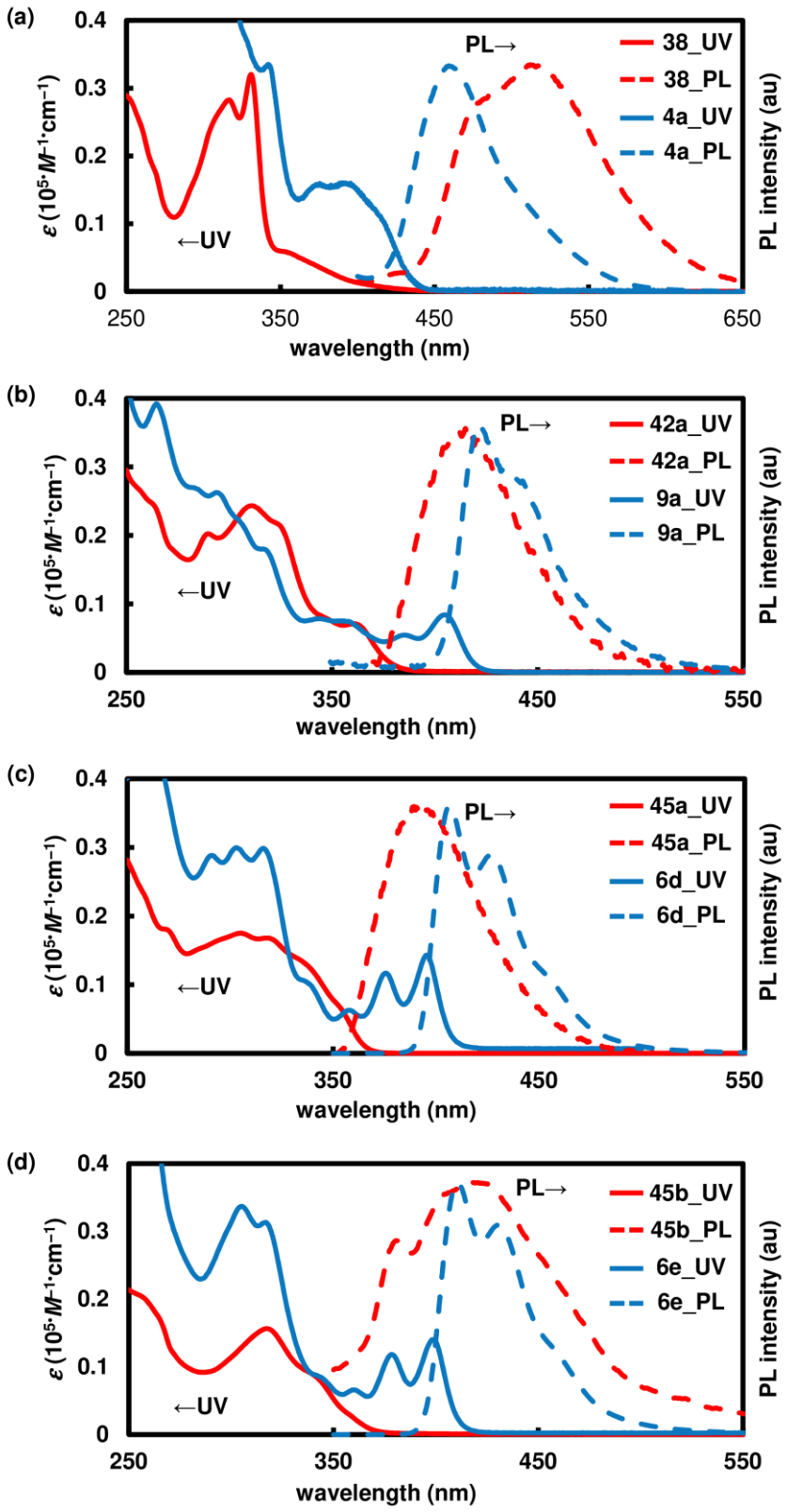

Figure 4.5. Comparison of photophysical properties between (a) **38** and **4a**, (b) **42a** and **9a**, (c) **45a** and **6d**, and (d) **45b** and **6e**.

The PL spectrum of phosphole-fused compound **38** was red-shifted compared to those of **42** and **45** and its benzene analogue **4a**. Such phenomenon is likely to attribute to intramolecular charge transfer (ICT) derived from the electron-donating thiophene units and the electron-accepting phosphole oxide unit.[13,14] Similar to the trend observed in absorption spectrum, the PL spectrum of cyclopentadiene-fused compound **42a** was blue-shifted compared to that of its benzene analogue **9a**.[5] The PL spectrum of the pyrrole-fused compounds **45a** and **45b** were also blue-shifted from that of cyclopentadiene-fused compound **42a** as well as those of their benzene analogues **6d** and **6e**. Therefore, (a) the replacement of the central cyclopentadiene ring of **38** with a pyrrole ring and (b) the replacement of two benzene rings of the pyrrole-fused aza[7]helicenes with two thiophene rings result in blue-shifted emission band, which is the same trend as observed in the absorption spectra. On the other hand, another emission maximum at the longer wavelength region was observed in PL spectrum of compound **45b**. The second emission maximum exhibited positive solvatochromism [λ_{em}: 399 nm (toluene) and 442 nm (MeOH)] and becomes more dominant as the solvent polarity increases (toluene [$E_T(30)$ = 33.9]; AcOEt [$E_T(30)$ = 38.1]; CH_2Cl_2 [$E_T(30)$ = 41.1]; CH_3CN [$E_T(30)$ = 46.0]; MeOH [$E_T(30)$ = 55.5, $E_T(30)$: solvent polarity parameter[15]], while the first emission maximum does not exhibited such solvatochromism (Figure 4.6). This result indicates that the first emission band is based on the locally excited state and the second emission band is based on the photo-induced ICT where the thiophene rings and the acetyl group act as electron-donor and electron-acceptor units, respectively.[11,12] Thus, the benzene analogue **6e** without the electron-donor unit does not exhibited such solvent dependency. Fluorescence quantum yields of **38**, **42a**, **45a**, and **45b** are much lower than those of their benzene analogues **4a**, **9a**, **6d**, and **6e** (Table

4.2), which may be due to much larger non-radiative rate constant (Table 4.3).

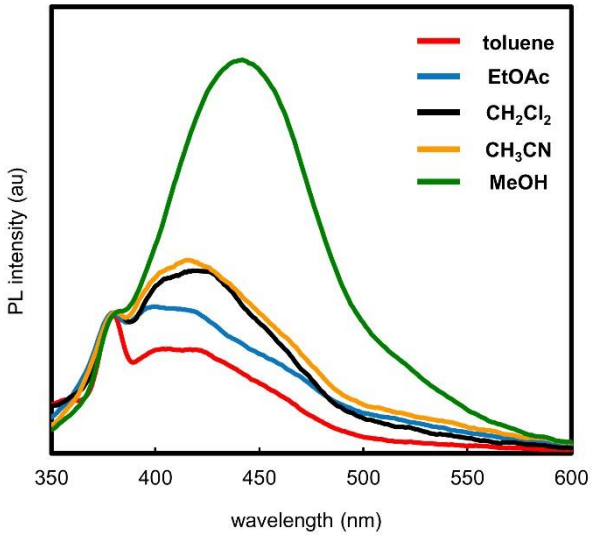

Figure 4.6. Solvent effect on PL spectrum of **45b**.

Table 4.3. Summary of Fluorescence Lifetime Measurement

	τ_1 (ns) [α_1]	τ_2 (ns) [α_2]	τ_{ave} (ns)[a]	Φ (%)	k_r ($\times 10^7$ s^{-1})[b]	k_{nr} ($\times 10^9$ s^{-1})[c]
38	0.18 [0.94]	0.68 [0.06]	0.21	0.17	0.81	4.8
42a	0.49 [1.00]	-	0.49	1.8	3.7	2.0
45a	0.16 [0.99]	1.29 [0.01]	0.17	0.29	1.7	5.9
45b	0.15 [0.91]	2.26 [0.09]	0.34	0.11	0.32	2.9
6d	4.16 [0.83]	6.46 [0.17]	4.55	8.4	1.8	0.20
6e	3.37 [0.99]	23.8 [0.01]	3.57	12.2	3.4	0.25

[a] $\tau_{ave} = \alpha_1 \cdot \tau_1 + \alpha_2 \cdot \tau_2$. [b] k_r (radiative rate constant) = Φ / τ_{ave}. [c] k_{nr} (non-radiative rate constant) = $(1-\Phi_f)/\tau_{ave}$.

4.4.2. Chiroptical properties

Chiroptical properties of **38** were also investigated. The specific rotation $[\alpha]_D^{23}$ of **38** with a shorter retention time in chiral HPLC showed −1660° (c = 0.049, CH_2Cl_2). The CD spectra of (−)-**38** exhibited a negative cotton effect at 403 nm, a positive Cotton effect at 331 nm followed by two negative Cotton effects at 305 nm and 253 nm (Figure 4.7). The dissymmetry factor (g_{abs}) was calculated to be 6.0×10^{-3} at 331 nm.

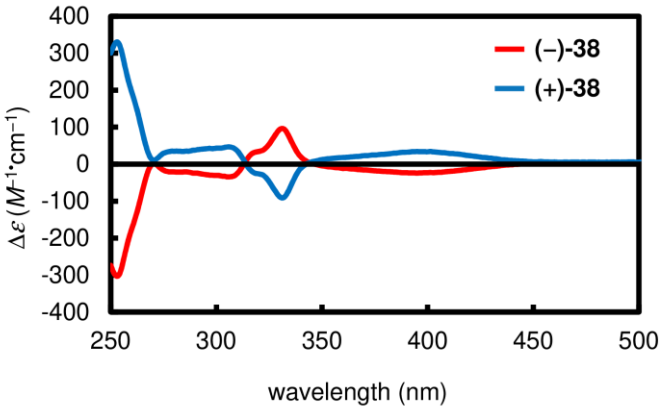

Figure 4.7. CD spectra of (+)- and (−)-**38**

4.5. Theoretical calculations

For understanding experimental photophysical properties, DFT and TD–DFT calculation were conducted at the B3LYP/6-31G(d) level of theory (Figures 4.8 and 4.9 and Table 4.4). The phosphole-fused compound **38** exhibited two lower energy transitions (411 nm and 370 nm) which are induced mainly from HOMO → LUMO and HOMO−1 → LUMO transitions (Table 4.4). However, the oscillator strengths of these two transitions are very low. Therefore, these transitions were related to a broad absorption band with low absorption coefficient at longer wavelength region. The

HOMO is mainly located on the two naphtho[2,1-*b*]thiophene units and the oxygen atom with a nodal plane at the phosphorus atom. On the other hand, the LUMO is largely located on the phospholo[2,3-*b*:5,4-*b*']dithiophene moiety. The phosphorus center apparently contributes to the LUMO through σ*–π* hyperconjugation.[13,14] Such orbital perturbation of the phosphole oxide moiety reduces the LUMO energy level, resulting in smaller HOMO–LUMO energy gap and lower-energy absorption than those of **42a**, **45a**, and **45b**. The lowest transition energy of cyclopentadiene-fused compound **42a** (370 nm) is lower than those of the pyrrole-fused compounds **45a** and **45b** (**45a**: 348 nm, **45b**: 362 nm). These effects of the central five-membered ring on absorption properties were also shown in their benzene analogues **4a**, **9a**, **6d**, and **6e**. Furthermore, the calculated transition energies of **38**, **42a**, **45a**, **45b**, **4a**, **9a**, **6d**, and **6e** qualitatively demonstrated the effects of the replacement of two benzene rings with two thiophene rings observed in their experimental absorption spectra.

The DFT calculations show a significant difference in LUMOs between **45a** and **45b**. The HOMO of **45b** is mainly distributed on one naphtho[2,1-*b*]thiophene and pyrrole units, while the LUMO is distributed on another naphtho[2,1-*b*]thiophene and acetyl units. The HOMO of **45a** is also distributed on one naphtho[2,1-*b*]thiophene and pyrrole units. On the other hand, the LUMO of **45a** is spread over the entire helical structure, and the contribution of the carbonyl group is very small. Both the HOMO and the LUMO of **6d** and **6e** are distributed over their helical structure. Furthermore, the HOMO and the LUMO of the related compounds, *N*-acetyldithieno[3,2-*b*:2',3'-*d*]pyrrole and *N*-acetyldithieno[3,2-*b*:3',2'-*d*]pyrrole, are spread over the entire molecules (Figure 4.9).[11,12] Considering all of these calculation results, the combination of electron-donating thiophene rings and an electron-withdrawing acethyl group and the extension of

the π-conjugated system cause photo-induced ICT of **45b**, resulting in the longer wavelength emission.

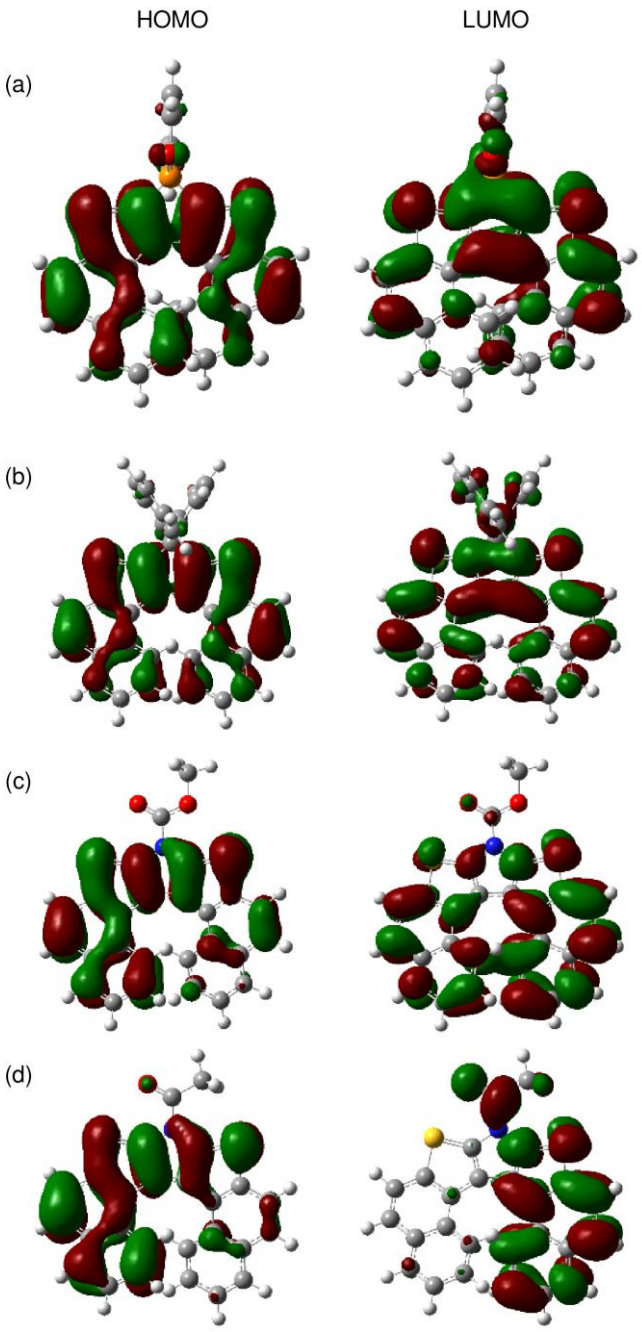

Figure 4.8. HOMOs and LUMOs of (a) **38**, (b) **42a**, (c) **45a**, and (d) **45b** calculated by DFT method at the B3LYP/6-31G(d) level of theory.

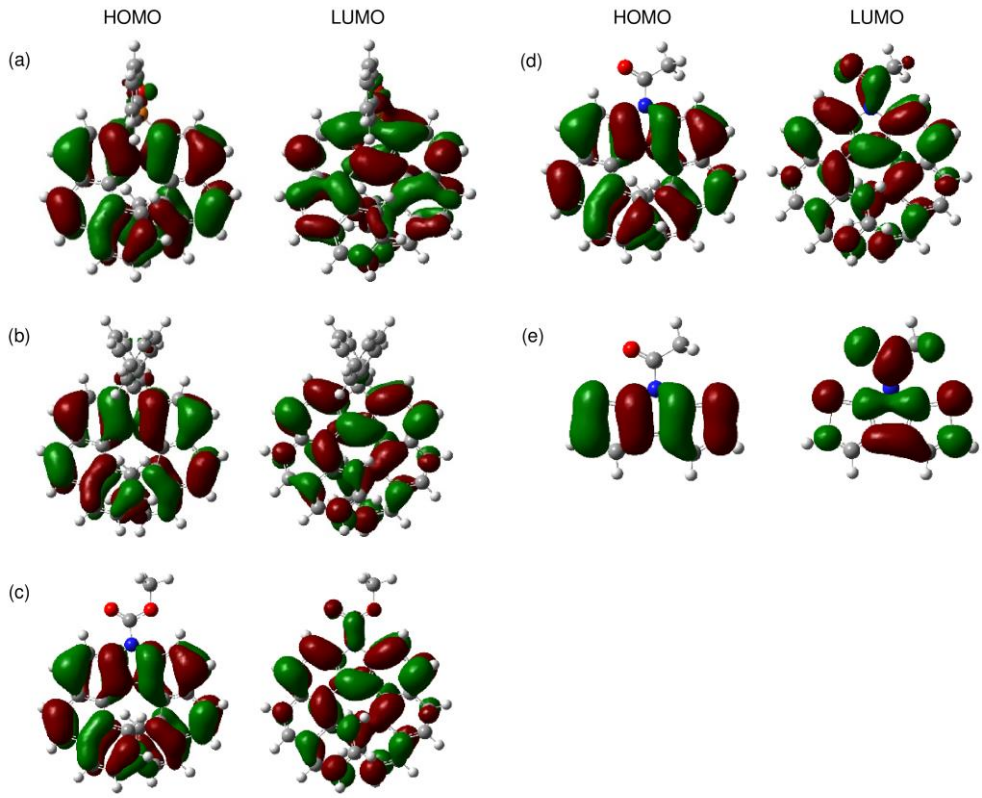

Figure 4.9. HOMOs and LUMOs of (a) **4a**, (b) **9a**, (c) **6d**, (d) **6e**, and (e) 1-(7*H*-dithieno[2,3-*b*:3',2'-*d*]pyrrol-7-yl)ethan-1-one calculated by DFT method at the B3LYP /6-31G(d) level of theory.

Table 4.4. The Selected Absorption of **38**, **42a**, **45a**, **45b**, **4a**, **9a**, **6d**, and **6e** Calculated by TD–DFT Method at the B3LYP /6-31G(d) Level of Theory.

	excited state	transition energy (eV)	wavelength (nm)	transition configulation (CI expansion coefficient)	oscillator strength, *f*
38	1	3.0193	411	HOMO → LUMO (0.701)	0.0091
	2	3.3503	370	HOMO−1 → LUMO (0.606)	0.0096
				HOMO → LUMO+1 (0.353)	
	3	3.6502	3.65	HOMO−2 → LUMO (0.659)	0.0698
				HOMO → LUMO+1 (−0.104)	
				HOMO → LUMO+2 (-0.182)	
	4	3.7009	335	HOMO−2 → LUMO (0.116)	0.3325
				HOMO−1 → LUMO (−0.340)	
				HOMO → LUMO+1 (0.583)	
42a	1	3.3469	370	HOMO → LUMO (0.700)	0.0171
	2	3.4457	360	HOMO−1 → LUMO (−0.267)	0.0816
				HOMO → LUMO+1 (0.643)	
	3	3.7989	326	HOMO−1 → LUMO (0.640)	0.2725
				HOMO → LUMO+1 (0.260)	
	4	3.8553	322	HOMO−2 → LUMO (0.101)	0.0368
				HOMO−1 → LUMO+1 (0.604)	
				HOMO → LUMO+2 (0.316)	
45a	1	3.5620	348	HOMO−1 → LUMO (0.186)	0.0416
				HOMO−1 → LUMO+1 (0.165)	
				HOMO → LUMO (0.632)	
				HOMO → LUMO+1 (0.141)	
	2	3.6419	340	HOMO−1 → LUMO (0.639)	0.1207
				HOMO−1 → LUMO+1 (−0.216)	
				HOMO → LUMO (−0.137)	
	3	3.7104	334	HOMO−1 → LUMO (−0.146)	0.0339
				HOMO−1 → LUMO+1 (−0.219)	
				HOMO → LUMO+1 (0.643)	
	4	3.8604	321	HOMO−1 → LUMO (0.128)	0.2121
				HOMO−1 → LUMO+1 (0.602)	
				HOMO → LUMO (−0.221)	
				HOMO → LUMO+1 (0.216)	

(continued)

	excited state	transition energy (eV)	wavelength (nm)	transition configulation (CI expansion coefficient)	oscillator strength, *f*
45b	1	3.4276	362	HOMO → LUMO (0.691) HOMO → LUMO (0.114)	0.0081
	2	3.5529	349	HOMO−1 → LUMO (−0.475) HOMO−1 → LUMO+1 (−0.152) HOMO → LUMO+1 (0.479)	0.0357
	3	3.6617	339	HOMO−1 →LUMO (−0.299) HOMO−1 → LUMO+1 (0.610) HOMO → LUMO+1 (−0.112)	0.0939
	4	3.7660	329	HOMO−1 → LUMO (0.409) HOMO−1 → LUMO+1 (0.284) HOMO → LUMO+1 (0.455)	0.2647
4a	1	3.0587	405	HOMO → LUMO (0.691)	0.0768
	2	3.2576	381	HOMO−1 → LUMO (0.581) HOMO → LUMO+1 (−0.378)	0.0113
	3	3.4599	358	HOMO−3 → LUMO+1 (0.105) HOMO−2 → LUMO (0.618) HOMO−1 → LUMO (−0.131) HOMO → LUMO (0.232)	0.0228
	4	3.5622	348	HOMO−2 → LUMO (0.638) HOMO−1 → LUMO (0.370) HOMO → LUMO+1 (0.567)	0.0012
9a	1	3.1644	392	HOMO → LUMO (0.677) HOMO → LUMO+1 (−0.137)	0.1363
	2	3.4662	358	HOMO−2 → LUMO+2 (0.108) HOMO−1 → LUMO (0.594) HOMO → LUMO+2 (0.341)	0.0055
	3	3.4804	356	HOMO−2 → LUMO (0.502) HOMO → LUMO (0.154) HOMO → LUMO+1 (0.460)	0.0224
	4	3.7248	333	HOMO−2 → LUMO (−0.486) HOMO → LUMO+1 (0.496)	0.0780

(continued)

	excited state	transition energy (eV)	wavelength (nm)	transition configulation (CI expansion coefficient)	oscillator strength, *f*
6d	1	3.2908	377	HOMO−1 → LUMO (0.142) HOMO−1 → LUMO+1 (−0.120) HOMO → LUMO (0.657) HOMO → LUMO+2 (−0.134)	0.1442
	2	3.3160	374	HOMO−1 → LUMO (0.626) HOMO → LUMO (−0.146) HOMO → LUMO+1 (0.256)	0.0444
	3	3.6304	341	HOMO−2 → LUMO (0.610) HOMO → LUMO (0.115) HOMO → LUMO+1 (0.110) HOMO → LUMO+2 (0.295)	0.0343
	4	3.8931	318	HOMO−3 → LUMO (0.101) HOMO−2 → LUMO (−0.311) HOMO−1 → LUMO (−0.109) HOMO−1 → LUMO+1 (0.188) HOMO−1 → LUMO+3 (−0.110) HOMO → LUMO (0.105) HOMO → LUMO+1 (0.402) HOMO → LUMO+2 (0.381)	0.0433
6e	1	3.2225	385	HOMO−1 → LUMO (0.182) HOMO → LUMO (0.655) HOMO → LUMO (−0.108)	0.1344
	2	3.2635	380	HOMO−1 → LUMO (0.624) HOMO → LUMO (−0.190) HOMO → LUMO+1 (0.343) HOMO → LUMO+2 (−0.148)	0.0678
	3	3.5390	350	HOMO−2 → LUMO (0.568) HOMO → LUMO+1 (0.343) HOMO → LUMO+2 (0.176)	0.0174
	4	3.7770	328	HOMO−2 → LUMO (−0.406) HOMO−1 → LUMO+1 (0.107) HOMO−1 →LUMO+2 (−0.115) HOMO → LUMO+1 (0.476) HOMO → LUMO+2 (0.240)	0.0247

4.6. Conclusion

The diversity-oriented synthesis of [7]helicenes and [7]helicene-like compounds was achieved by using 1,1′-binaphtho[2,1-*b*]thiophene (**33**) as a common precursor. The precursor **33** was successfully synthesized and converted into the desired helical molecules **38**, **42**, and **45**. X-ray crystallographic analysis revealed their helical structures. The absorption and fluorescence properties of them were investigated and compared with those of their benzene analogues. To better understand photophysical properties, theoretical calculations were also conducted. The introduction of five-membered rings to helicene skeletons led to significant changes in photophysical properties. The compounds in which a phosphole ring is located at the center exhibits the longest absorption and emission bands. The replacement with two thiophene rings causes blue-shifted absorption spectra compared to those of their parent benzene analogues. In case of the introduction of a five-membered ring with an electron-withdrawing character, the combination with electron-donating thiophene rings induced red-shifted emission which would be attributed to ICT. These results would be of importance for the molecular design of π-conjugated helical skeleton to improve their properties.

4.7. Experimental section

4.7.1 General

All manipulations involving air- and/or moisture-sensitive compounds were carried out using the standard Schlenk technique under argon. Analytical thin-layer chromatography was performed on glass plates coated with 0.25 mm 230–400 mesh silica gel containing a fluorescent indicator. Column chromatography was performed by using silica gel (spherical neutral, particle size: 63–210 mm). The recycling preparative HPLC was performed using YMC-GPC T-2000 and T-4000 columns (chloroform as an eluent). Most of the reagents were purchased from commercial suppliers, such as Sigma-Aldrich Co. LLC, Tokyo Chemical Industry Co., Ltd., and Kanto Chemical Co., Inc., and used without further purification unless otherwise specified. Commercially available anhydrous solvents were used for air- and/or moisture sensitive reactions. NMR spectra were recorded in $CDCl_3$, CD_2Cl_2, DMSO-d_6, and acetone-d_6, on a JEOL ECX400 spectrometer (^{1}H 400 MHz; ^{13}C 101 MHz) or on a JEOL ECA500 spectrometer (^{1}H 500 MHz; ^{13}C 126 MHz; ^{31}P 202 MHz). Chemical shifts are reported in ppm relative to the internal standard signal (0 ppm for Me_4Si in $CDCl_3$) or the solvent residual signal (2.50 ppm for DMSO-d_6, 5.32 ppm for CD_2Cl_2, 2.05 ppm for acetone-d_6) for ^{1}H and the deuterated solvent signal (77.16 ppm for $CDCl_3$, 39.52 ppm for DMSO-d_6, 206.26 ppm for acetone-d_6, 73.8 ppm for $Cl_2CDCDCl_2$) for ^{13}C. Data are presented as follows: chemical shift, multiplicity (s = singlet, d = doublet, t = triplet, td = triplet of doublets, m = multiplet and/or multiple resonances), coupling constant in hertz (Hz), and signal area integration in natural numbers. Melting points were determined on a melting point apparatus. High resolution mass spectra were recorded using a Bruker Daltonics micrOTOF-QII mass spectrometer by an atmospheric pressure chemical ionization-time-of-flight (APCI–TOF) or electrospray ionization-time-of-flight (ESI–TOF) method. UV–Vis absorption spectra were recorded on a JASCO V–650 spectrophotometer. Photoluminescence spectra were recorded on a JASCO FP–6500 spectrofluorometer. Absolute quantum yields were determined using an absolute quantum yield measurement system with a JASCO ILF–533 integrating sphere. The fluorescence lifetimes were measured using a Hamamatsu Photonics C4334 streak camera. Circular dichroism (CD) spectra were recorded on a JASCO J–720 spectrometer. Optical rotations were measured on a JASCO P–2200 polarimeter using a 50 mm cell. Chiral HPLC analyses were carried out using a DAICEL CHIRALPAK® IA-3 column (4.6 mm 250 mm).

4.7.2. Synthetic procedure

2-(4-Bromothiophen-3-yl)benzaldehyde (36). 2-(2-Bromophenyl)-1,3-dioxolane (9.0 g, 39 mmol) in THF (50 mL) was placed in a 200 mL three-necked flask and was cooled to –78 °C. To the solution was added BuLi (2.6 M in hexane, 18 mL, 47 mmol), and the resulting mixture was stirred for 1 h. After a mixture of $ZnBr_2$ (8.9 g, 39 mmol) and THF (50 mL) at –78 °C was transferred to the solution, the resulting mixture was warmed to 0 °C. After stirring for 1 h, $Pd(PPh_3)_4$ (2.3 g, 2.0 mmol) and 3,4-dibromothiophene (4.4 mL, 39 mmol) were added to the solution. The resulting solution was degassed by three freeze–pump–thaw cycles, and then refluxed for 40 h. The reaction was quenched with saturated aqueous NH_4Cl (10 mL), and the resulting mixture was filtered through a pad of celite®. The filtrate was concentrated under reduced pressure. The resulting crude residue was purified by silica-gel column chromatography with EtOAc/hexane (1/9) as an eluent to give the coupling product with inseparable by-products.

The obtained coupling product, 1 M aqueous HCl (50 mL), and methanol (50 mL) were placed in a 300 mL flask, and the resulting mixture was stirred at room temperature until completion of the reaction, which was monitored by TLC. Brine (50 mL) was added to the reaction mixture, and the resulting mixture was extracted with AcOEt (50 mL × 3). The combined organic layers were dried over Na_2SO_4, filtered, and concentrated under reduced pressure. The resulting crude residue was purified by silica-gel column chromatography with EtOAc/hexane (1/9) as an eluent to give **36** as a yellowish oil (6.2 g, 59% yield for 2 steps): ^{1}H NMR (400 MHz, $CDCl_3$) δ 9.86 (s, 1H), 8.03 (dd, J = 7.8, 1.4 Hz, 1H), 7.64 (td, J = 7.6, 1.6 Hz, 1H), 7.53 (t, J = 7.3 Hz, 1H), 7.41 (d, J = 3.6 Hz, 1H), 7.37 (dd, J = 7.6, 1.6 Hz, 1H), 7.30 (d, J = 3.2 Hz, 1H); ^{13}C NMR (101 MHz, $CDCl_3$) δ 191.6, 138.6, 138.4, 134.5, 133.7, 131.6, 128.8, 127.6, 125.7, 124.1, 112.7; HRMS–APCI$^+$ (m/z) calcd for $C_{11}H_8BrOS^+$ ($[M + H]^+$) 266.9474 (monoisotopic ion), found 266.9478.

1-Bromonaphtho[2,1-*b*]thiophene (37). A mixture of potassium *tert*-butoxide (6.2 g, 55 mmol) in THF (50 mL) was added to a 200 mL three-necked flask containing the mixture of (methoxymethyl)triphenyl-phosphonium chloride (19 g, 55 mmol) in Et_2O (50 mL), and the resulting mixture was stirred at room temperature for 1 h. To the mixture was added a solution of **36** (5.4 g, 20 mmol) in THF (50 mL), and the resulting mixture was stirred at room temperature for 15 h. The precipitate was removed off by filtration, and the filtrate was concentrated under reduced pressure. The resulting crude residue was purified by silica-gel column chromatography with AcOEt/hexane (1/20) as

an eluent to give a mixture of *E*/*Z*-isomers of 3-bromo-4-[2-(2-methoxyvinyl)phenyl]thiophene as a colorless oil (3.5 g).

A mixture of *E*/*Z*-isomers of 3-bromo-4-[2-(2-methoxyvinyl)phenyl]thiophene (3.5 g, 12 mmol), methanesulfonic acid (0.78 mL, 12 mmol), and CH_2Cl_2 (50 mL) in a 200 mL flask was stirred at 0 °C for 18 h. The reaction was quenched with aqueous NH_4Cl (50 mL), and the resulting mixture was extracted with CH_2Cl_2 (20 mL × 3). The combined organic layers were dried over Na_2SO_4, filtered, and concentrated under reduced pressure. The resulting crude residue was purified by recrystallization from hexane and silica-gel column chromatography with hexane as an eluent to give **37** as a colorless solid (2.9 g, 53% yield for 2 steps): m.p. 80–81 °C; ^{1}H NMR (400 MHz, $CDCl_3$) δ 9.64 (d, *J* = 8.7 Hz, 1H), 7.94 (dd, *J* = 8.4 Hz, 1.6 Hz, 1H), 7.82–7.74 (m, 2H), 7.67–7.62 (m, 1H), 7.58–7.54 (m, 2H); ^{13}C NMR (101 MHz, $CDCl_3$) δ 138.2, 132.0, 130.2, 129.6, 128.9, 126.8, 126.3, 125.9, 124.6, 122.8, 120.7, 107.1; HRMS–APCI$^+$ (*m*/*z*) calcd for $C_{12}H_8BrS^+$ ($[M + H]^+$) 262.9525 (monoisotopic ion), found 262.9533.

1,1′-Binaphtho[2,1-*b*]thiophene (33). A mixture of **37** (2.6 g, 10 mmol), bis(pinacolato)diboron (1.3 g, 5.0 mmol), $PdCl_2$(dppf) (0.29 g, 0.40 mmol), K_2CO_3 (4.1 g, 30 mmol), and 1,4-dioxane (59 mL) in a 200 mL three-necked flask was degassed by three freeze–pump–thaw cycles and stirred at 80 °C for 65 h. The resulting mixture was filtered through a pad of celite®, and the filtrate was washed with water (100 mL) and saturated aqueous $NaHCO_3$ (100 mL), dried over Na_2SO_4, and concentrated under reduced pressure. The resulting crude residue was purified by silica-gel column chromatography with $CHCl_3$/hexane (1/4) as an eluent to give **33** as a colorless solid (1.5 g, 80% yield): m.p. 216–217 °C; ^{1}H NMR (400 MHz, $CDCl_3$) δ 7.97 (d, *J* = 8.7 Hz, 2H), 7.83 (d, *J* = 7.8 Hz, 2H), 7.78 (d, *J* = 8.8 Hz, 2H), 7.53–7.50 (m, 4H), 7.29–7.25 (m 2H), 6.98–6.93 (m, 2H); ^{13}C NMR (101 MHz, $CDCl_3$) δ 138.8, 135.5, 133.7, 131.9, 130.2, 128.6, 126.5, 126.3, 125.6, 125.2, 123.2, 121.1; HRMS–APCI$^+$ (*m*/*z*) calcd for $C_{24}H_{15}S_2^+$ ($[M + H]^+$) 367.0610, found 367.0604.

8-Phenyl-8*H*-dinaphtho[2,1-*b*:2′,1′-*b*′]phospholo[3,2-*d*:4,5-*d*′]dithiophene 8-oxide (38). To a mixture of **33** (0.037g, 0.10 mmol) and Et_2O (5 mL) in a 20 mL Schlenk tube was added BuLi (2.6 M in hexane, 0.10 mL, 0.26 mmol) dropwise at 0 °C. After stirring at room temperature for 30 min, dichlorophenylphosphine (14 μL, 0.093 mmol) was added to the solution at room temperature. The resulting mixture was stirred for 24 h, and the reaction was quenched with water (10 mL). The resulting mixture was extracted with CH_2Cl_2 (10 mL × 3), and the combined organic layers were dried over

Na_2SO_4, filtered, and concentrated under reduced pressure. The resulting residue was dissolved in THF (3 mL), and 30% aqueous H_2O_2 (1 mL) was added to the solution. After stirring for 18 h, the reaction was quenched with water (10 mL). The resulting mixture was extracted with CH_2Cl_2 (10 mL × 3), and the combined organic layers were dried over Na_2SO_4, filtered, and concentrated under reduced pressure. The resulting crude residue was purified by silica-gel column chromatography with $CHCl_3$/AcOEt (20/1) as an eluent and by recycling preparative HPLC to give **38** as a green solid (7.6 mg, 16% yield): m.p. 255–256 °C; ^{1}H NMR (500 MHz, $CDCl_3$) δ 7.92–7.85 (m, 7H), 7.80 (d, *J* = 8.6 Hz, 1H), 7.76 (d, *J* = 7.5 Hz, 1H), 7.73 (d, *J* = 6.9 Hz, 1H), 7.53–7.50 (m, 1H), 7.41–7.38 (m, 2H), 7.37– 7.32 (m, 2H), 6.72–6.66 (m, 2H); ^{13}C NMR (101 MHz, $CDCl_3$) δ 148.4 (d, *J*cp = 5.8 Hz), 147.9 (d, *J*cp = 5.8 Hz) 147.3 (d, J_{cp} = 19.2 Hz), 147.2 (d, J_{cp} = 18.2 Hz), 137.0 (d, J_{cp} = 112.1 Hz), 134.7 (d, J_{cp} = 113.1 Hz), 132.9 (d, J_{cp} = 2.9 Hz), 131.9, 131.8, 131.3 (d, J_{cp} = 11.5 Hz), 130.4 (d, J_{cp} = 11.5 Hz), 130.3 (d, J_{cp} = 116.0 Hz), 129.7 (d, J_{cp} = 12.5 Hz), 129.6, 129.4, 129.2 (d, J_{cp} = 13.4 Hz), 128.6, 128.4, 127.9, 127.8, 127.6, 127.5, 126.3, 126.2, 125.2, 125.1, 121.34 (d, J_{cp} = 1.9 Hz), 121.26 (d, J_{cp} = 1.9 Hz); ^{31}P NMR (202 MHz, $CDCl_3$) δ 21.1; HRMS–APCI$^+$ (*m*/*z*) calcd for $C_{30}H_{18}OPS_2$ ($[M + H]^+$) 489.0532, found 489.0536.

Methyl 1,1′-binaphtho[2,1-*b*]thiophene-2-carboxylate (40). To a mixture of **33** (0.036 g, 0.098 mmol) and THF (3.6 mL) in a 20 mL Schlenk tube was added BuLi (2.6 M in hexane, 0.09 mL, 0.24 mmol) dropwise at 0 °C. After stirring at room temperature for 30 min, methyl chloroformate (0.023 mL, 0.30 mmol) was added to the reaction mixture at room temperature. The resulting mixture was stirred for 17 h, and the reaction was quenched with water (10 mL). Brine (10 mL) was added, and the resulting mixture was extracted with CH_2Cl_2 (20 mL × 3), and the combined organic layers were dried over Na_2SO_4, filtered, and concentrated under reduced pressure. The resulting crude residue was purified by silica-gel column chromatography with $CHCl_3$/ hexane (1/1) as an eluent to give **40** as a colorless solid (33 mg 79% yield): m.p. 230–231 °C; ^{1}H NMR (500 MHz, $CDCl_3$) δ 8.03 (d, *J* = 9.2 Hz, 1H), 7.97 (d, *J* = 9.2 Hz, 1H), 7.92 (d, *J* = 9.2 Hz, 1H), 7.89–7.86 (m, 2H), 7.82 (d, *J* = 8.6 Hz, 1H), 7.44–7.40 (m, 3H), 7.36–7.30 (m, 2H), 7.03 (t, *J* = 6.4 Hz, 2H), 3.61 (s, 3H); ^{13}C NMR (126 MHz, $CDCl_3$) δ 162.5, 141.5, 140.4, 138.9, 134.2, 134.0, 133.4, 132.0, 131.9, 130.8, 130.2, 129.5, 129.4, 129.0, 128.8, 127.3, 126.5, 126.2, 125.8, 125.1, 124.2, 123.2, 122.8, 121.2, 120.6, 52.4; HRMS–APCI$^+$ (*m*/*z*) calcd for $C_{26}H_{17}O_2S_2^+$ ($[M + H]^+$) 425.0665, found 425.0669.

([1,1′-Binaphtho[2,1-*b*]thiophen]-2-yl)diphenylmethanol (41a). To a mixture

of **40** (0.19 g, 0.44 mmol) and THF (10 mL) in a 30 mL Schlenk tube was added phenylmagnesium bromide (1.0 M in THF, 1.7 mL, 1.7 mmol). The resulting mixture was stirred at 40 °C for 23 h and cooled to room temperature. The reaction was quenched with saturated aqueous NH_4Cl (20 mL), and the resulting mixture was extracted with AcOEt (10 mL × 3). The combined organic layers were dried over Na_2SO_4, filtered, and concentrated under reduced pressure. The crude residue was suspended with hexane, and the resulting precipitate was collected to give **41a** as a colorless solid (0.21 g, 87% yield): m.p. >300 °C; ^{1}H NMR (400 MHz, DMSO-d_6, 100 °C) δ 8.08 (d, J = 8.7 Hz, 1H), 7.88 (d, J = 9.2 Hz, 2H), 7.83 (d, J = 8.5 Hz, 2H), 7.71 (d, J = 8.8 Hz, 1H), 7.31–7.21 (m, 6H), 7.13–7.10 (m, 3H), 7.02 (d, J = 9.2 Hz, 2H), 6.97–6.91 (m, 3H), 6.81–6.77 (m, 1H), 6.59–6.54 (m, 3H), 6.15 (s, 1H); The ^{13}C NMR spectrum was not recorded because of low solubility; HRMS–APCI$^+$ (*m*/*z*) calcd for $C_{37}H_{23}S_2^+$ ([M – OH]$^+$) 531.1236, found 531.1237.

([1,1′-binaphtho[2,1-*b*]thiophen]-2-yl)bis(4-*tert*-butylphenyl)methanol (41b). According to the procedure described for **41a**, **41b** was obtained as a colorless solid (130 mg, 84% yield) with **40** (0.10 g, 0.23 mmol) and (4-*tert*-butylphenyl)magnesium bromide (1.0 M in THF, 0.94 mL, 0.94 mmol): m.p. 196–197 °C; ^{1}H NMR (400 MHz, DMSO-d_6, 100 °C) δ 8.08 (d, J = 9.2 Hz, 1H), 7.87–7.85 (m, 2H), 7.82 (d, J = 8.7 Hz, 1H), 7.78 (dd, J = 8.7, 1.4 Hz, 1H), 7.67 (d, J = 8.8 Hz, 1H), 7.34 (s, 1H), 7.27–7.18 (m, 5H), 7.09–7.07 (m, 2H), 6.97 (d, J = 8.7, 2H), 6.94–6.90 (m, 2H), 6.76–6.72 (m, 1H), 6.65 (d, J = 8.7 Hz, 2H), 6.10–6.09 (m, 1H), 1.21 (s, 9H), 1.02 (s, 9H); ^{13}C NMR (126 MHz, DMSO-d_6, 100 °C) δ 150.7, 148.8, 148.0, 142.8, 141.9, 136.9, 135.6, 133.9, 133.6, 133.0, 131.1, 130.7, 130.6, 129.4, 129.2, 128.1, 127.5, 126.9 (three carbons), 125.04 (two carbons), 125.00, 124.95, 124.6, 124.01, 123.95, 123.3, 122.5, 122.4, 121.5, 120.2, 78.8, 34.4, 33.1, 30.5, 30.4; HRMS–APCI$^+$ (*m*/*z*) calcd for $C_{45}H_{39}S_2^+$ ([M – OH]$^+$) 643.2488, found 643.2500.

8,8-Diphenyl-8*H*-cyclopenta[1,2-*b*:4,3-*b*′]dinaphtho-[1,2-*d*:1′,2′-*d*′]dithiophene (42a). A mixture of **41a** (0.19 g, 0.35 mmol) and CH_2Cl_2 (10 mL) was placed in a 20 mL Schlenk tube, and TfOH (3.1 mL, 0.035 mmol) was added. The resulting mixture was stirred at room temperature for 30 min and concentrated under reduced pressure. The resulting residue was purified by silica-gel column chromatography with $CHCl_3$ as an eluent and by recycling preparative HPLC to give **42a** as a colorless solid (0.10 g, 58% yield): m.p. 224–225 °C; ^{1}H NMR (400 MHz, CD_2Cl_2, 35 °C) δ 8.07 (d, J = 8.2 Hz, 2H), 7.94 (d, J = 7.8 Hz, 2H), 7.91 (d, J = 8.7 Hz, 2H), 7.80 (d, J = 8.7 Hz,

2H), 7.49–7.47 (m, 4H), 7.41–7.37 (m, 2H), 7.34–7.28 (m, 6H), 6.85–6.81 (m, 2H); the ^{13}C NMR spectrum was not measured because of low solubility; HRMS–APCI$^+$ (*m*/*z*) calcd for $C_{37}H_{23}S_2^+$ ([M + H]$^+$) 531.1236, found 531.1245.

8,8-Bis(4-*tert*-butylphenyl)-8*H*-cyclopenta[1,2-*b*:4,3-*b′*]dinaphtho[2,1-*d*:1′,2′-*d′*]dithiophene (42b). The crude residue was obtained with **41b** (0.51 g, 0.77 mmol), CH_2Cl_2 (14 mL), and TfOH (6.8 mL, 0.077 mmol) according to the procedure described for **42a**. Purification by silica-gel column chromatography with $CHCl_3$/hexane (2/1) as an eluent gave **42b** as a colorless solid (0.45 g, 91% yield): m.p. >300 °C; ^1H NMR (500 MHz, $CDCl_3$) δ 8.07 (d, *J* = 8.4 Hz, 2H), 7.90 (d, *J* = 7.5 Hz, 2H), 7.87 (d, *J* = 8.6 Hz, 2H), 7.76 (d, *J* = 8.6 Hz, 2H), 7.40–7.35 (m, 6H), 7.30– 7.28 (m, 4H), 6.84–6.81 (m, 2H), 1.27 (s, 18 H); ^{13}C NMR (126 MHz, $CDCl_3$) δ 155.8, 150.3, 142.2, 141.6, 137.1, 131.9, 129.33, 129.30, 129.1, 127.7, 127.4, 125.7, 125.4, 125.1, 124.4, 121.6, 64.0, 34.6, 31.4; HRMS–APCI$^+$ (*m*/*z*) calcd for $C_{45}H_{39}S_2$ ([M + H]$^+$) 643.2488, found 643.2509.

1,10 -Binaphtho[2,1-*b*]thiophen-2-amine (43). A mixture of **40** (0.14 g, 0.33 mmol), KOH (0.106 g, 1.9 mmol), THF (8 mL), and H_2O (1 mL) in a 50 mL flask was refluxed until completion of the reaction, which was monitored by TLC. The mixture was concentrated under reduced pressure until most of THF was removed, and the mixture was acidified with 1 M HCl at 0 °C. The resulting mixture was extracted with CH_2Cl_2 (10 mL × 3), and the combined organic layers were dried over Na_2SO_4, filtered, and concentrated under reduced pressure. The obtained crude residue was used without further purification.

A mixture of diphenylphosphoryl azide (0.078 mL, 0.36 mmol) and diisopropylamine (0.056 mL, 0.40 mmoL) in THF (2 mL) and ^{t}BuOH (4 mL) was added to the crude residue, and the resulting mixture was refluxed for 22 h. After concentrating under reduced pressure, 12 M HCl (2 mL) and THF (7 mL) were added to the residue. The resulting mixture was stirred until completion of the reaction, which was monitored by TLC. The resulting mixture was diluted with water (30 mL) and extracted with CH_2Cl_2 (10 mL × 3). The combined organic layers were dried over Na_2SO_4, filtered, and concentrated under reduced pressure. The resulting crude residue was purified by silica-gel column chromatography with $CHCl_3$/hexane (1/1) as an eluent to give **43** as a green solid (0.089 g, 71% yield): m.p. 90–91 °C; ^1H NMR (400 MHz, DMSO-d_6) δ 8.19 (d, *J* = 8.8 Hz, 1H), 7.97 (d, *J* = 7.8 Hz, 1H), 7.91–7.86 (m, 4H), 7.80 (d, *J* = 7.8 Hz, 1H), 7.55 (d, *J* = 8.8 Hz, 1H), 7.35 (t, *J* = 7.2 Hz, 1H), 7.20–7.16 (m, 2H), 7.11 (t, *J* = 7.6 Hz, 1H), 6.82 (t, *J* = 7.6 Hz, 1H), 5.79 (s, 2H); ^{13}C NMR (101 MHz, DMSO-d_6) δ 151.4,

139.0, 134.5, 133.1, 133.0, 131.9, 131.3, 130.0, 128.5 (two carbons), 128.0, 127.7, 126.2, 126.1, 125.6, 125.1, 124.7, 124.3, 122.4, 122.2, 121.7, 120.8, 120.7, 107.6; HRMS–ESI$^+$ (*m*/*z*) calcd for $C_{24}H_{16}NS_2$ ([M + H]$^+$) 382.0719, found 382.0707.

Methyl 1,1′-binaphtho[2,1-*b*]thiophene-2-carbamate (44a). A mixture of **43** (0.073 g, 0.19 mmol), methyl chloroformate (0.034 mL, 0.41 mmol), and toluene (0.60 mL) in a 20 mL Schlenk tube was refluxed with stirring for 3 h. The resulting mixture was concentrated under reduced pressure to give **44a** as a green solid (0.079 g, 94% yield): m.p. 100–101 °C; ^{1}H NMR (400 MHz, DMSO-d_6) δ 10.14 (s, 1H), 8.22 (d, J = 8.8 Hz, 1H), 8.08 (d, J = 8.8 Hz, 1H), 7.97 (d, J = 7.8 Hz, 1H), 7.93–7.85 (m, 3H), 7.78 (d, J = 8.8 Hz, 1H), 7.53 (d, J = 8.8 Hz, 1H), 7.33 (t, J = 6.8 Hz, 1H), 7.25 (t, J = 7.2 Hz, 1H), 7.13 (d, J = 8.8 Hz, 1H), 7.05 (t, J = 8.0 Hz, 1H), 6.88 (t, J = 8.4 Hz, 1H), 3.61 (s, 3H); ^{13}C NMR (126 MHz, DMSO-d_6, 100 °C) δ 153.9, 138.5, 138.3, 132.9, 131.5, 131.3, 131.24, 131.20, 131.0, 129.4, 128.4, 128.1, 127.9, 127.3, 125.5, 125.1, 124.9, 124.4, 124.1, 123.8, 121.8, 121.5, 120.8, 120.1, 119.1, 51.7; HRMS–APCI$^+$ (*m*/*z*) calcd for $C_{26}H_{18}NO_2S_2$ ([M + H]$^+$) 440.0774, found 440.0779.

***N*-([1,1′-Binaphtho[2,1-*b*]thiophen]-2-yl)acetamide (44b).** A mixture of **43** (0.037 g, 0.097 mmol) and Ac_2O (0.011 mL, 0.12 mmol), and CH_2Cl_2 (0.60 mL) in a 20 mL Schlenk tube was stirred at room temperature for 18 h. The reaction was quenched with saturated aqueous $NaHCO_3$ (20 mL), and the resulting mixture was extracted with CH_2Cl_2 (10 mL × 3). The combined organic layers were dried over Na_2SO_4, filtered, and concentrated under reduced pressure. The obtained crude residue was purified by silica-gel column chromatography with CH_2Cl_2 as an eluent to give **44b** as a green solid (0.032 g, 78% yield): m.p. 255–256 °C; ^{1}H NMR (500 MHz, DMSO-d_6) δ 10.29 (s, 1H), 8.25 (d, J = 8.5 Hz, 1H), 8.08 (d, J = 8.5 Hz, 1H), 7.99–7.96 (m, 2H), 7.94 (d, J = 8.6 Hz, 1H), 7.89 (d, J = 8.0 Hz, 1H), 7.77 (d, J = 8.5 Hz, 1H), 7.51 (d, J = 8.5 Hz, 1H), 7.33 (t, J = 7.0 Hz, 1H), 7.24 (t, J = 7.0 Hz, 1H), 7.06–7.03 (m, 2H), 6.86 (t, J = 7.0 Hz, 1H), 2.04 (s, 3H); ^{13}C NMR (126 MHz, DMSO-d_6) δ 168.4, 139.1, 137.7, 133.5, 131.7, 131.6 (two carbons), 131.4, 130.7, 129.8, 128.7, 128.6, 128.5, 128.4, 126.3, 125.7, 125.5, 125.1, 124.6, 124.0, 122.1, 121.6 (2 carbons), 120.8, 116.4, 22.6; HRMS–APCI$^+$ (*m*/*z*) calcd for $C_{26}H_{18}NOS_2$ ([M + H]$^+$) 424.0825, found 424.0830.

Methyl 8*H*-bis(naphtho[1′,2′:4,5]thieno)[2,3-*b*:3′,2′-*d*]pyrrole-8-carboxylate (45a). A mixture of **44a** (0.079 g, 0.18 mmol), $Pd(OAc)_2$ (2.2 mg, 9.0 μmol), $Cu(OAc)_2$ (33 mg, 0.18 mmol), powdered molecular sieves (41 mg), and xylene (1.8 mL) was placed

in a 20 mL Schlenk tube and degassed by three freeze–pump–thaw cycles. The mixture was refluxed for 20 h. The reaction was quenched with 30% ammonia solution (1 mL), and water (20 mL) was added. The resulting mixture was extracted with CH_2Cl_2 (10 mL × 3), and the combined organic layers were dried over Na_2SO_4, filtered, and concentrated under reduced pressure. The obtained crude residue was purified by silica-gel column chromatography with $CHCl_3$/hexane (2/1) as an eluent to give **45a** as a colorless solid (8.4 mg, 11% yield): m.p. 227–228 °C; ^{1}H NMR (400 MHz, $CDCl_3$, 50 °C) δ 8.29 (d, J = 8.4 Hz, 2H), 7.94 (d, J = 7.8 Hz, 2H), 7.90 (d, J = 8.7 Hz, 2H), 7.81 (d, J = 8.0 Hz, 2H), 7.42 (t, J = 6.8 Hz, 2H), 6.97 (t, J = 6.8 Hz, 2H), 4.26 (s, 3H); ^{13}C NMR (101 MHz, $Cl_2CDCDCl_2$, 60 °C) δ 149.4, 135.7, 131.8, 129.5, 128.3 127.7, 127.3, 125.3, 124.7, 124.4, 122.3, 121.3, 55.1; HRMS–APCI$^+$ (*m*/*z*) calcd for $C_{26}H_{16}NO_2S_2$ ([M + H]$^+$) 438.0617, found 438.0614.

1-[8*H*-Bis(naphtho[1′,2′:4,5]thieno)[2,3-*b*:3′,2′-*d*]pyrrol-8-yl]ethan-1-one (45b). The crude residue was obtained with **44b** (0.042 g, 0.10 mmol), $Pd(OAc)_2$ (1.4 mg, 5.0 μmol), $Cu(OAc)_2$ (19 mg, 0.10 mmol), powdered molecular sieves (21 mg), and xylene (1 mL) according to the procedure for **45a**. Purification by silica-gel column chromatography with CH_2Cl_2 as an eluent and by preparative HPLC gave **45b** as a colorless solid (7.5 mg, 18% yield): m.p. 260–261 °C; ^{1}H NMR (500 MHz, $CDCl_3$, 40 °C) δ 8.24 (d, J = 7.5 Hz, 2H), 7.94 (d, J = 8.0 Hz, 2H), 7.89 (d, J = 8.6 Hz, 2H), 7.82 (d, J = 8.5 Hz, 2H), 7.42 (t, J = 7.5 Hz, 2H), 6.95 (t, J = 7.0 Hz, 2H), 2.89 (s, 3H); ^{13}C NMR (101 MHz, DMSO-d_6, 100 °C) δ 165.9, 135.5, 135.0, 131.4, 128.2, 127.4, 127.1, 126.2, 124.9, 124.4, 123.7, 121.2, 121.1, 22.4; HRMS–APCI$^+$ (*m*/*z*) calcd for $C_{26}H_{16}NOS_2$ ([M + H]$^+$) 422.0668, found 422.0661.

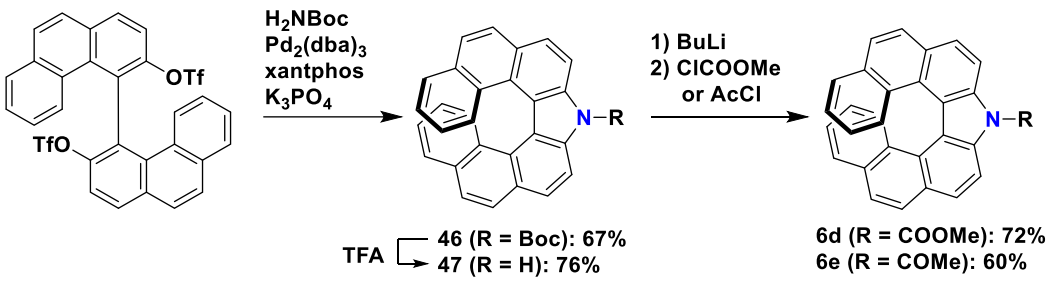

***tert*-Butyl 9*H*-dinaphtho[2,1-*c*:1',2'-*g*]carbazole-9-carboxylate (46).** A mixture of *rac*-[4,4′-biphenanthrene]-3,3′-diyl bis(trifluoromethanesulfonate) (0.14 g,

0.20 mmol), *tert*-butyl carbamate (31 mg, 0.26 mmol), $Pd_2(dba)_3$(16 mg, 0.015 mmol), xantphos (15 mg, 0.026 mmol), anhydrous K_3PO_4 (0.15 g, 0.71 mmol), and xylene (15 mL) in a Schlenk tube was stirred at 100 °C for 49 h. The resulting mixture was washed with 1 M aqueous HCl, dried over anhydrous Na_2SO_4, filtered, and concentrated under reduced pressure. The resulting crude residue was purified by silica-gel column chromatography with CH_2Cl_2/hexane (3/2) as an eluent to give **46** as a colorless solid (65 mg, 67%): ^{1}H NMR (400 MHz, $CDCl_3$) δ 8.90 (d, *J* = 8.7 Hz, 2H), 8.11 (d, *J* =8.7 Hz, 2H), 7.97 (d, *J* = 8.7 Hz, 2H), 7.85 (d, *J* = 8.7 Hz, 2H), 7.78 (d, *J* = 7.3 Hz, 2H), 7.46 (d, *J* =8.2 Hz, 2H), 7.20-7.16 (m, 2H), 6.32-6.28 (m, 2H), 1.93 (s, 9H); ^{13}C NMR (101 MHz, $CDCl_3$) δ 151.1, 138.3, 131.4, 130.4, 128.7, 127.8, 127.6, 126.51, 126.45, 126.3, 125.9, 123.2, 120.5, 115.3, 85.0, 28.6; HRMS–APCI$^+$ (*m*/*z*) calcd for $C_{29}H_{18}NO_2^+$ ($[M-C_4H_9+2H]^+$), 412.1333; found, 412.1346.

9*H*-Dinaphtho[2,1-*c*:1',2'-*g*]carbazole (47). To the solution of **46** (0.13 g, 0.28 mmol) in CH_2Cl_2 (2 mL) was added trifluoroacetic acid (0.64 mL, 8.3 mmol) at 0 ℃. The resulting mixture was stirred at room temperature for 13 h. The reaction was quenched with saturated aqueous $NaHCO_3$, and the resulting mixture was extracted with CH_2Cl_2. The combined organic layers were dried over Na_2SO_4, filtered, and concentrated under reduced pressure. The resulting crude residue was purified by silica-gel column chromatography with AcOEt/hexane (1/2) as an eluent to give **47** as a brownish solid (78 mg, 76% yield): ^{1}H NMR (400 MHz, acetone-d_6) δ 11.71 (s, 1H), 8.15-8.06 (m, 6H), 7.86 (d, *J* = 8.4 Hz, 4H), 7.50 (d, *J* =8.8 Hz, 2H), 7.18-7.14 (m, 2H), 6.22-6.18 (t, 2H); ^{13}C NMR (101 MHz, acetone-d_6) δ 140.1, 140.0, 132.4, 131.3, 128.7, 127.9, 127.8, 127.3, 126.7, 124.9, 123.3, 117.5, 117.4, 113.2, 113.1; HRMS–APCI$^+$ (*m*/*z*) calcd for $C_{28}H_{18}N^+$ ($[M+H]^+$), 368.1434; found, 368.1457.

Methyl 9*H*-dinaphtho[2,1-*c*:1',2'-*g*]carbazole-9-carboxylate (6d). BuLi (2.6 M in hexane, 0.045 mL, 0.12 mmol) was added dropwise to the solution of **47** (0.037 g, 0.10 mmol) in THF (1.5 mL) at 0 °C. After stirring at room temperature for 30 min, methyl chloroformate (0.011 mL, 0.14 mmol) was added to the reaction mixture at room temperature. The resulting mixture was stirred for overnight, and the reaction was quenched with water (20 mL). The resulting mixture was extracted with CH_2Cl_2 (10 mL × 3), and the combined organic layers were dried over Na_2SO_4, filtered, and concentrated under reduced pressure. The resulting crude residue was purified by silica-gel column chromatography with CH_2Cl_2/hexane (1/1) as an eluent to give **6d** as a colorless solid (31 mg, 72% yield): m.p. 235-236 °C; ^{1}H NMR (400 MHz, $CDCl_3$) δ 8.79 (d, *J* = 9.2 Hz, 2H),

8.05 (d, J = 9.2 Hz, 2H), 7.91 (d, J = 8.8 Hz, 2H), 7.80 (d, J = 8.8 Hz, 2H), 7.72 (d, J = 8.4 Hz, 2H), 7.38 (d, J = 8.4 Hz, 2H), 7.13 (dt, J = 6.8, 1.2 Hz, 2H), 6.24 (dt, J = 7.2, 1.2 Hz, 2H), 4.26 (s, 3H); ^{13}C NMR (101 MHz, $CDCl_3$) δ 153.1, 138.0, 131.4, 130.4, 129.0, 128.0, 127.6, 126.6, 126.44 (two carbons), 126.40, 126.1, 123.3, 120.9, 115.2, 54.2; HRMS–APCI (*m/z*) calcd for $C_{30}H_{20}NO_2^+$ ($[M+H]^+$) 426.1489, found 426.1494.

1-(9*H*-Dinaphtho[2,1-*c*:1',2'-*g*]carbazol-9-yl)ethanone (6e). BuLi (2.6 M in hexane, 0.045 mL, 0.12 mmol) was added dropwise to the solution of **47** (0.037 g, 0.10 mmol) in THF (1.5 mL) at 0 °C. After stirring at room temperature for 30 min, acetyl chloride (0.011 mL, 0.16 mmol) was added to the reaction mixture at room temperature. The resulting mixture was stirred for overnight, and the reaction was quenched with water (20 mL). The resulting mixture was extracted with CH_2Cl_2 (10 mL × 3), and the combined organic layers were dried over Na_2SO_4, filtered, and concentrated under reduced pressure. The resulting crude residue was purified by silica-gel column chromatography with CH_2Cl_2/hexane (1/1) as an eluent to give **6e** as a colorless solid (23 mg, 60% yield): m.p. 236-237 °C; ^{1}H NMR (400 MHz, $CDCl_3$) δ 8.62 (d, J = 8.8 Hz, 2H), 8.07 (d, J = 8.4 Hz, 2H), 7.92 (d, J = 8.8 Hz, 2H), 7.82 (d, J = 8.8 Hz, 2H), 7.73 (d, J = 6.8 Hz, 2H), 7.38 (d, J = 8.0 Hz, 2H), 7.14 (dt, J = 6.8, 1.6 Hz, 2H), 6.26 (dt, J = 7.6, 1.6 Hz, 2H), 3.12 (s, 3H); ^{13}C NMR (101 MHz, $CDCl_3$) δ 170.8, 138.1, 131.5, 130.4, 129.0, 128.0, 127.6, 126.63, 126.57, 126.5, 126.4, 126.3, 123.4, 121.2, 114.8, 28.6; HRMS–APCI (*m/z*) calcd for $C_{30}H_{20}NO^+$ ($[M+H]^+$) 410.1540, found 410.1545.

4.7.3. X-ray Crystallography

For X-ray crystallographic analyses, suitable single crystals were selected under ambient conditions, mounted using a nylon loop filled with paraffin oil, and transferred to the goniometer of a RIGAKU R-AXIS RAPID diffractometer with a graphite-monochromated Cu−Kα irradiation (α = 1.54187 Å). The structures were solved by a direct method (SIR 2008[16]) and refined by full-matrix least-squares techniques against F^2 (SHELXL-2014[17,18]). The intensities were corrected for Lorentz and polarization effects. All non-hydrogen atoms were refined anisotropically. Hydrogen atoms were placed using AFIX instructions.

4.7.4. Theoretical calculations

The DFT and TD–DFT calculations were performed by using the Gaussian 09 program[19] at the B3LYP/6–31G(d) level with workstation at Research Center for Computational Science, National Institutes of Natural Sciences, Okazaki, Japan. The

starting molecular models for DFT geometry optimizations were built and optimized with MMFF molecular mechanics by using the Spartan ’08 package (Wavefunction, Inc., Irvine, CA, USA). Twelve singlet states were calculated in TD–DFT calculations. The visualization of the molecular orbitals was performed using GaussView 5 (Gaussian, Inc., Wallingford, CT, USA).

4.8. References

(1) Harvey, R. G.; Dai, Q.; Ran, C.; Penning, T. M. *J. Org. Chem.* **2004**, *69*, 2024–2032.
(2) Li, G.; Wang, E.; Chen, H.; Li, H.; Liu, Y.; Eang, P. G. *Tetrahedron* **2008**, *64*, 9033–9043.
(3) Tsang, W. C. P.; Zheng, N.; Buchwald, S. L. *J. Am. Chem. Soc.* **2005**, *127*, 14560–14561.
(4) Nakano, K.; Oyama, H.; Nishimura, Y.; Nakasako, S.; Nozaki, K. *Angew. Chem. Int. Ed.* **2012**, *51*, 695–699.
(5) Oyama, H.; Akiyama, M.; Nakano, K.; Naito, M.; Nobusawa, K.; Nozaki, K. *Org. Lett.* **2016**, *18*, 3654–3657.
(6) Nakano, K.; Hidehira, Y.; Takahashi, K.; Hiyama, T.; Nozaki, K. *Angew. Chem. Int. Ed.* **2005**, *44*, 7136–7138.
(7) Gordon, T. J.; Szabo, L. D.; Linder, T.; Berlinguette, C. P.; Baumgartner, T. *C. R. Chimie* **2010**, *13*, 971–979.
(8) Durben, S.; Linder, T.; Baumgartner, T. *New J. Chem.* **2010**, *34*, 1585–1592.
(9) Hanamura, H.; Nemoto, N. *Polymer* **2011**, *52*, 5282–5289.
(10) Hanamura, H.; Nemoto, N. *Polymer* **2014**, *55*, 6672–6679.
(11) Evenson, S. J.; Rasmussen, S. C. *Org. Lett.* **2010**, *12*, 4054–4057.
(12) Evenson, S. J.; Pappenfus, T. M.; Delgado, M. C. R.; Radke-Wohlers, K. R.; Navarretec, J. T. L.; Rasmussen, S. C. *Phys. Chem. Chem. Phys.* **2012**, *14*, 6101–6111.
(13) Baumgartner, T.; Réau, R. *Chem. Rev.* **2006**, *106*, 4681–4727.
(14) Baumgartner, T. *Acc. Chem. Res.* **2014**, *47*, 1613–1622.
(15) Reichardt, C. *Angew. Chem. Int. Ed.* **1979**, *18*, 98–110.
(16) Burla, M. C. B.; Caliandro, R.; Camalli, M.; Carrozzini, B.; Cascarano, G. L.; De Caro, L.; Giacovazzo, C.; Polidori, G.; Siliqi, D.; Spagna, R. *J. Appl. Cryst.* **2007**, *40*, 609–613.
(17) Sheldrick, G. *Acta Crystallogr. A* **2008**, *64*, 112–122.
(18) Sheldrick, G. *Acta Crystallogr. C Struct. Chem.* **2015**, *C71*, 3–8.
(19) Frisch, M. J.; Trucks, G. W.; Schlegel, H. B.; Scuseria, G. E.; Robb, M. A.; Cheeseman, J. R.; Scalmani, G.; Barone, V.; Mennucci, B.; Petersson, G. A.; Nakatsuji, H.; Caricato, M.; Li, X.; Hratchian, H. P.; Izmaylov, A. F.; Bloino, J.; Zheng, G.; Sonnenberg, J. L.; Hada, M.; Ehara, M.; Toyota, K.; Fukuda, R.; Hasegawa, J.; Ishida, M.; Nakajima, T.; Honda, Y.; Kitao, O.; Nakai, H.; Vreven, T.; Montgomery, Jr. J. A., Peralta, J. E.; Ogliaro, F.; Bearpark, M.; Heyd, J. J.; Brothers, E.; Kudin, K. N.; Staroverov, V. N.; Kobayashi, R.; Normand, J.; Raghavachari, K.; Rendell, A.; Burant, J. C.; Iyengar,

S. S.; Tomasi, J.; Cossi, M.; Rega, N.; Millam, J. M.; Klene, M.; Knox, J. E.; Cross, J. B.; Bakken, V.; Adamo, C.; Jaramillo, J.; Gomperts, R.; Stratmann, R. E.; Yazyev, O.; Austin, A. J.; Cammi, R.; Pomelli, C.; Ochterski, J. W.; Martin, R. L.; Morokuma, K.; Zakrzewski, V. G.; Voth, G. A.; Salvador, P.; Dannenberg, J. J.; Dapprich, S.; Daniels, A. D.; Farkas, Ö.; Foresman, J. B.; Ortiz, J. V.; Cioslowski, J.; Fox, D. J. Gaussian 09, Revision D.01; Gaussian, Inc.: Wallingford CT, **2009**.

Chapter 5

Conclusion and Perspective

The purpose of this study is (a) establishment of efficient methods for the synthesis of helicenes and helicene-like compounds from common precursors and (b) evaluation of properties of newly synthesized helicenes and helicene-like compounds to elucidate structure–property relationship.

In Chapter 2, 3,3'-dibromo-4,4'-biphenanthrene as a promising precursor was prepared through a new synthetic route. Its synthesis ever reported requires harsh reaction conditions and is difficult to be reproduced, but the new route in this thesis avoids such conditions. However, the new route requires lengthy multistep sequence and the total yield could not be improved. The transformations of thia[7]helicene to aza[7]helicenes and [7]helicene-like compounds were successfully achieved via aromatic metamorphosis. The dianion obtained by desulfurative dilithiation of thia[7]helicene was found to react with an dielectrophiles to give the corresponding helicene-like compounds. Furthermore, dinucleophiles is able to be introduced with thia[7]helicene *S*,*S*-dioxide. This methodology is free of transition metal catalysts and can derivatize thia[7]helicene to a variety of aza[7]helicenes and [7]helicene-like compounds at a later stage of the synthetic sequence.

In Chapter 3, the spiro-double silole-fused [7]helicene-like compound was successfully synthesized using 3,3'-dibromo-4,4'-biphenanthrene as the precursor. This is the first report on the synthesis of an optically resolvable spiro-double helicene-like compound. The combination of the silicon-centered spiro fusion and the π-extended helical structure was found to offer unique optical properties attributable to the LUMO spiro-conjugation between the two silole-fused [7]helicene-like units.

In Chapter 4, the synthesis of 1,1'-binaphtho[2,1-*b*]thiophene as a common precursor has led to the successful and efficient synthesis of new helical compounds

containing a cyclopentadiene, pyrrole, or phosphole ring. The thiophene ring in the helical structure was found to work as an electron-donor and induce intramolecular charge transfer in the presence of electron-withdrawing unit, affording a red-shifted emission.

In conclusion, the syntheses of helicene precursors were achieved, and they were efficiently converted into a variety of new helicenes and helicene-like compounds. Through evaluation of their photophysical properties and comparison of them with those of the related compounds, the effects of heteroles and cyclopentadiene units on photophysical properties were clarified. The establishment of these efficient synthetic methods in this thesis will contribute to the search for novel helicenes and helicene-like compounds with desirable properties. It is expected to efficiently synthesize a series of helicenes and helicene-like compounds with heteroatom(s) and cyclopentadiene ring(s) at different positions by designing the suitable precursor. With the development of new helicenes and helicene-like compounds, the relationship between the structure and physicochemical properties would be clarified, providing the design guide for more highly functional helicene-based materials.

List of Publication

Parts of the present Thesis have been published in the following journals.

(1) Synthesis and properties of [7]helicene and [7]helicene-like compounds with a cyclopenta[1,2-*b*:4,3-*b*']dithiophene or dithieno[2,3-*b*:3',2'-*d*]heterole skelton
Uematsu, K.; Noguchi, K.; Nakano, K. *Phys. Chem. Chem. Phys.* **2018**, *20*, 3286–3295.
[Chapter 4]

(2) Synthesis and Properties of Spiro-double Sila[7]helicene: The LUMO Spiro-conjugation
Terada, N.; Uematsu, K.; Higuchi, R.; Tokimaru, Y.; Sato, Y.; Nakano, K.; Nozaki, K. *Chem. Eur. J.* **2021**, *27*, 9342–9349.
[Chapters 2 and 3]

(3) Transformation of Thia[7]helicene to Aza[7]helicenes and [7]Helicene-like Compounds via Aromatic Metamorphosis
Uematsu, K.; Hayasaka, C.; Takase, K.; Noguchi, K.; Nakano, K. *Molecules* **2022**, *27*, 606–617.
[Chapter 2]

Acknowledgements

The study presented in this Thesis has been carried out under the direction of Dr. Koji Nakano at Tokyo University of Agriculture and Technology. The author would like to express his sincerest gratitude to Dr. Koji Nakano for his constant support, guidance, encouragement, and enthusiasm throughout this study.

The author is deeply grateful to Professor Keiichi Noguchi at Tokyo University of Agriculture and Technology for his valuable discussions and technical assistance for NMR and MS measurements and X-ray crystallography analysis. The author also wishes to thank Professor Kyoko Nozaki and her group members at The University of Tokyo for their technical assistance for the optical resolution with chiral HPLC and helpful discussion for X-ray crystallography analysis and theoretical calculations.

The author would like to thank all members of the Dr. Nakano's group at Tokyo University of Agriculture and Technology for their kindness.

Financial support from Teijin Scholarship Foundation is greatly appreciated.

Finally, the author wishes to express sincerest gratitude to his families for their warm support and heartfelt encouragement.